REPUBLIQUE DU CAMEROUN
Paix-Travail-Patrie

UNIVERSITY DE YAOUNDE I

CENTRE DE RECHERCHE ET DE FORMATION DOCTORALE EN SCIENCE TECHNOLOGIE ET GEOSCIENCES

UNITE DE RECHERCHE ET DE FORMATION DOCTORALE PHYSIQUE APPLICATIONS

B.P. 812 Yaoundé
Email: crfd_stg@uy1.uninet.cm

REPUBLIC OF CAMEROON
Peace-Work-Fatherland

THE UNIVERSITY OF YAOUNDE I

POSTGRADUATE SCHOOL OF SCIENCE, TECHNOLOGY AND GEOSCIENCES

RESEARCH AND POSTGRADUATE TRAINING UNIT FOR PHYSICS AND APPLICATIONS

P.O. Box: 812 Yaounde
Email: crfd_stg@uy1.uninet.cm

LABORATOIRE DE MECANIQUE, MATERIAUX ET STRUCTURE

MECHANICS, MATERIALS, AND STRUCTURE LABORATORY

Study of structural and magnetic properties of Fe/Cu/Fe multilayers using a computational approach

Thesis submitted in partial fulfilment of the requirements for the award of a Doctorate/**Ph. D. in Physics**

Option: Materials Science

By

NDE KENGNE Jules Berlin

Registration number: **07W597**

Master's in Physics

Supervised by

ZEKENG Serge Sylvain

Professor, The University of Yaounde I

Year 2021

BIBLIOTHEQUE UNIVERSITAIRE UY1

UNIVERSITÉ DE YAOUNDÉ I
THE UNIVERSITY OF YAOUNDE I

FACULTÉ DES SCIENCES
FACULTY OF SCIENCE

DÉPARTEMENT DE PHYSIQUE
DEPARTMENT OF PHYSICS

ATTESTATION DE CORRECTION DE LA THÈSE DE DOCTORAT/Ph.D

Nous, Professeur **NANA NBENDJO Blaise Roméo** et Professeur **NDJAKA Jean Marie Bienvenu**, respectivement Examinateur et Président du jury de la Thèse de Doctorat/Ph.D de Monsieur **NDE KENGNE Jules Berlin**, Matricule **07W597**, préparée sous la direction du Professeur **ZEKENG Serge Sylvain,** intitulée : « **Study of structural and magnetic properties of Fe/Cu/Fe multilayers using a computational approach** », soutenue le **Lundi, 05 Avril 2021**, en vue de l'obtention du grade de Docteur/Ph.D en Physique, Spécialité **Mécanique et Matériaux,** Option **Sciences des Matériaux,** attestons que toutes les corrections demandées par le jury de soutenance ont été effectuées.

En foi de quoi, la présente attestation lui est délivrée pour servir et valoir ce que de droit.

Fait à Yaoundé le 13 APR 2021

Examinateur	Le Chef de Département de Physique	Le Président du jury
Pr NANA NBENDJO Blaise Roméo	Pr NDJAKA Jean-Marie Bienvenu	Pr NDJAKA Jean-Marie Bienvenu

UNIVERSITE DE YAOUNDE I FACULTE DES SCIENCES DEPARTEMENT DE PHYSIQUE Le Chef de Département

REPUBLIQUE DU CAMEROUN
Paix-Travail-Patrie

UNIVERSITY DE YAOUNDE I

CENTRE DE RECHERCHE ET DE FORMATION DOCTORALE EN SCIENCE TECHNOLOGIE ET GEOSCIENCES

UNITE DE RECHERCHE ET DE FORMATION DOCTORALE PHYSIQUE APPLICATIONS

B.P. 812 Yaoundé
Email: crfd_stg@uy1.uninet.cm

REPUBLIC OF CAMEROON
Peace-Work-Fatherland

THE UNIVERSITY OF YAOUNDE I

POSTGRADUATE SCHOOL OF SCIENCE, TECHNOLOGY AND GEOSCIENCES

RESEARCH AND POSTGRADUATE TRAINING UNIT FOR PHYSICS AND APPLICATIONS

P.O. Box: 812 Yaounde
Email: crfd_stg@uy1.uninet.cm

LABORATOIRE DE MECANIQUE, MATERIAUX ET STRUCTURE

MECHANICS, MATERIALS, AND STRUCTURE LABORATORY

Study of structural and magnetic properties of Fe/Cu/Fe multilayers using a computational approach

Thesis submitted in partial fulfilment of the requirements for the award of a Doctorate/**Ph. D. in Physics**

Option: Materials Science

By

NDE KENGNE Jules Berlin

Registration number: **07W597**

Master's in Physics

Supervised by

ZEKENG Serge Sylvain

Professor, The University of Yaounde I

Year 2021

Acknowledgements

I thank the Almighty God for His guidance, strength, and knowledge given to me throughout this thesis.

I seize this opportunity to express my profound gratitude to my supervisor, Prof Serge Sylvain Zekeng, Professor of Physics, University of Yaounde I, Yaounde, Cameroon. His guidance, suggestions, and fruitful discussions have made my journey as a post-graduate student a pleasant experience. I found such great joy working with him, discussing with him not only like supervisor and student but also like father and son. His constant motivations boosted my mindset to finish this graduate work.

I am indebted to Dr. Bernard Fongang, Assistant Professor, University of Texas Health Science Center at San Antonio, Texas, USA, for his motivations. His high implication has brought this thesis to great success. He was always ready to provide lucid explanations of the different concepts involved. Sharing his greatest success in science has been a fantastic experience. Thank you.

I am grateful to Prof Jean Marie B. Ndjaka, Professor of Physics, The University of Yaounde I, Yaounde, Cameroon, for accepting me as a graduate student in the Laboratory of Material Sciences at the Department of Physics, University of Yaounde I. Your teachings, your sense of humor, your primary concern being our success, etc., have been of highest importance to us, not only as scientists but also in our everyday life. Thank you.

I would like to thank the Graduate Committee Members for accepting to serve on this graduate committee. Their guidance and critical thinking will help to improve the quality of this work.

I am grateful with the Lectures of the Materials Science Laboratory, Department of Physics, University of Yaounde I and all the Lecturers of the Department of Physics for their teachings, encouragement, and the knowledge they have impacted on me.

I am grateful to the Director of the graduate school for allowing this thesis work to be conducted in his school.

I express my special thanks to the post-graduate Students in the Materials Science Laboratory and the post-graduate Students of the Department of Physics, University of Yaounde I, for their interactions, exchange, and excellent discussions.

I would like to express my gratitude to the University of Yaounde I for providing a joyful and peaceful environment and for accompanying us towards our success.

My special thanks also goes to my parents and my parents in Law for their supports. I equally want to thank them for their love and encouragement.

My special thanks equally goes to my lovely family for their support throughout this work. Special thanks also goes to my friends and others for their constant support and motivations.

Finally, I thank my wife Gaelle Djouka for her constant support, encouragement, inspiration, and motivation given to me throughout this thesis work.

Jules Berlin Nde, Kengne

Dedication

To my lovely late Dad, Papa Kengne Michel,

Who has always been supportive to me wherever he is

I miss you Dad, and you know that.

Contents

Abstract vii

Résumé viii

List of Abbreviations ix

List of Tables x

List of Figures xi

General Introduction 1

Chapter 1 Literature Review **6**

1-1. Introduction 6

1-2. Origin of the ferromagnetism in different materials 7

1-3. Structural and magnetic properties of thin films and magnetic multilayer systems 11

1-3.1 Influence of the structure of each layer on the magnetic properties 12

1-3.2 Giant magnetoresistance effect observed in magnetic multilayer systems 14

1-4. Structural and magnetic properties of thin films and magnetic multilayers Fe/Cu/Fe 18

1-5. Experimental methods of preparation and characterization of magnetic multilayer systems 21

1-5.1 Synthesis of nanomaterial. 22

1-5.2 Experimental approach to fabricate the multilayers Fe/Cu/Fe. 24

1-5.3 Characterization of the multilayer systems Fe/Cu/Fe 26

1-6. Iron and copper structures – Bragg's law 32

1-8. Conclusion 36

Chapter 2 Numerical Methodology **38**

2-1. Introduction 38

2-2. Voronoï diagram approach applied to the preparation of the multilayer systems.... 38

2-3. Definition of the form of the Hamiltonian used in this thesis 44

2-4. Computational approach of characterization of magnetic multilayer systems 47

2-4-1. Molecular dynamics method to investigate the properties of interacting particles.....48

2-4-2. Monte Carlo versus Molecular dynamics.....49

2-4-3. Metropolis Monte Carlo statistical method to investigate the properties of interacting particles.....50

2-5. Metropolis Monte Carlo method to investigate the properties of magnetic multilayers 56

2-6. Data analysis..... 61

2-7. Conclusion 63

Chapter 3 Results and Discussion 65

3-1. Introduction..... 65

3-2 Structural properties of Fe/Cu/Fe multilayers..... 67

3-2.1 Test of the simulation model.....67

3-2.2 Properties of the magnetic bilayer systems 69

3-2.3 Structural characterization of the trilayer systems.....75

3-4. Magnetic properties of multilayer systems Fe/Cu/Fe. 88

3-5. Conclusion 93

General conclusion and future outlooks.....95

References.....97

Publication from this thesis.....103

Abstract

This thesis presents the results of our investigations on the structural and magnetic properties of FM/NM/FM (FM for ferromagnetic and NM for non-magnetic) multilayer systems based on the fundamental from statistical physics and numerical methods.

Interest in magnetic multilayers has recently emerged as they are promising candidates for magnetic storage media, magneto-resistive sensors, and personalized medical treatment. As these artificial materials show substantial differences in properties compared to conventional materials, many experimental and theoretical works have been dedicated to shed light on the observed differences, and many hypotheses on their structural differences have been tested. However, little is known about the influence of the interfaces between FM and NM layers on the magnetism of the multilayer systems. We have used atomistic Monte Carlo simulations to analyze the effect of the non-magnetic layer at the interface between FM and NM layers. We constructed the multilayers model composed of iron (Fe) and copper (Cu) based on the Voronoï diagram.

From our numerical approaches, we have shown that the structural and magnetic properties of each layer depend on its thickness and the interface morphology. The Fe and Cu layers can adopt either the body-centered-cubic, BCC, or face-centered-cubic, FCC; at the same time, the interface can assume amorphous, BCC, FCC, or even a mixture of BCC and FCC structures depending on the layers' thicknesses. On the other hand, we have also observed reduced magnetization (smaller amplitude compared to the magnetization of the bulk of Fe) at the interface, characterized by the BCC Fe. A fluctuating susceptibility was also observed near the Curie temperature for both the Fe layer and the interface. It is probably related to the reduced thicknesses. These results are in good agreement with the experiment. This model of magnetic multilayers could hopefully help to get new insight into the mechanism governing the interfaces of FM/NM/FM multilayer systems by providing atomistic details of the changes observed in these magnetic multilayers, which are of great importance in the industries of magnetic recording media (when exploring the giant magnetoresistance, GMR, effect) and Nanomagnetic Sensors (when exploring the giant magneto impedance, GMI, effect).

Keywords: Nanotechnology; Nanomaterials; Magnetic multilayers; Physics of surface and interface; Computational Physics; Monte Carlo simulations; Voronoï diagram

Résumé

Cette thèse porte sur l'étude des propriétés structurale et magnétique des multicouches FM/NM/FM (FM pour ferromagnétique et NM pour non-magnétique) en utilisant une approche originale basée sur la physique statistique et les méthodes numériques.

L'intérêt portée sur les multicouches magnétiques vient du fait que ces systèmes artificiels présentent des propriétés complètement différentes de celles des éléments conventionnels, c'est-à-dire Fe et Cu dans nos travaux. Ces propriétés nouvelles présentent beaucoup d'avantages selon la litérature. Toutefois, la question de leur origine liée vraissemblablement aux épaisseurs individuelles des couches et aux agencements susceptibles de conduire à des effets magnétiques spectaculaires reste pour certains aspects un sujet de débats au sein de la communauté scientifique. Nous avons utilisé la méthode de Monte Carlo avec le critère de Metropolis pour caractériser les effets de l'interface sur les différentes multicouches. Nous avons construit nos systèmes de multicouches à base de fer (Fe) pour FM et de cuivre (Cu) pour NM en utilisant la méthode de construction dite du diagramme de Voronoï.

En utilisant une approche numérique, nous montrons que les propriétés structurale et magnétique de chaque couche du système sont déterminées par les épaisseurs des couches et la nature de l'interface entre les deux couches. Le Fe et le Cu peuvent adopter des structures cubique centrée, CC, cubique à face centrée, CFC, alors que l'interface quant à elle peut être de structure amorphe, CC, CFC, ou un mélange des deux dernières structures. Un magnétisme (amplitude très réduite par rapport à celle relative à la couche massive de fer) a été observé à l'interface, sûrement à cause de la présence des atomes de Fe. En effet, il a été montré que tant que la structure du Fe démeure CC, le magnétisme sera toujours observé. Au voisinage de la temperature de Curie, La susceptibilité magnétique présente des fluctuations à l'interface, en relation avec la grandeur des épaisseurs des couches adjacentes.

Ces résultats sont en accord avec ceux des études expérimentales menées sur des structures comparables, et pourront aider à comprendre l'origine des effets exhibés par ces multicouches, qui ont une portée technologique très importante, et notamment dans la creation de la magnéto-résistance géante et de la la magnéto-impédance géante.

Mots clés: Nanotechnologie; Nanomatériaux; Multicouches magnétiques; Physique des surfaces et interfaces; Physique numérique; Simulations Monte Carlo; Diagramme de Voronoï

List of Abbreviations

AFM: Antiferromagnetic

BCC: Body Centered Cubic

Cu: Copper

CVD: Chemical Vapour Deposition

EAM: Embedded-atom Method

FCC: Face Centered Cubic

Fe: Iron

FM: Ferromagnetic

GMI: Giant Magneto Impedance

GMR: Giant Magnetoresistance

MEAM: Modified Embedded-Atom Method

MD: Molecular dynamics

MR: Magnetoresistance

MC: Monte Carlo

MCM: Monte Carlo Metropolis

NM: Non-magnetic

PVD: Physical Vapour Deposition

TMR: Transverse Magnetoresistance

UHV: Ultra-High Vacuum

List of Tables

Table 1-1. Approximate relative permeability μ/μ_0 of copper, iron, and other common materials used for comparison 8
Table 1-2. Selection rules for the diffraction peaks in cubic systems 34
Table 1-3. Allowed list of values ($h^2+k^2+l^2$) of different atomic planes found in the cubic system 35
Table 2-1. Parameters used in the energy function. 47

List of Figures

Figure 1-1. Magnetic domains in a ferromagnetic material. (a) shows the rearrangement of the system into domains to minimize the energy of the system; (b) shows the magnetization of different domains in the absence of external magnetic field; (c) shows the orientations of the magnetization in the presence of the external magnetic field. The field is applied in the direction of dominant moments and the rest of the moments will undergo a torsional transformation upon increase of the field. 9

Figure 1-2. Magnetic and hysteresis loop for a ferromagnetic material. (a) show a system with easy magnetization and (b) shows a system with hard magnetization and high dissipated energy defined by the enclosed surface. 10

Figure 1-3. Mössbauer absorption spectra at 300K and 4K for Fe/Mg multilayers with various Fe layer thicknesses. The thickness of Fe is varied and the results are compared to that of bulk Fe, as shown above. When the thickness of Fe is as low as 10 Å, the behavior remains similar to that of the bulk Fe [37]. 14

Figure 1-4. Magnetoresistance at 4.2K of three Fe/Cr/Fe superlattices as a function of the applied field. The current and the applied field are along the (110) in the plane of the layers [14]. 16

Figure 1-5. Variation of the magnetoresistance ratio as a function of the thickness of the copper. The thickness of the Fe is kept at 15 Å and that of Cu is varied from 4 to 60 Å [41]..... 19

Figure 1-6. Structural changes observed in the multilayer systems Fe/Cu/Fe and Fe/Cu/Ni [5]..... 20

Figure 1-7. a) Schematic representation of the formation of nanostructures via the top-down and bottom-up approaches. b) A tapered probe, manipulated by a macroscopic machine, allows “writing” small features by scratching the probe apex on a soft polymer surface; c) Example of the self-assembling set to occur on previously chemically-functionalized surfaces; chemisorption happens due to interactions between adsorbing molecules and specific sites on the substrate. The resulting nano-electronics material emerges with much more useful functions when proper shapes and microstructures are provided [60]. 23

Figure 1-8. Future of the top-down and bottom-up approaches [59] 24

Figure 1-9. Principle of fabrication of thin films and multilayers using the physical vapor deposition (PVD). 25

Figure 1-10. Low-angle X-ray reflectivity data for a series of (Cu 25 Å / Fe t_{Fe} Å) x36 multilayers with nominal t_{Fe} ranging from 11 down to 5 Å. The appearance of the first peak from the right upon increasing the thickness of the Fe layer can be interpreted as the structural transition [23]. 27

Figure 1-11. . High-angle X-ray reflectivity data for a series of (Cu 25 Å / Fe t_{Fe} Å) x36 multilayers with nominal t_{Fe} ranging from 11 down to 5 Å. One can see the appearance of the Cu(200) on the structure of Fe upon increasing the thickness of the Fe [23]..... 28

Figure 1-12. Conversion-electron Mössbauer spectra taken at room temperature (vertical bars) and calculated fits (solid lines) for a series of of (Cu 25 Å / Fe t_{Fe} Å) x36 multilayers with nominal t_{Fe} ranging from 11 down to 5 Å. One can see the appearance of the Cu(200) on the structure of Fe upon increasing the thickness of the Fe [23]. 31

Figure 1-13. Unit cells of Fe (a), BCC, and Cu (b), FCC. 34

Figure 2-1. Descartes decomposition of the space into vortices [64]. 39

Figure 2-2. Example of the 2D construction of the Voronoï diagram. The distance from p to p_1 is less than the distance from p to any other points; p' is located at the boundary between p_1 and p_3 40

Figure 2-3. Flowchart to simulate a single layer based on Voronoï diagram. 42

Figure 2-4. Example of a magnetic multilayer system composed of Fe (blue) and Cu (red) layer, prepared with the Voronoï method, used in our study. We have used the free boundary conditions by first choosing a large simulation box, and analyze a reduced box, as shown in the figure. 43

F**igure 2-5.** Flowchart of the biased classical Monte Carlo Metropolis algorithm used in our simulations 58

Figure 2-6. Example of the spins configuration used the Heisenberg model. Left panel shows ferromagnetic arrangement whereas the right panel shows the antiferromagnetic arrangement. 60

Figure 2-7. Flowchart describing the procedure to investigate the magnetic properties..... 61

Figure 2-8. Example of the radial distribution function calculation. The pink atom at the center is taken as reference and atoms in blue are located at the distance r from the atom in pink. 63

Figure 3-1. Atomic representation of the pure structures of (a) Fe (blue) and (b) Cu (red). The structures are obtained by Voronoï construction. 66

Figure 3-2. Radial distribution function (RDF) of pure bulky Fe (a) and Cu (b). The two first planes are also shown for both elements. 66

Figure 3-3. An amorphous system composed of 50% Fe (blue) and 50% Cu (red) before (a) and after (b) simulated annealing. One can see that even outside of the simulation box, atoms form agglomeratess of the same type; thus justifying the capability of our potential to reproduce the different interactions 67

Figure 3-4. RDF of Fe before (a) and after (b) simulated annealing process. The conserved atomic density versus inter-plane distance is shown. One can also notice the absence of a few peaks from (b), which shows the distribution of the pure Fe after the simulated annealing process. 68

Figure 3-5. RDF of Cu before (a) and after (b) simulated annealing process. The conserved atomic density versus inter-plane distance is shown. 69

Figure 3-6. Structure of Fe/Cu (the thicknesses of Fe and Cu layers are 5 and 15 Å, respectively) before (a) and after (b) simulated annealing. One can see the presence of Fe atoms even in the bulk of Cu, due to their reduced size as compared to that of Cu. 69

Figure 3-7. RDF of the bilayer system Fe_5/Cu_{15}. The FCC structure of Cu is conserved (a); the structure of Fe is similar to that of the interface (b-d). One can see that due to the lower thicknesses of both layers, 15 and 5 Å for Cu and Fe respectively, the structure of the bulk Cu is conserved through the system. 70

Figure 3-8. The bilayer $Fe_{15}Cu_5$ system before (a) and after (b) simulated annealing. Cu is completely at the interface due to its low thickness 71

Figure 3-9. RDF of the bilayer system of Fe_{15}/Cu_5. The BCC structure of Fe is conserved (a); the structure of Cu is similar to that of the interface (b-d). One can notice the presence of the first atomic plan of the FCC structure of Cu. This is due to the large atomic radius of Cu as compared to that of Fe. Near the interface, Cu atoms tend to dominate and dictate the FCC structure of Cu. 72

Figure 3-10. RDF of the Fe_{35}/Cu_{35}, when Fe is deposited on Cu, with the same thickness, 35 Å. The FCC structure of Cu is reproduced (a). The structure of Fe (b) is similar to that observed at the interface (c, d). These observations confirm the hypothesis that investigations on bilayer systems may take into account the substrate layer as it may primarily affect the structure of the system. 73

Figure 3-11. Structure of Fe_{35}/Cu_{35} before (a) and after (b) simulated annealing. 74

Figure 3-12. RDF of the Fe_{35}/Cu_{35}, when Cu is deposited on Fe, with the same thickness, 35 Å. The BCC structure of Fe clearly reproduced (a). Although the structure of Cu layer (b) is similar to that of the interface (c, d), the presence of the second peak less pronounced (b) implies the (200) second atomic plane of Fe. Both interfaces, Cu-Fe and Fe-Cu, show the same distribution. 74

Figure 3-13. The trilayer system $Fe_7/Cu_{25}/Fe_7$. The atomic planes of Fe and Cu are shown in blue and red respectively. One can see that the Fe layers are almost consumed by the interfaces Fe-Cu and Cu-Fe. 75

Figure 3-14. RDF of the $Fe_7/Cu_{25}/Fe_7$ system. At a sufficiently large value of the thickness of Cu (a) and lower value of the thickness of Fe (b), the FCC structure of Cu is conserved (a) while the Fe layer copies both FCC and BCC structures for its first two atomic planes and adopts an amorphous structure beyond. The presence of the FCC structure at the interface can be seen even beyond the first atomic planes (c, b). This means that the structure of the largest thickness dominates the system. 76

Figure 3-15. The trilayers system $Fe_{18}/Cu_{25}/Fe_{18}$. The atomic planes of Fe and Cu are shown in blue and red, respectively. One can see the formation of the atomic plane of Fe layers upon increasing its thickness. At the interface, atoms prefer to form agglomerates of the same type, leading to the transition from the amorphous to mixed FCC and BCC structures. 77

Figure 3-16. RDF of the $Fe_{18}/Cu_{25}Fe_{18}$ system. The Cu layer conserves its FCC structure regardless of the Fe layer. In contrast to the bilayer system, increasing the thickness of the Fe layer leads to a smooth transition from a mixture (FCC and BCC) to the BCC structure, as seen in the pure structure of Fe (b). The

interface structures remain dominated by the FCC structure (c, d), although the first is disturbed due to the transition observed in the Fe structure. 78

Figure 3-17. The trilayer $Fe_{25}/Cu_{25}/Fe_{25}$ system. The atomic planes of Fe and Cu are shown in blue and red, respectively. Each layer shows the well-pronounced atomic planes as a result of the formation of the structures similar to that of the bulk..... 79

Figure 3-18. RDF of the $Fe_{25}/Cu_{25}/Fe_{25}$ system. Cu layer remains FCC (a), while the Fe layer shows the presence of the BCC atomic plan through the layer (b). The large atomic radius of Cu can justify the presence of the FCC structure in the Fe layer, a third small peak (b) compared to that of Fe, which dominates the interface. The interface shows a mixture of both FCC and BCC structure (c, d). 80

Figure 3-19. RDF of the $Fe_{34}/Cu_{25}/Fe_{34}$ system. No considerable change is observed either for the Cu layer, FCC (a), Fe layer, BCC (b) distorted at the interface by the presence of the Cu atoms, and both interfaces remain mixed dominated by the FCC structure. 81

Figure 3-20 The trilayers $Fe_{21}/Cu_{6}/Fe_{21}$ system before (a) and after (b) the simulated annealing. The atomic planes of Fe and Cu are shown in blue and red, respectively. One can see the presence of Fe atoms even in the bulk of the Cu layer. Additionally, the atoms of Cu disturb the structure of the Fe layer on multiple planes, thus justifying the less pronounced structure of the Fe layer close to the interface. The interfaces remain dominated by the atoms of Fe, which impose the formation of the BCC structure. 82

Figure 3-21. RDF of the $Fe_{21}/Cu_{6}/Fe_{21}$ system. (a) shows the conserved BCC structure of the Fe layer, although disturbed by the presence of Cu atoms on the first atomic planes. (b) shows the mixed structure (BCC and FCC) of the Cu, where the first peak implies the presence of BCC at the surface of Cu. The less pronounced presence of the BCC structure beyond the first atomic plane could be justified by the large atomic radius of the Cu, which limits the interpenetration of the Cu atoms into the Fe bulk. The interfaces are dominated by the FCC structure, probably due to its high proportion at the interface (c, d)..... 83

Figure 3-22 The trilayer system $Fe_{21}/Cu_{13}/Fe_{21}$ before (a) and after (b) the simulated annealing. The atomic planes of Fe and Cu are shown in blue and red respectively. One can see the formation of the different atomic planes of Cu, while the atoms of the interface tend to interact with atoms of the same type. These observations can help to explain the transition observed in Figure 3-23 84

Figure 3-23. RDF of the $Fe_{21}/Cu_{13}/Fe_{21}$ system. Fe has conserved its BCC structure, less disturbed by the presence of the Cu atoms (a). During the growth process, atoms of Cu will tend to form an agglomerates composed uniquely of Cu atoms, thus limiting the disturbance of the Fe layer at the interface. (b) shows the FCC structure of Cu, while the effect of the transition is seen at the interface (c, d). 84

Figure 3-24. Visualization of the trilayer system $Fe_{21}/Cu_{24}/Fe_{21}$. before (a) and after (b) the simulated annealing. The atomic planes of Fe and Cu are shown in blue and red respectively..... 85

Figure 3-25. RDF of $Fe_{21}/Cu_{24}/Fe_{21}$ system. The disturbance is again seen at the interface of the Fe layer (a), which is still BCC, as the thickness of the Cu continues to grow. (b) shows the FCC structure of the Cu layer. In the presence of a high atomic proportion of Cu at the interface, Fe atoms will tend to copy the FCC

structure of the interface (c, d) for the first atomic planes. This can justify the mixed structure dominated by the FCC of the interface. 86

Figure 3-26. Structure visualization of $Fe_{21}/Cu_{40}/Fe_{21}$ before (a) and after (b) the simulated annealing. Increasing the thickness of Cu may disturb the structure of Fe. 87

Figure 3-27. RDF of $Fe_{21}/Cu_{40}/Fe_{21}$ system. The disturbance of the Fe layer is seen upon a high increase of the Cu layer thickness. The structure of the Fe layer remains BCC but disturbed at the interface (a). (b) show the well-defined structure of the Cu layer as compared to the pure Cu, while the mixed structure of the interface is highly dominated by the FCC structure, second peak from the left (c, d). 87

Figure 3-28. Multilayer system $Fe_{34}/Cu_{25}/Fe_{34}$. (a) and (c) show the magnetization of the Fe layer and the interface, respectively. The magnetic susceptibility if shown by (b) and (d) for the Fe layer and the interface, respectively. The Curie temperature of the system is around 275.9 K. 89

Figure 3-29. Multilayer system $Fe_{25}/Cu_{25}/Fe_{25}$. (a) and (c) show the magnetization of the Fe layer and the interface, respectively. The magnetic susceptibility if shown by (b) and (d) for both the Fe layer and the interface respectively. A slight increase in the Curie temperature of the system is observed, which is around 275.5 K. Additionally, one can observe the disturbance of the magnetization of the interface..... 90

Figure 3-30. Multilayer system $Fe_{18}/Cu_{25}/Fe_{18}$. (a) and (c) show the magnetization of the Fe layer and the interface, respectively. The magnetic susceptibility if shown by (b) and (d) for both the Fe layer and the interface respectively. The disturbance of the magnetization of the interface is seen (c). The Curie temperature of the system remains close to 275.5 K. 91

Figure 3-31. Multilayer system of $Fe_7/Cu_{25}/Fe_7$. (a) and (c) show the relative magnetization of the Fe layer and the interface, respectively. The relative magnetic susceptibility if shown by (b) and (d) for both the Fe layer and the interface, respectively. The high disturbance of the magnetization observed at the interface could be due to the presence of Cu atoms at the interface, which reduces the interlayer coupling between both layers of Fe..... 92

General Introduction

There is a growing body of literature that recognizes the importance of nanomaterials as the root of progress in many areas of materials science. Indeed, as the size of the materials reduces into the nanometer range, they exhibit peculiar and exciting physical, chemical, mechanical, magnetic, and electrical properties compared to their conventional counterparts [1]. These novel properties are not only attractive to the understanding of the fundamental mechanism governing those artificially made materials but also have interesting industrial applications [1-3].

The growing interest in nanomaterials is also paramount to the development of new magnetic materials for a variety of critical technological applications [4, 5]. For this aim, nanomaterials have experienced rapid growth in recent years due to their applications in a wide variety of technological areas such as electronics, catalysis, ceramics, magnetic data storage, structural components[1, 4, 5].

To meet the technological demands in these areas and to follow up with Moore's law, the size of the materials should be reduced to the nanometer scale while its performance increases. For example, the miniaturization of functional electronic devices like transistors, diodes, inductors, and sensors demands the placement or assembly of nanometer-scale components into well-defined structures [6-8]. This new field based on nanomaterials has been named as nanotechnology and has emerged as a new branch of science and technology, which is quite diverse and incorporates areas ranging from microelectronics to molecular biology [1, 4]. The term nanotechnology reminds us of Richard Feynman back to 1959, during his great talk where he stated that "*The principles of Physics, as far as I can see, do not speak against the possibility of maneuvering things atom by atom. It is not an attempt to violate any laws; it is something in principle that can be done, but in practice, it has not been done because we are too big*". The tremendous efforts in advancing science and technology for the last two decades have seen the possibility to economically arrange atoms in most of the ways permitted by physical laws with a reasonably general acceptance[2]. Nanomaterials can be classified into nano-crystalline materials and nanoparticles. The formers are polycrystalline bulk materials devitrified from the previously synthesized amorphous precursor through appropriate thermal treatment with grain sizes in the nanometer range (less than 100 nm). In comparison, the latter refers to ultra-fine dispersive particles with diameters below 100 nm [1,

7]. In other words, nanomaterials describe materials characterized by structural features in the range of $\approx 1 - 100$ nm corresponding typically to $\leq 50 - 5\times10^7$ atoms, respectively. Nanomaterials are interesting from the fundamental point of view due to their tiny size. For example, the increasing surface to volume ratio when the size of the element decreases results in a significant increase of the grain boundaries (i.e., surface energies), especially in the "real" nanometer range (≤ 10 nm). Nanomaterials have a wide range of applications, from medicine to electronics.

Studies of magneto electronics have greatly benefited from the development of nanomaterials. These studies, in the nanomagnetic scale, have attracted considerable attention as they involve a fascinating fundamental science and have numerous industrial applications [1, 4, 5, 9, 10]. Magnetic multilayers are the critical configurations in this field, which allow the utilization of unique micro-magnetic, magneto-optic, and magneto-electronic phenomena which cannot be realized with conventional materials [4, 5]. The wide range of applications of magnetic multilayers has been possible due to the improved understanding of the interface-dominated magnetic phenomena, which is the result of the considerable amount of recent advances in materials synthesis, characterization techniques and methods of advanced measurement facilities on the nanometer scale, theoretical, and computational methods [1, 2].

Magnetic multilayers are artificial materials composed of alternated ferromagnetic and non-magnetic or ferromagnetic and antiferromagnetic layers. They are made of metals or rare earth materials or even a combination of both metals and rare earth [2, 11-13]. Their unusual properties mostly result from the surface and interface effects, including symmetry breaking, and electronic environment (charge transfer and magnetic interactions). Due to both a continuous basic-science interest and still industrial applications, our understanding of the domain configurations, inter-domain boundaries, and, in general, of the micro-magnetics, i.e., the detailed energy balance in a ferromagnetic material, can be considered reasonably profound [1, 13]. However, the underlying mechanisms involved at the interface of ferromagnetic and non-ferromagnetic when the sizes of the layers reduce remains debatable. This mechanism is rarely precise simply because of the complicated behavior of multiphase materials at the interface. This thesis addresses several questions about the observed new properties that might improve our understanding of these new phenomena and the design of new technological applications, using computational methods based on Monte Carlo combined with the Metropolis criterion. For example, the bulk of the magnetic

layer, which is far from the interface, always shows a ferromagnetic crystalline structure, which is not the case at the vicinity of the interface. This layer configuration has the property to be electrically less resistant. At the interface between both layers, an amorphous configuration could be observed at the transition. The amorphous configuration has better magnetic behavior (permeability μ and magnetization M_s) due to the absence of crystalline magnetic anisotropy (symmetry breaking). Also, it has been shown that the magnetic state of a ferromagnetic can affect the electrical transport properties of the materials. For example, the relative orientation of the magnetic moments in magnetic multilayers underlies the phenomenon of giant magnetoresistance [14, 15]. Throughout this thesis, we used metallic magnetic multilayer systems composed of FM/NM/FM, where FM stands for ferromagnetic (here iron Fe), and NM stands for non-magnetic (here copper Cu).

The aim of the thesis is then to investigate in detail the effect of Cu non-magnetic spacer layer on the structural and magnetic properties of the system, and to provide insight into the structural and magnetic properties of interfaces between Fe and Cu. We have systematically varied the different thicknesses of Fe and Cu ($Fe_x/Cu_y/Fe_x$, where x and y represent the thicknesses of Fe and Cu respectively), according to the available experiments, and investigated the impact of the spacer layer on the properties of the system. The behavior of interfaces between both layers is of particular interest as they show properties that deviate considerably from the bulk. Although a few reports are available on the study of FM/NM/FM properties [5, 13, 16-19], the atomistic detail of the mechanism governing the unusual behavior at the interface and its impact on the magnetic properties of the system is still debatable. In the present work, a detailed study of the interface properties, including the change in magnetic properties of the system when varying the thicknesses of different layers were investigated.

The thesis is structured as follows: In the first chapter, we will discuss the importance of the present work in terms of advancing our understanding of the fundamental physics of magnetic multilayer systems and their growing industrial applications. In the second chapter, we shall present the numerical approach to synthesize and to characterize the metallic magnetic multilayer systems. Besides, we introduce the mathematical model used in this work to build the multilayer samples that mimic experimental ones, including the numerical method of characterizing them. Chapter

three covers the essentials of our findings, and we shall compare the results of our simulations to the experimental results.

Chapter 1 Literature Review

1-1. Introduction

Magneto-electronics is undoubtedly one of the most expanding fields in basic research, as well as in industrial applications. Magnetic multilayers are the critical configurations that present phenomena that cannot be realized based on conventional materials. These phenomena range from micro-magnetic, magneto-optic, and magneto-electronic. For quite some time, it has been noticed that magnetic properties at surfaces and interfaces deviate from those of bulk materials [2]. Due to the considerable progress made in the development of techniques suitable for the high-quality deposition of magnetic thin films, the surface and interface-determined properties of magnetic materials have attracted much interest [1, 2]. The reason for this is twofold: On the one hand, it is possible to use magnetic thin film systems to tailor unique properties that cannot be achieved solely by employing bulk materials.

On the other hand, in particular, in the magnetic recording industry, we have, as in the whole information technology, a rigorous trend to further miniaturize essential components. This miniaturization requires thin-film technology as the primary approach for device fabrication. It is thus not surprising that current research in magnetism is concentrated on ultrathin magnetic films to a considerable amount

The high interest in multilayer materials started back a few decades when X-ray spectroscopists, who were interested in the optical properties, attempted to prepare multilayers by combining heavy and light elements to fabricate X-ray mirrors. The poor vacuum conditions significantly limited further investigation of the physical properties. The introduction of high vacuum techniques around 1970 by Esaki in the field of thin-film has seen a considerable jump in the study of nanomaterials, as it allows the fabrication of multilayer systems with controlled thickness in the monolayer scale. This procedure was then used to fabricate the semiconductor super-lattices, such as Gallium-Arsenic/Aluminum-Arsenic, GaAs/AlAs [20].

The same approach was later applied to fabricate multilayer systems composed of metallic elements around 1980 [21]. The introduction of metallic multilayers was motivated by the unusual properties observed at the surface and interface of the magnetic component during its growth. In

this chapter, we will review some essential findings on magnetic multilayer systems, including the discovery of the giant magnetoresistance (GMR), which has considerable technological applications in the domain of electronics, and the giant magneto-impedance, mostly applied in the area of sensors. We will first discuss the origin of the ferromagnetism in different materials, the introduction to some key findings in the field of magnetic multilayers, particularly in systems composed of Fe/Cu/Fe will follow, and we will end this chapter with a conclusion.

1-2. Origin of the ferromagnetism in different materials

Each magnetic material is characterized by its magnetization (M), which is the total magnetization per unit volume; in the presence of intrinsic field H, M is defined by Equation (1.1)

$$M = \chi_m H \tag{1.1}$$

The magnetic flux density B observed within the magnet is the result of the driving force of the externally applied magnetic field H and that resulting from the internal magnetization M. The flux density B is given by Equation (1.2)

$$B = \mu_o (H + M) \tag{1.2}$$

By replacing M from Equation (1.1) into Equation (1.2), we get the relationship between the magnetic flux density, the external magnetic field, and the susceptibility of the material, as shown in Equation (1.3).

$$B = \mu_o H (1 + \chi_m) \tag{1.3}$$

Since $B = \mu H = \mu_o H (1 + \chi_m) = \mu_o (H + M)$, we can write the magnetic permeability as $\mu = \mu_o (1 + \chi_m) = \mu_r \mu_0$, where μ_r is the relative permeability ($\mu_r \sim 1$ for the paramagnetic and diamagnetic, $\mu_r >> 1$ for ferromagnetic materials) and μ_0 the free permeability; χ_m stands for the magnetic susceptibility of the material. Because of quantum effects, χ_m is negative for diamagnetic materials so that $\mu < \mu_0$. Examples of such material are silver, copper, and water. On the other hand, paramagnetic materials, such as aluminum, have slightly positive magnetic susceptibility χ_m

while ferromagnetic materials such as iron (Fe), cobalt (Co), and nickel (Ni) have a substantial magnetic susceptibility (Table 1-1).

Table 1-1. Approximate relative permeability μ/μ_0 of copper, iron, and other common materials used for comparison

Element	Relative permeability	Element	Relative permeability
Bismuth	0.99983	Aluminum	1.00002
Silver	0.99998	Cobalt	250
Lead	0.999983	Nickel	600
Copper	0.999991	Mid steel	2000
Water	0.999991	Iron	5000
Vacuum	1.000000	Mumeltal	100000
Air	1.0000004	Supermalloy	1000000

The sharp difference between ordinary materials with $\mu \cong \mu_0$ and ferromagnetic materials having $\mu \gg \mu_0$ is due to the spontaneous alignment of atomic moments in the same direction, to increase the applied field, reorienting the remaining moments. That is, if the susceptibility of a material is above some threshold, then the atomic magnetic moments spontaneously align over regions of size limited by grain structure or energy considerations, as suggested in Figure 1-1 a.

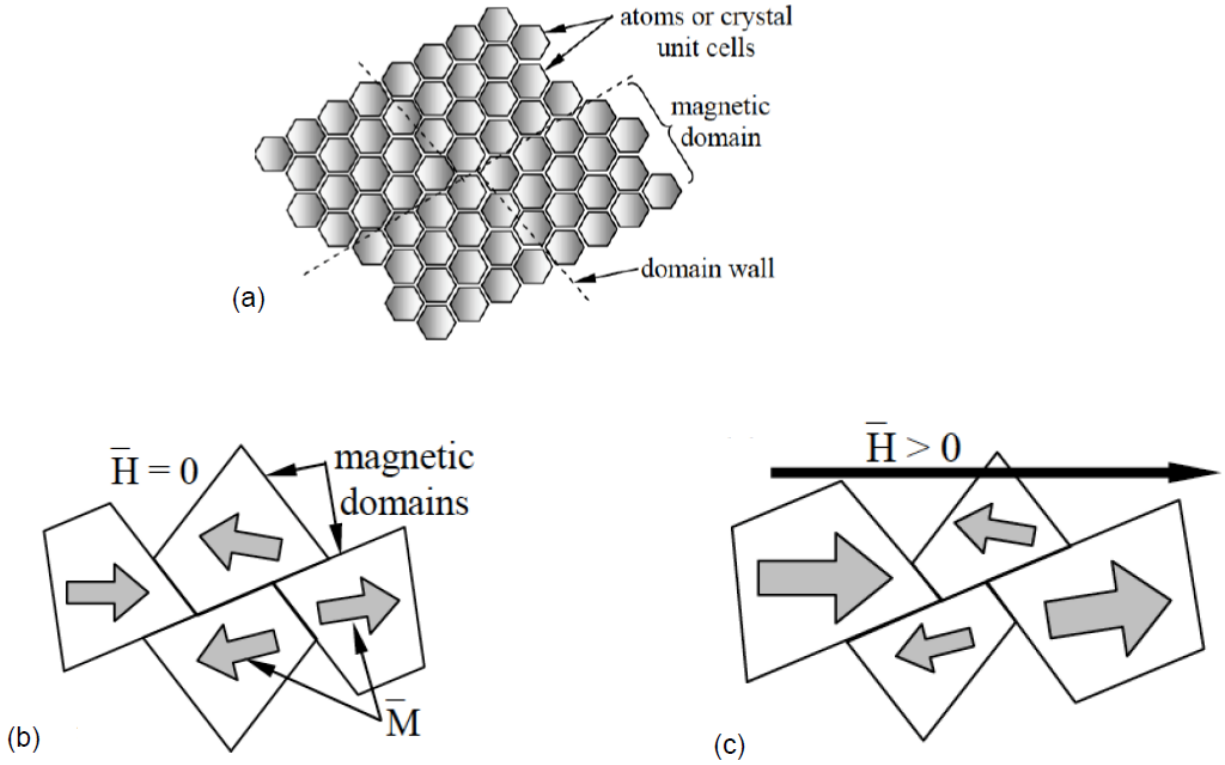

Figure 1-1. Magnetic domains in a ferromagnetic material. (a) shows the rearrangement of the system into domains to minimize the energy of the system; (b) shows the magnetization of different domains in the absence of external magnetic field; (c) shows the orientations of the magnetization in the presence of the external magnetic field. The field is applied in the direction of dominant moments and the rest of the moments will undergo a torsional transformation upon increase of the field.

These regions of nearly perfect alignment are called magnetic domains. These domains are usually quite small (we can think of Neel block) to minimize the stored magnetic energy, μH^2. In this regime, if only energy considerations control domain size, then the size of those domains oriented in the general direction of the applied magnetic field grows as the field increases. In contrast, other domains shrink, as can be seen in Figure 1-1 b and c. Since domain walls cannot easily move across grain walls, the granular structure of the material can be engineered to control magnetic properties (we can start to think about multilayer systems). If the domain walls move smoothly, the magnetic susceptibility is large.

At a sufficiently high magnetic field, all domains will expand to their maximum size and/or rotate in the direction of H. This corresponds to the maximum value of M and magnetic saturation. The resulting typically non-linear behavior of the magnetization curve relating B and H for ferromagnetic materials is shown in Figure 1-2 a. The slope of the B versus H curve is approximately equal to the permeability μ of the material near the origin and μ_0, the permeability of the vacuum, beyond the saturation. If the domains resist the change and dissipate energy when doing so, the hysteresis curve of Figure 1-2 b is observed. The energy dissipated is defined by the enclosed area in the figure as the field H oscillates.

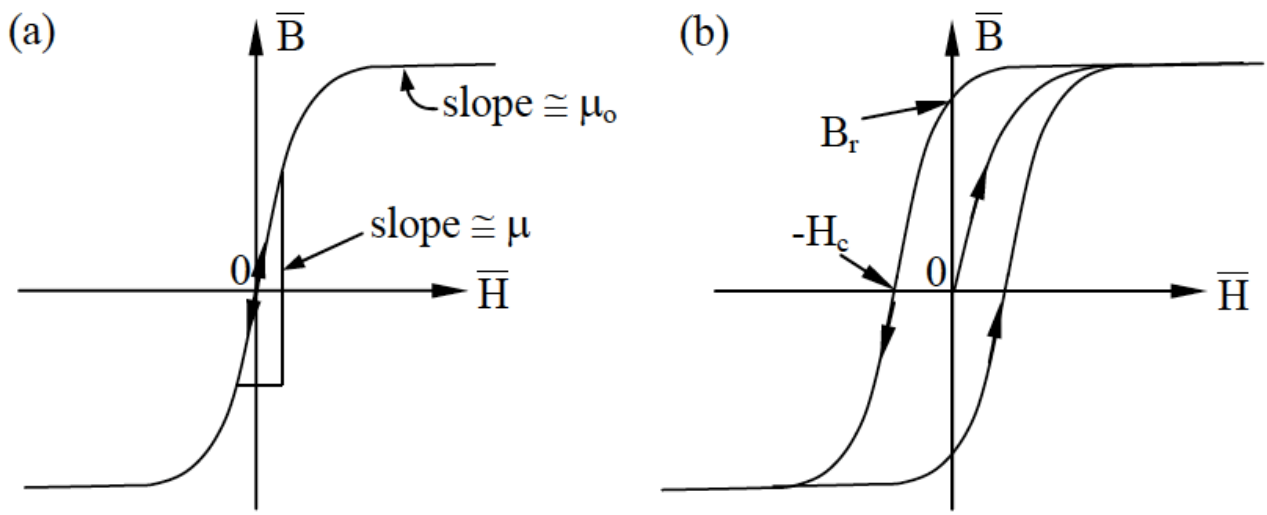

Figure 1-2. Magnetic and hysteresis loop for a ferromagnetic material. (a) show a system with easy magnetization and (b) shows a system with hard magnetization and high dissipated energy defined by the enclosed surface.

Hard magnetic materials have large values of residual flux density Br and magnetic coercive force or coercivity Hc as illustrated in Figure 1-2 b.

1-3. Structural and magnetic properties of thin films and magnetic multilayer systems

Numerous factors are at the origin of the unusual properties of magnetic multilayer systems as compared to the conventional bulk materials. One likely factor is the exchange coupling between thin films of a ferromagnetic layer separated by a non-magnetic or antiferromagnetic layer. The exchange coupling has been used to explain the phenomena called giant magnetoresistance (GMR) [1, 2, 13, 15, 22]. Under suitable circumstances, the exchange-coupled multilayers exhibit a drastic change in their electrical resistance under the influence of varying external field [15] (The resistance decreases considerably when an external magnetic field is applied). Since this was quite surprising for a metallic system, the effect was named the GMR effect. This effect was first observed in Fe/Cr multilayer systems and was later seen in other systems such as Fe/Cu [12, 18, 23, 24]. However, the fundamental physics underlying the interlayer exchange coupling and the GMR effect is still not well understood. For instance, the spacer thickness to which the oscillating coupling or the maximum of GMR is observed remains debatable.

Moreover, the increasing percentage of atoms at the interface with the decrease of the layer thicknesses can make the structural properties of metallic multilayer systems deviate significantly from those of their bulk counterparts [6, 25]. These structural changes have been linked to interesting phenomena used in the industry [1]. In addition to the surface and interface effects, electronic transport through multilayer structures can also affect the properties of magnetic multilayers. Although many techniques have been developed for the preparation and characterization of magnetic multilayers, there are subtle differences among those techniques that can sometimes lead to the misinterpretations of results. For example, various deposition rates and growth temperatures can produce unexpected structural changes in the multilayer system. Furthermore, the multilayer systems such as that composed of Fe and Cu may also experience considerable unwanted interdiffusion at the interface, although they are often chosen for their mutual insolubility [17, 26].

The artificially made magnetic multilayers systems composed of magnetic and magnetic (e.g., iron-rare earth, iron-chromium) or magnetic and non-magnetic (e.g., iron-copper) layers have attracted much attention due to their high transferability to the industrial scale [2]. The still-

growing interest of these systems comes from the fact that they can be carefully manipulated to tailor their properties with their desired effects. Considerable efforts are being made to understand the origin of the observed differences, which is paramount to further modification, as they imply many technological applications, and tremendous results are present in the literature [19, 27-33]. Before we go deep into the topic, let us discuss the history of the magnetic multilayers and the state of the art of its investigations for both research purpose and industrial applications.

Back in 1969, Liebermann and coworkers first observed the unusual properties in ultrathin material during the growth. They concluded that the magnetization of an ultrathin ferromagnetic metal, Fe, Co, or Ni, measured during the film growth is always smaller than the bulk value, and the decrease roughly corresponds to two atoms layers' magnetization. Therefore, they claimed that one surface layer in the ferromagnetic metal loses its magnetic moment independently of the total thickness, and it is the "dead layer" [34]. These findings became of high interest to the experimental and theoretical physicists, and many investigations on nanomagnetic materials have emerged.

Shinjo et al. later proved the non-existence of the dead layer during their Mössbauer study [35]. They deposited ^{57}Co source atoms on the surface of Fe and Co, by electrodeposition and the Mössbauer source spectra were measured. The observed spectra from the ferromagnetic metal surface showed magnetically split patterns for both Fe and Co [35]. Additionally, they showed that the surface atoms have bulk-like magnetic moments, although the hyperfine fields are fairly distributed, and the average value is a little smaller than the bulk.

1-3.1 Influence of the structure of each layer on the magnetic properties

How different thicknesses of layers forming the magnetic multilayer systems affect the magnetism of the system remains a subject of intense debate. Answering this preoccupation is paramount to deriving the critical values of different thicknesses that allow each layer to adopt the structure similar to the bulky material. Modern devices have the magnetic element with much-reduced size, varying from nanometer to Angstrom. It implies that magnetic multilayer systems with reduced dimensionalities are of high interest for many technological applications.

For this aim, researchers have been working to improve the dimensionalities of magnetic multilayer systems, while keeping at least the properties observed in the bulk materials. Investigations performed on different samples with different Fe layer thicknesses have shown a similar trend [36]. Initially, Fe atoms deposited on non-magnetic substrate form fractional monolayers until there are sufficient Fe atoms to cover the whole surface. The crystal structure is regarded as amorphous but there is a stable ferromagnetic order in the Fe layer, which has an easy direction perpendicular to the film plane and the Curie temperature is relatively low. As the thickness of the deposited Fe layer approaches 0.8 nm (8 Å), the magnetization direction gradually turns toward the film plane. A drastic change in the structure from amorphous to crystalline BCC occurs between 0.8 and 1.5 nm (15 Å). The Curie temperature increases to a higher temperature greater than room temperature in association with the crystallographic structure transformation [36].

The results from the spectra for 15Å Fe layers revealed that they were entirely ferromagnetic and the observed hyperfine field value was the same as the pure bulk Fe value. The results further showed that the BCC Fe layer did not include impurities from the non-magnetic substrate. If the sample included a significant amount of impurities, the amorphous structure would be stable and the transformation to a BCC structure would not take place. We notice that the amorphous phase of Fe alloys in bulk form can be obtained by mixing some non-magnetic metalloid elements (such as B, C, N, etc.). However, the amorphous form of pure Fe is known to be unstable. This means that the interdiffusion in the ultrathin amorphous Fe layer during film growth was negligible. It can, therefore be concluded that the structure of an ultrathin Fe layer deposited on a non-magnetic substrate is amorphous, as long as the thickness remains below a critical value, which lies between 0.8 and 1.5 nm. If the thickness exceeds the critical value, a sudden transformation to BCC takes place [37].

An example of Mössbauer characterization (which is one of the most used method) of a multilayer system is shown in Figure 1-3. One can see that even when the Fe thickness is as low as 10 Å, the system still exhibits the magnetic properties as evidenced by the different spectra from the Mössbauer measurements [37].

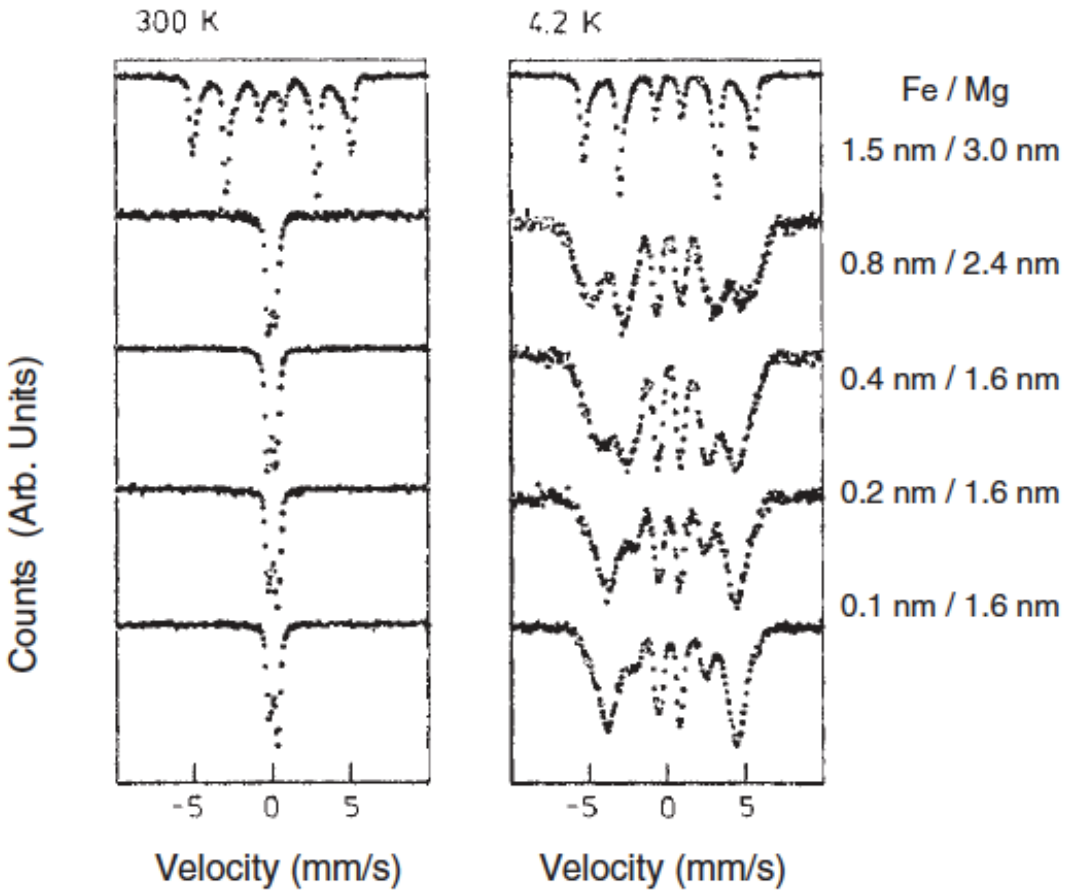

Figure 1-3. Mössbauer absorption spectra at 300K and 4K for Fe/Mg multilayers with various Fe layer thicknesses. The thickness of Fe is varied and the results are compared to that of bulk Fe, as shown above. When the thickness of Fe is as low as 10 Å, the behavior remains similar to that of bulk Fe [37].

1-3.2 Giant magnetoresistance effect observed in magnetic multilayer systems

Magnetoresistance (MR) is the change observed in the ferromagnetic materials in the presence of an external magnetic field due to the alignment of the magnetic moments to the direction of the applied field. In magnetic multilayer systems, the thickness of the non-magnetic interlayer may lead to the ferromagnetic or antiferromagnetic coupling between the adjacent magnetic layers. The MR is observed when the relative orientation of the magnetizations in adjacent layers change upon an externally-applied magnetic field. The most significant effect occurs when an antiferromagnetic

arrangement is changed into a ferromagnetic arrangement, for example, due to an applied field. The antiferromagnetic interlayer exchange can provide an antiferromagnetic arrangement between two consecutive ferromagnetic layers. It is worth noting that these observations are present in all ferromagnetic materials. However, in the magnetic multilayer configuration, the change was increased by many degrees of magnitude and it was termed giant magnetoresistance. The GMR effect was discovered conjointly by P. Grünberg and A. Fert around 1986 - 1989, both groups working independently on the Fe/Cr/Fe multilayer systems. Their efforts in the field of magnetics multilayers were recognized with the award of the Nobel Prize in Physics in 2007.

P. Grünberg et al. during their investigation of the magnetic properties of the Fe/Cr/Fe measured the magnetic behaviors of the system by changing the thickness of the Cr spacer layers. They found a strong antiferromagnetic exchange interaction between the two Fe layers, separated by a Cr layer when the Cr layer thickness was around 1 nm. The Fe layers' magnetizations were spontaneously oriented antiparallel to each other and aligned parallel if a sizeable external field was applied. They further measured the magnetoresistance of Fe/Cr/Fe films and found that the resistance when the two magnetizations were antiparallel was larger than when they were parallel. This result indicates that the conductance is affected by the magnetic spin structure, which is the physical principle of the GMR effect. However, the observed MR ratio in the three-layer system, (about 1.5%), was not large enough to draw a significant impact [22].

Around the same period, in 1988, A. Fert and coworkers were also investigating the magnetic properties of Fe/Cr/Fe. They were interested in the role of interlayer coupling using samples with a multilayered structure. They have prepared epitaxial Fe/Cr multilayers with various Cr layer thicknesses and measured the magnetic properties including the magnetoresistance. Figure 1-4 summarizes their findings. They observed surprising results for the resistance measurements in the presence of external fields. For the [Fe (3 nm)/Cr (0.9 nm)]x60 sample for instance, the resistance at 4.2K decreased to almost a half at the saturation field. The MR ratio was nearly 20% even at room temperature, which is strikingly significant value in comparison with the conventional MR changes. They termed the observed change "giant magnetoresistance, GMR" [14]. Ferromagnetic alloys have been shown to exhibit the anisotropic magnetoresistance (AMR), but the MR ratio is not more than a few percent at room temperature. The results of Fert's GMR experiment confirmed

the existence of a robust antiferromagnetic interlayer coupling between Fe layers separated by a Cr layer [14].

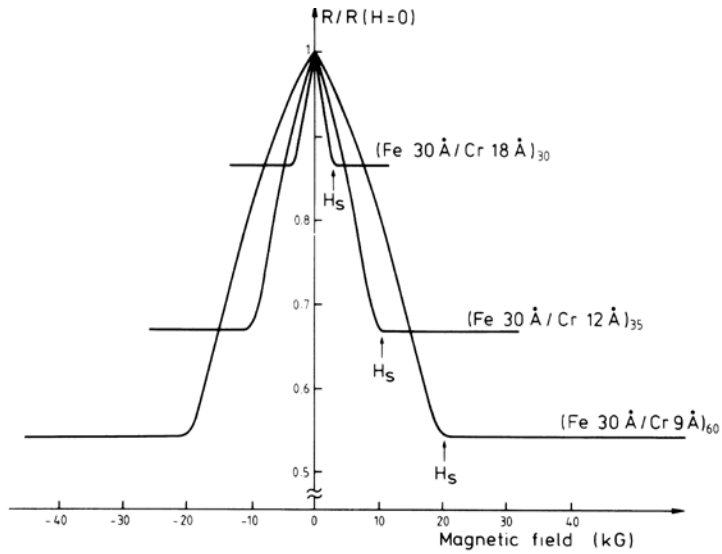

Figure 1-4. Magnetoresistance at 4.2K of three Fe/Cr/Fe superlattices as a function of the applied field. The current and the applied field are along the (110) in the plane of the layers [14].

The observed GMR was explained by considering the spin-dependent scattering of conduction electrons. The scattering probability for conduction electrons at the interface of the ferromagnetic layer should depend on the spin direction, up or down. For instance, an up-spin electron can penetrate without scattering from a Cr layer into a Fe layer having up-spin magnetization, while a down-spin electron is scattered. If the Fe layers have an antiparallel magnetic structure, both up- and down-spin electrons soon meet a Fe layer having a magnetization in the opposite direction (within two Fe layers' distance), so the probability of scattering is high for both types of electrons. On the other hand, if all the Fe layers have parallel magnetizations, down-spin electrons are scattered at every Fe layer whereas up-spin electrons can move across a long distance without scattering. In other words, the mean-free-path of up-spin electrons can be considerably long, while that of down-spin electrons must be very short. The total conductance of the system is the sum of conductance due to up- and down-spin electrons. Because of the long mean free path of up spin electrons, the total resistance is much smaller in the parallel magnetization state than in the antiparallel state [14, 31, 38-40].

The discovery of the GMR effect raised two key issues: interlayer coupling and spin-dependent scattering. Also, for the Fe/Cr/Fe sandwich system, the existence of antiferromagnetic interlayer coupling was reported for Fe/Cu, Co/Cu multilayers and many other systems [12, 23, 41]. If the interlayer coupling is antiferromagnetic, the GMR effect is almost always observed. That is, the resistance in the antiferromagnetic state is more significant than that in the ferromagnetic state. In a study of Co/Cu multilayers with various Cu layer thicknesses, a fantastic result was obtained: the interlayer coupling strength across the Cu layer oscillated with the variation in the Cu layer thickness [42]. Since the antiferromagnetic coupling causes MR effect, the observed MR ratio showed a periodic change as a function of the Cu layer thickness. In other words, MR measurements can be used to verify that the sign of interlayer coupling is negative. Parkin et al. prepared multilayers combining Co and various non-magnetic metals and found that the oscillation of interlayer coupling occurs rather generally with a wavelength of 10–15 Å[43].

The GMR effect is caused by the change in the magnetic structure between antiparallel and parallel alignments. In the case of Fe/Cr and also Co/Cu multilayers, the antiparallel configuration that originates from the antiferromagnetic interlayer exchange coupling is converted into a ferromagnetic configuration by an externally applied magnetic field. The magnitude of the external field necessary for this conversion depends on the strength of the interlayer coupling. Because of the strong interlayer coupling, the magnetic field required to induce the MR effect in Fe/Cr multilayers is significantly large (about 2T). The coupling of the Co/Cu system is smaller. However, the saturation field is still too high for the MR effect to be exploited in technological applications such as magnetic recording sensors.

The technological application of GMR effect was first realized as magnetic recording heads by using non-coupled sandwich films with two magnetic components, such as [NiFe (15 nm)/Cu (2.6 nm)/ FeNi (15 nm)/FeMn (10 nm)], by IBM group [44]. An antiferromagnetic FeMn layer is attached to one of the NiFe layers to increase the coercive force, while the other NiFe layer behaves freely as a soft magnet. These magnetic layers are called the “pinned layer” and the “free layer”, respectively. Although the MR ratio of the spin-valve system is not large, satisfactorily high magnetoresistance sensitivity was achieved.

Concerning enhancement of the MR ratio, the next breakthrough was obtained in the studies of tunneling magnetoresistance, TMR [45, 46]. In TMR systems, the non-magnetic metal spacer layer in a non-coupled GMR system was replaced by an insulator spacer layer (i.e., tunneling barrier). In 1996, a MR ratio of about 18% at 300K was reported. In 2004, using MgO as the material for the tunneling barrier, a MR ratio of more than 100% was achieved [47, 48].

In recent computers, the capacity of magnetic recording has been dramatically advanced with the adoption of a perpendicular magnetic recording method invented by Iwasaki [49]. To analyze information from magnetic recording with extremely high density, read-out heads are required to have enough sensitivity for very small field variation. Magneto-resistive sensors using the non-coupled GMR principle (i.e., GMR head and TMR head) fulfill this requirement and are currently being used in commercial computers.

GMR can be used for the detection of magnetic fields. However, the range of applications of such field sensors is surprisingly extensive. They can be utilized to read information from tapes, hard disks, floppies, magnetic strips in electronic devices, and computers. Furthermore, they can be employed for sensing the position and/or the speed of moving parts. The moving part for this purpose has to be equipped with a small permanent magnet or a magnetic strip. Using a strip yields the possibility to store further information if required. A control of moving parts, for example, is of interest at many places in automobiles (e.g., ABS), in robotics, assembly lines, etc. Sensors based on GMR are not only very sensitive but can also be made very small. The field of magnetism of surface and interface is relatively new in physics, and critical technological applications are still to come. Further development of magnetic multilayer studies could make use of perpendicularly magnetized films (e.g., Co/Pt multilayers) as recording media materials and magnetic sensors.

1-4. Structural and magnetic properties of thin films and magnetic multilayers Fe/Cu/Fe

Although multilayer systems composed of Fe/Cr/Fe present high variation of the resistance (magnetoresistance), it is worth noting that the non-magnetic interlayer Cr shows antiferromagnetic ordering at room temperature. Therefore, it would require higher external magnetic field to return the magnetic moments of the ferromagnetic Fe at the interface between Fe and Cr. For this reason, other metals are often used as the interlayer spacers such as Cu.

Many studies have been conducted by using the system Fe/Cu/Fe to investigate the effect of the spacer layer on the magnetic properties of the system such as the GMR. By varying the thickness of the spacer Cu from 4 to 60 Å, Petroff and coworkers [41] have observed high variation of the magnetoresistance ratio at the Cu's thickness between 10 and 20 Å. The samples were prepared using the sputtering technique. Interestingly, although the oscillation peaks in the Fe/Cu/Fe and Co/Cu/Co [42] systems occur at the same thickness of Cu, both multilayer systems have completely opposite phases. Our hypothesis is that the observed opposite phases could be due to the structural change, since Cu and Fe crystallize in the same cubic system whereas Cu and Co (hexagonal close-packed, hcp) do not. This range coincided with that of Cr when similar study was performed on the Fe/Cr/Fe [14] system. Therefore, it would be interesting to investigate the structural changes around these values during our simulations.

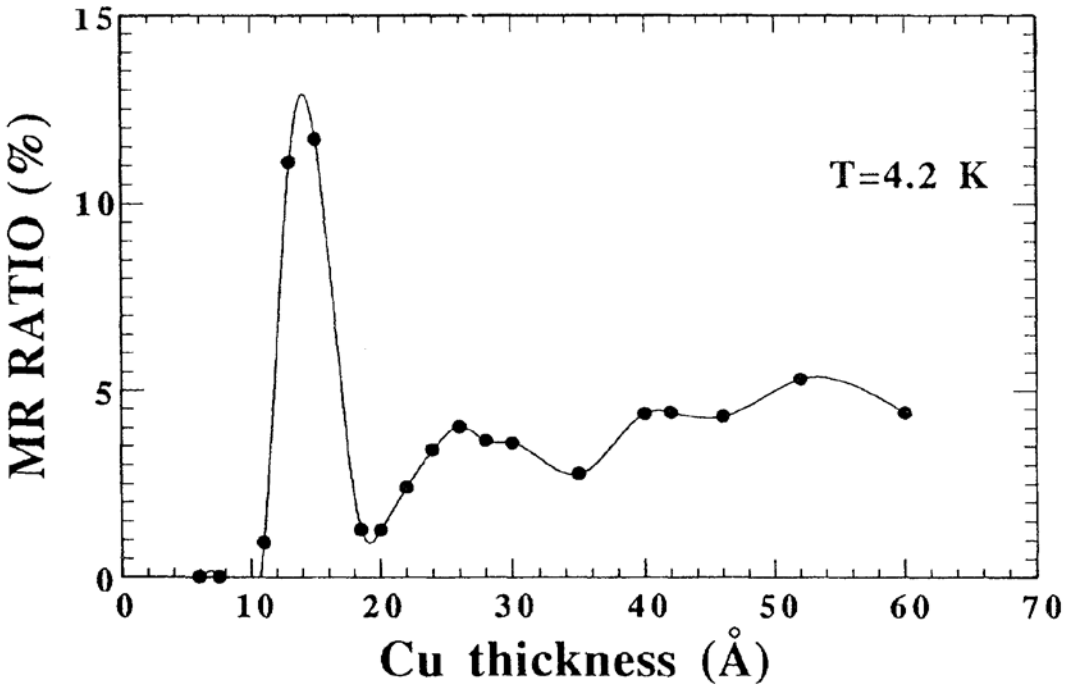

Figure 1-5. Variation of the magnetoresistance ratio as a function of the thickness of the copper. The thickness of the Fe is kept at 15 Å and that of Cu is varied from 4 to 60 Å [41].

Another interesting results on the Fe/Cu/Fe multilayers came from the investigations of Mardani et al. [5], where they used the evaporation technique to fabricate the multilayers Fe/Cu/Fe. Using the X-ray (see Figure 1-6) diffraction technique to characterize the structural changes in the system, they showed that the Cu layer crystallizes in BCC structure, which is surprising since Cu crystallizes in a FCC structure. These results show that by appropriately choosing the thickness of the spacer layer, we would not only modulate the structure of the system, but also the magnetic properties of the adjacent ferromagnetic layers as well as the overall properties of the system.

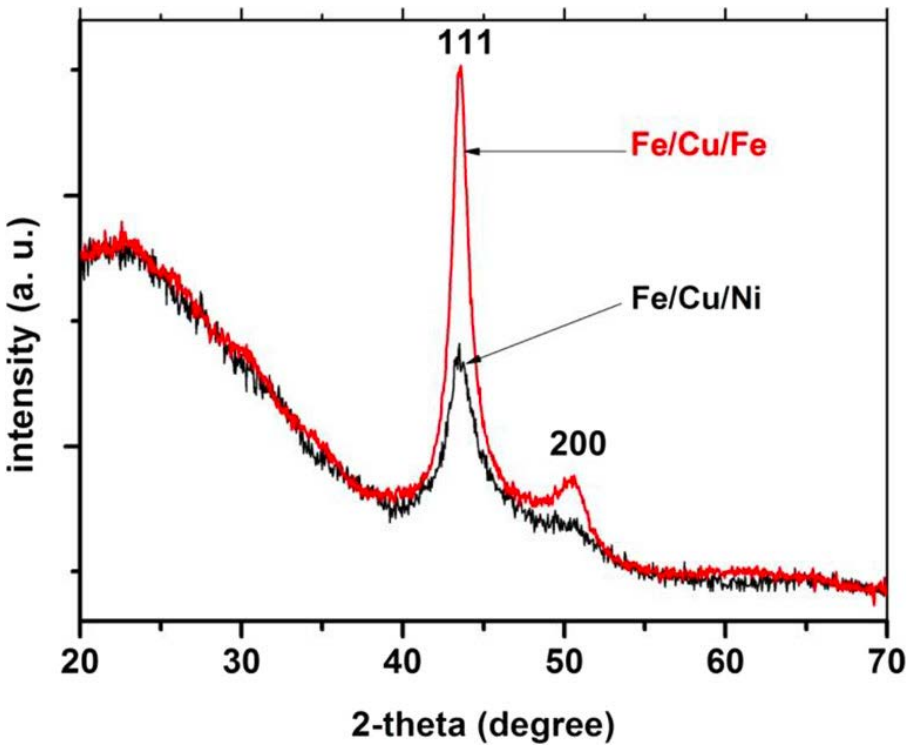

Figure 1-6. Structural changes observed in the multilayer systems Fe/Cu/Fe and Fe/Cu/Ni [5].

Magnetic multilayer systems composed of Fe and Cu are particularly attractive for many reasons including the non-solubility of Fe and Cu in nature, the availability of both elements for the smooth technological transfer, the fact that ɣ-Fe can be stabilized down to low temperature either as small Fe precipitates in a Cu matrix or thin epitaxial Fe films on a Cu buffer layer, among others [41, 50-54]. Epitaxial Cu/Fe multilayers are possible due to the similarity of their lattice constants Cu ~ 3.615 Å at 295 K and ɣ-Fe ~ 3.588 Å at 293 K, extrapolated from bulk ɣ-Fe data above 1185 K,

or 3.5757 Å at 80 K, measure for ɣ-Fe precipitates in Cu. It has been shown that Fe undergoes unusual structural changes, correlated with its magnetic behavior for epitaxial growth of Fe by evaporation onto Cu. Furthermore, several groups have suggested that the room temperature growth of Fe on Cu (100) leads to three distinct phases:

1- ferromagnetic FCT (face-centered tetragonal) structure for films with less than five monolayers;
2- an antiferromagnetic bulk FCC structure with a ferromagnetically ordered surface layer for films between 5 and 11 monolayers; and
3- A ferromagnetic BCC structure for films thicker than 13 monolayers. It has to be noticed here that most of the works were done on bilayer systems with Fe films grown by evaporation on a Cu substrate [51].

Numerous studies have also shown the dependency of the structural and magnetic properties on the layer thicknesses. For instance, Cheng et al. [55] during their work on magnetron-sputtered Fe/Cu multilayers using extended X-ray absorption fine structure spectroscopy suggested that the crystal structure of Fe changes from distorted bcc to FCC Fe with decreasing Fe layer thickness. They found the FCC sample to be ferromagnetic with a reduced Curie temperature. Pankhurst et al. [56] on Mössbauer's study of evaporated Fe/Cu multilayers showed that samples with Fe thicknesses of ~5 Å have roughly equal quantities of ferromagnetic BCC Fe and antiferromagnetic FCC Fe.

The additional complications introduced by the growth of the multilayer samples can make the study of the structural dependence of the magnetic properties even more complicated. For instance, the non-similarity between the two interfaces Fe/Cu and Cu/Fe has to be considered; also, the structural imperfections can lead to the formation of an island structure with dislocated sub-multilayers for ultrathin Fe layers. This may produce a composite granular solid which consists of nanometer-sized Fe grains embedded in the Cu medium and may exhibit superparamagnetic behavior [13].

1-5. Experimental methods of preparation and characterization of magnetic multilayer systems

1-5.1 Synthesis of nanomaterial.

Nanotechnology has grown at a tremendous rate for the past three decades, and recent advances in nanostructured materials and nanodevices have opened up new opportunities in a variety of applications, ranging from information and communication technology to healthcare and medicine. The two possible methods of fabrication, the top-down and bottom-up approaches, widely used to fabricate the nanomaterial systems will be discussed here, covering the merits and drawbacks of each approach. As an example of a top-down procedure, the fabrication of electronic integrated circuits. The foreseen limitations of the procedure could be related to the further miniaturization. The bottom-up approach, through self-assembly and supramolecular chemistry, provides a new exciting alternative route either combined with the top-down approach or on its own [57].

The top-down approach starts from a large piece and subsequently uses more delicate and finer tools for creating correspondingly smaller structures (Figure 1-7.a). In other words, the nanomaterial system is obtained by reducing the size of the bulk materials. Top-down routes are included in the typical solid-state processing of the materials. This route is based on the bulk material and makes it smaller, thus breaking up larger particles by the use of physical processes like crushing, milling or grinding. Usually this route is not suitable for preparing uniformly shaped materials, and it is challenging to realize tiny particles even with high energy consumption. The biggest problem with the top-down approach is the imperfection of the surface structure. Such imperfection would have a significant impact on the physical properties and surface chemistry of nanostructures and nanomaterials [58, 59]. It is well known that the conventional top-down technique can cause significant crystallographic damage to the processed patterns (Figure 1-7.b).

In the bottom-up approach, smaller components of atomic or molecular dimensions self-assemble together, according to a natural physical principle or an externally applied driving force, to give rise to more substantial and more organized systems (Figure 1-7.a). This approach refers to the build-up of material from the bottom: atom-by-atom, molecule-by-molecule or cluster-by-cluster. This route is more often used for preparing most of the nano-scale materials with the ability to generate a uniform size, shape and distribution. It effectively covers chemical synthesis and precisely controlled the reaction to inhibit further particle growth. Although the bottom-up

approach is nothing new, it plays an essential role in the fabrication and processing of nanostructures and nanomaterials (Figure 1-7.c) [60].

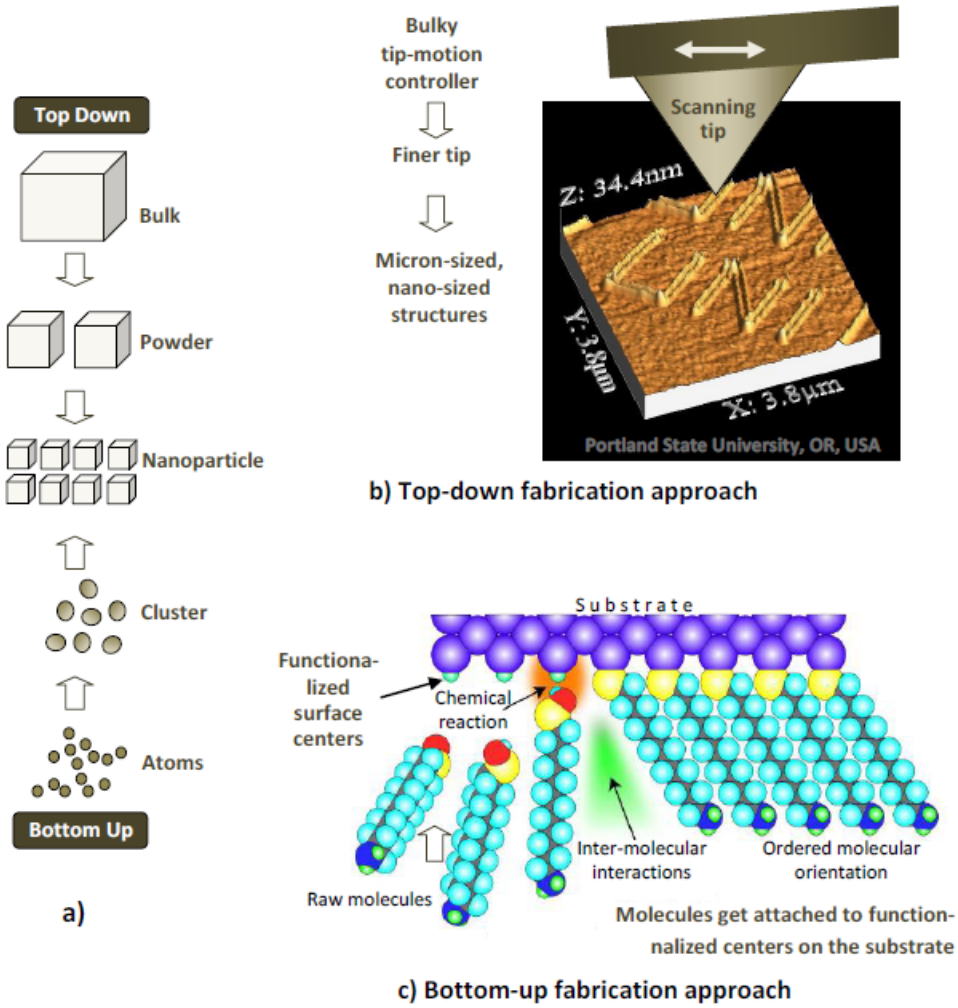

Figure 1-7. a) Schematic representation of the formation of nanostructures via the top-down and bottom-up approaches. b) A tapered probe, manipulated by a macroscopic machine, allows "writing" small features by scratching the probe apex on a soft polymer surface; c) Example of the self-assembling set to occur on previously chemically-functionalized surfaces; chemisorption happens due to interactions between adsorbing molecules and specific sites on the substrate. The resulting nano-electronics material emerges with much more useful functions when proper shapes and microstructures are provided [60].

The future of both methods of fabrication of nanomaterials is predicted in Figure 1-8, where one can see the state of the art of the utilization of each approach. Top-down is mostly suitable for

large systems in the order of micro-meter while using bottom-up, it is possible to obtain systems in the order of Angstrom.

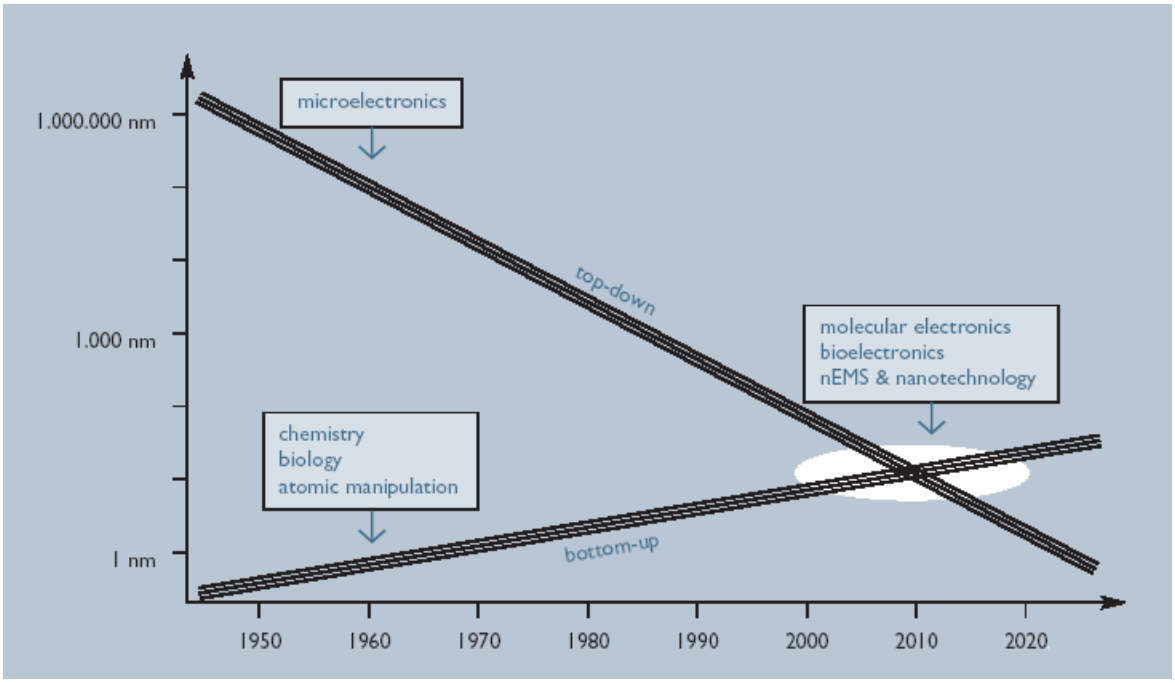

Figure 1-8. Future of the top-down and bottom-up approaches [59]

1-5.2 Experimental approach to fabricate the multilayers Fe/Cu/Fe.

Progress in nanomaterials is closely coupled to the progress in the development of tools being suitable to directly observe phenomena in real space at high resolution. While for basic research it is only important that suitable methods somewhere exist, it is of particular importance for concentrated applied research that methods exist which can be widely employed locally at many places.

Various experimental techniques have been used to fabricate the multilayer systems. These techniques are based on the following general approaches: chemical vapor deposition (CVD), the physical vapor deposition (PVD), and the mechanical annealing.

Depending on the type of study, the quality of samples, and the available funding, one can choose the PVD, CVD, or the mechanical annealing approach. Mechanical annealing approach is based

on top-down model, thus, the size and the quality of the final samples may not be accurate. Instead, the experimental set-up is easy and rapid, the cost is relatively low as compared to the PVD and CVD approaches.

PVD and CVD are all based on bottom-up model. Comparatively to the CVD approach, PVD requires low temperature, the cost is relatively low, samples are non-uniform, the deposition rate is high, and the target must be tuned. A schematic diagram of the PVD experiment is shown in Figure 1-9.

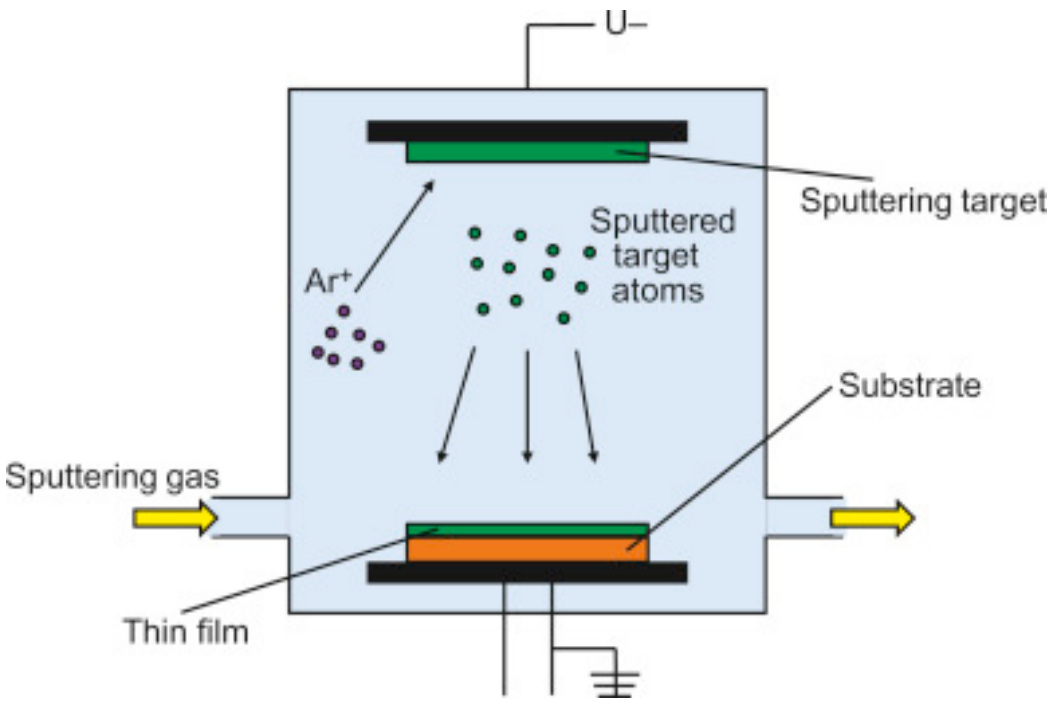

Figure 1-9. Principle of fabrication of thin films and multilayers using the physical vapor deposition (PVD).

As an example of the fabrication of the multilayer Fe/Cu, Lee and coworkers use the dc magnetron sputtering onto silicon subtract technique as described below: They prepared a series of Cu/Fe with the nominal individual layer thicknesses ranging from 25 down to 5 Å and with the total number of bilayers between 12 and 36. The pressure at the base before each deposition was less than $2x10^{-7}$ Torr. The deposition rates for Cu and Fe were determined by low-angle X-ray reflectivity measurements on single layer films and found to be 2.1 and 1.2 Å/s, respectively. The

samples were prepared at room temperature to minimize interdiffusion of Cu and Fe, and capped with 15 Å of Cu to reduce oxidation effects [23].

1-5.3 Characterization of the multilayer systems Fe/Cu/Fe

There are numerous methods to characterize the experimentally obtained multilayer systems. Among these methods of characterization, X-ray crystallography and Mössbauer spectroscopy are widely used.

X-ray crystallography is one of the most widely used techniques by the experimentalists to determine the atomic and molecular structure of a crystal, in which the crystalline structure causes a beam of incident X-rays to diffract into many specific directions. By measuring the intensities of these diffracted beams, the density of electrons within the crystal can be obtained. From this electron density, the mean positions of the atoms in the crystal can be determined, including their chemical bonds, their crystallographic disorder, etc. X-ray crystallography is complemented by various other techniques to obtain the structural detailed of the system. These include fiber diffraction, powder diffraction, or the small-angle X-ray scattering (XAXS). For thin film systems methods such as electron crystallography, low-angle X-ray reflectivity, high angle X-ray diffraction, etc. Lee et al. have used the low-angle X-ray reflectivity and high angle X-ray diffraction to characterize the multilayer systems Fe/Cu with variable thickness of the Fe layer [23]. Their sample structures were characterized by low and high angle X-ray diffraction (XRD) using Cu *K* radiation with the scattering vector perpendicular to the film surface (see Figure 1-10 and Figure 1-11).

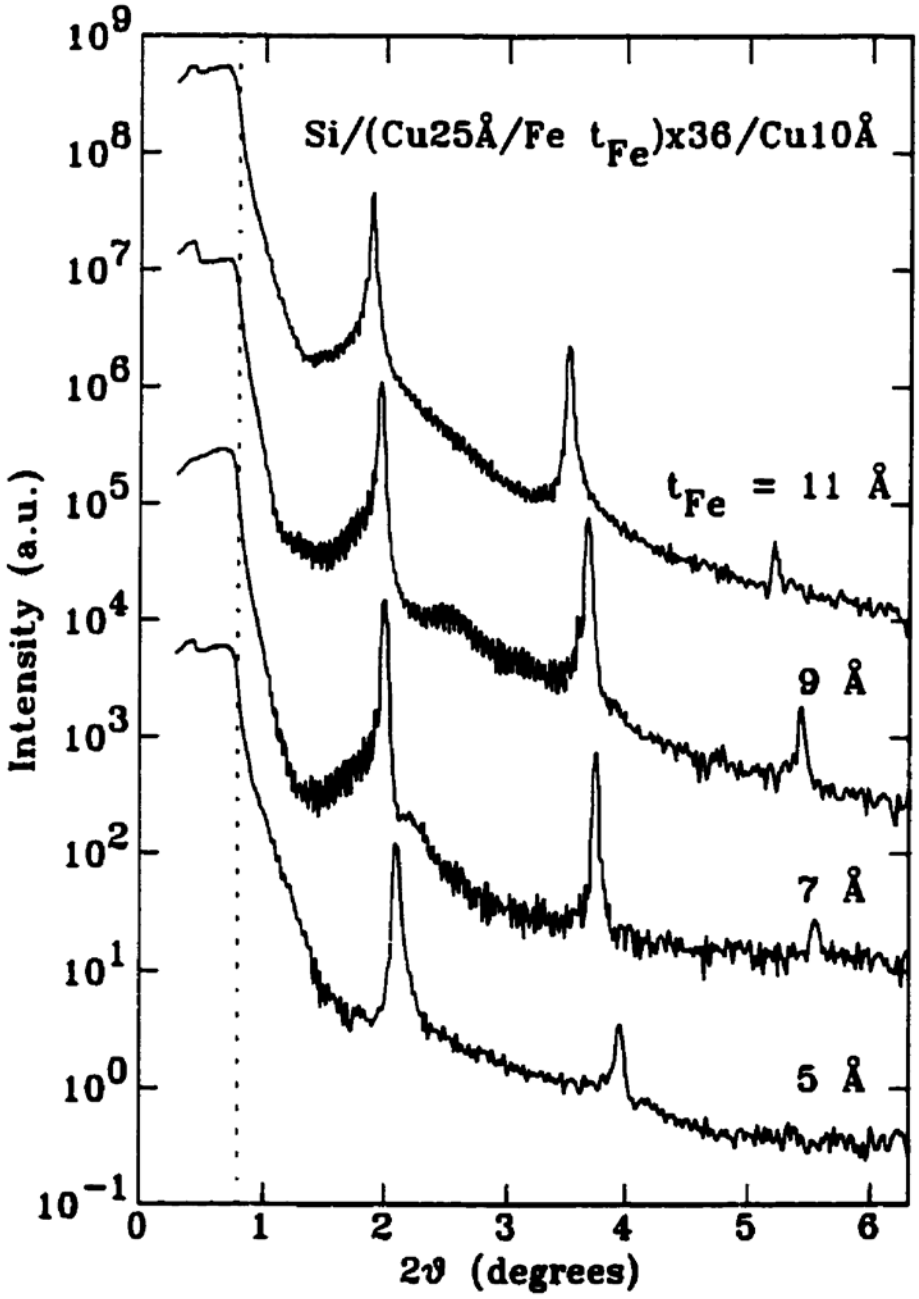

Figure 1-10. Low-angle X-ray reflectivity data for a series of (Cu 25 Å / Fe t_{Fe} Å) x36 multilayers with nominal t_{Fe} ranging from 11 down to 5 Å. The appearance of the first peak from the right upon increasing the thickness of the Fe layer can be interpreted as the structural transition [23].

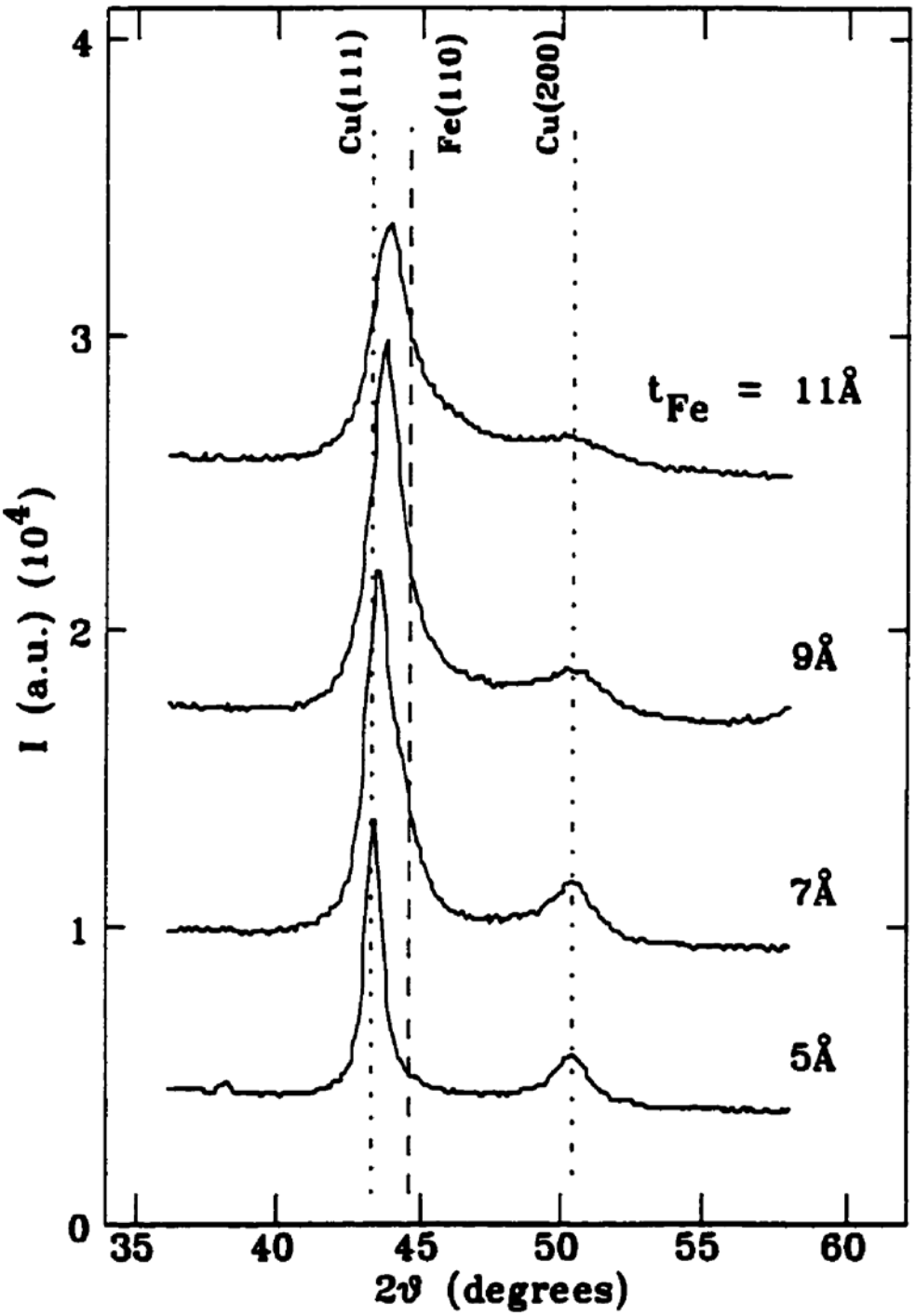

Figure 1-11. . High-angle X-ray reflectivity data for a series of (Cu 25 Å / Fe t_{Fe} Å) x36 multilayers with nominal t_{Fe} ranging from 11 down to 5 Å. One can see the appearance of the Cu(200) on the structure of Fe upon increasing the thickness of the Fe [23].

Another highly used method of characterization of the multilayer systems is that of the Mössbauer spectroscopy. The Mössbauer effect was discovered in 1957 by Mössbauer [61] and involved the recoilless emission of a gamma-ray (γ-ray) by an excited nucleus with subsequent recoilless absorption by another nucleus. Mössbauer spectroscopy has found numerous applications in physics, chemistry, and biology, and one notable early success was the measurement of the gravitational redshift [62]. This spectroscopic technique continues to make significant contributions, such as 2004-2005's analysis of soil on the surface of Mars [63], with spectra collected in situ. Rudolf Mössbauer was awarded the 1961 Nobel Prize of Physics for his work. Since then, numerous experimental investigations on magnetic multilayers have taken place exploiting the properties of ^{57}Fe.

Mössbauer spectroscopy is a prominent tool to study the properties of magnetic materials, exploiting the fact that ^{57}Fe is the most convenient nucleus for Mössbauer measurements [63]. During the magnetism investigation, the most crucial information obtained from the Mössbauer spectra is the hyperfine fields, which are magnetic field acting on the nuclei and are closely related to the local magnetic moment of 3d electron spins. The Mössbauer spectra for ^{57}Fe in magnetically ordered and have six-line patterns, and the hyperfine field is estimated from the magnitude of the six-line splitting. In contrast, paramagnetic and diamagnetic materials show single unresolved lines, so a magnetically split spectrum is a reliable evidence of the existence of magnetic order [21, 61, 63].

The Mössbauer effect occurs in a nucleus when the energy difference between its ground and excited states is sufficiently small [63]. ^{57}Fe is one of the stable isotopes included in natural Fe, but the natural abundance is only about 2%. Natural Fe is composed mostly of ^{56}Fe, which is unrelated to the Mössbauer effect. Therefore, to obtain Mössbauer absorption spectra from a sample containing natural Fe, the Fe concentration must be significantly large. If a sample can be enriched in the isotope ^{57}Fe, the necessary concentration of Fe in the sample is considerably reduced. A designed sample for a specific research purpose can be synthesized by combining pure ^{57}Fe and pure ^{56}Fe isotopes. As will be mentioned shortly, depth-selectively enriched multilayers are typical examples of artificially designed samples. The potential of the Mössbauer spectroscopy as a tool for materials research is remarkably enhanced if ^{57}Fe isotope can be utilized. Isotopes

enriched in ^{57}Fe and also ^{56}Fe, up to nearly 100%, can be purchased commercially, but they are very costly [61, 63].

The procedure for preparing interface-selectively enriched samples is as follows. In the UHV atmosphere, a pure ^{56}Fe layer with sufficient thickness is deposited on an appropriate substrate. A Mössbauer probing layer of ^{57}Fe, a few atomic layers thick, is then deposited on the ^{56}Fe layer. Finally, the surface is covered by a non-magnetic material, such as V, Cu, Ag, Sb, or MgO. Although the prepared sample is sufficiently thick to exhibit bulk magnetic properties, the ^{57}Fe probes are located only at the interface region of the Fe film. Therefore, the Mössbauer spectra for such interface-selectively enriched samples should reveal the properties of the Fe interface in contact with a non-magnetic material. The structure of the interface-selectively enriched sample for the Mössbauer absorption measurements can therefore be visualized. The layer thickness is controlled by operating the shutters. To control the width in units of 0.1 nm, the depositing rate has to be very slow. Avoidance of contamination during deposition requires the use of the UHV atmosphere [21, 61].

An example of the Mössbauer spectra is shown in Figure 1-12. Magneto-transport measurements between 77 and 300 K were carried out using a high-resolution ac bridge. The AC susceptibility and magnetization of samples were measured between 5 and 290 K using a commercial ac susceptometer. Conversion-electron Mössbauer spectroscopy (CEMS) measurements were performed at room temperature using a gas-flow proportional counter with premixed He/4% CH4. CEMS data were analyzed using a nonlinear least-squares fitting with overlapped Lorentzian curves to obtain the hyperfine parameters. Typical linewidths (half width at half maximum) were ~ 0.25 mm/s. All isomer shifts given below are relative to bulk α-Fe at room temperature.

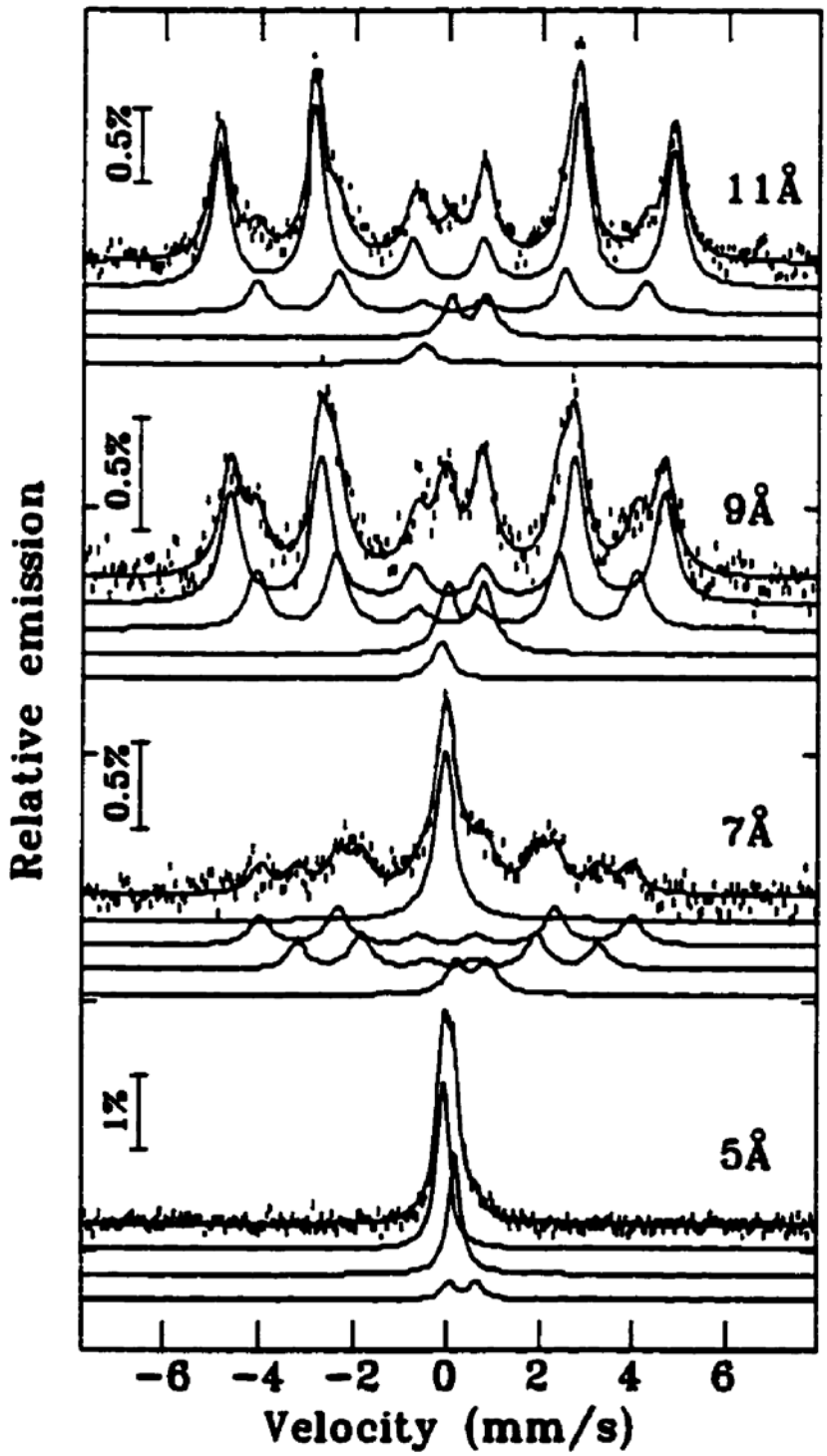

Figure 1-12. Conversion-electron Mössbauer spectra taken at room temperature (vertical bars) and calculated fits (solid lines) for a series of of (Cu 25 Å / Fe t_{Fe} Å) x36 multilayers with nominal t_{Fe} ranging from 11 down to 5 Å. One can see the appearance of the Cu(200) on the structure of Fe upon increasing the thickness of the Fe [23].

1-6. Iron and copper structures – Bragg's law

Iron is the 26th element in the periodic table, which is symbolized by Fe. Iron is a transition metal that belongs to group 8 of the periodic table. In its metallic state, Iron is rare in the Earth's crust, however, iron ores are the most common on Earth's crust. The electronic configuration of iron is given by [Ar]$3d^6 4s^2$, its atomic radius is 126-pm, and the covalent radius for the low spin is 132±3 pm and that of the high spin is 152±6 pm. The lattice parameter of iron is 286.65 pm. Iron exists in many isotropic forms, ranging from ^{54}Fe to ^{60}Fe, with ^{56}Fe the most abundant (~91.75%). Iron is a ferromagnetic element; the Curie temperature below which the transition from paramagnetic to ferromagnetic is observed is 770 ℃. Interestingly, under specific temperature and pressure, Fe exists in three allotropic forms: alpha iron (α-Fe), gamma iron (γ-Fe), and delta iron (δ-Fe); a fourth allotropic form might also exist at very high pressure, known as epsilon iron (ε-Fe). In the diagram of different allotropic forms of Fe, α-Fe, which has a BCC crystal structure, exists when the temperature is below 910 ℃; α-Fe is the most thermodynamically stable form of Fe. It is paramagnetic at high temperature (i.e., above the Curie temperature, which is ~771 ℃) and becomes ferromagnetic below the Curie temperature. As the temperature increases, $912 < T < 1394$ ℃, Fe becomes γ-Fe, which has an FCC crystal structure. A further increase, $1394 < T < 1538$ ℃, turns Fe unto δ-Fe, which has a BCC crystal structure.

Copper is the transition metal found in the periodic table with atomic number 29 and is symbolized by Cu. Among all the metal, copper is one of a few that can be found in the directly usable form. The atomic radius of copper is 128 pm, the covalent radius is 132±4 pm, and the Van der Walls radius is 140 pm. Copper is a noble metal that crystallizes in the face centered cubic; its electronic structure configuration is given by [Ar]$3d^{10} 4s^1$. Copper has 4 isotopes which vary from ^{63}Cu to ^{67}Cu, and ^{63}Cu is the most abundant (69.15%). In contrast to iron, copper is a non-magnetic element.

The choice of Fe and Cu for our studies has many advantages including the availability of both materials, environmental factors, the cost of both materials for subsequent technological applications, the similarity between both materials in terms of electronic structure (both are cubic), etc.

Fe and Cu are both cubic systems, Body-Centered Cubic (BCC), and Face Centered Cubic (FCC), respectively. In both, elements atoms are arranged regularly and the smallest possible arrangement is called a unit cell; for example Figure 1-13 illustrates both BCC and FCC systems. The distance between planes can be determined using Bragg's Law, which states

$$2d\sin(\theta) = n\lambda \tag{1.4}$$

where *d* is the distance between two consecutive planes, θ is the angle between the incident Rayleigh beam and the first plane, n is the diffraction order, and λ is the wavelength. Equation (1.4) shows that for a given diffraction order, the diffraction angle (θ) increases as the inter-planar distance *d* decreases.

For a cubic system, the relationship among the plane spacing *d*, the lattice parameter a, and the Miller's indices *hkl* is given by Equation (1.5).

$$\frac{1}{d^2} = \frac{h^2 + k^2 + l^2}{a^2} \tag{1.5}$$

Combining Equations 4 and 5 leads to the Equation (1.6):

$$d_{hkl} = \frac{na}{\sqrt{(h^2 + k^2 + l^2)}} \tag{1.6}$$

$$\lambda = \frac{2a\sin(\theta)}{\sqrt{(h^2 + k^2 + l^2)}} \tag{1.7}$$

and

$$\sin^2(\theta) = \frac{\lambda^2(h^2 + k^2 + l^2)}{2a^2} \tag{1.8}$$

The diffraction experiments provide quantitative information on the volume (the lattice constant a) and the shape characteristics (BCC or FCC) of the unit cell. The intensity of diffraction peaks depends on the phase relationships between the radiation scattered by all the atoms in the unit cell. As a result, the intensity of a particular peak, whose presence is predicted by Bragg's law, might be zero. This is explained by Bragg's law, which deals with the size and the shape of the unit cell, instead of the atomic positions. The structure factor, F_{hkl}, which is a function of the atomic

scattering factor (f_i) and the Miller indices (h, k, and l) of scattering planes determines the existence of a reflection. Missing reflections when the structure factor is zero. The rules which govern the presence of particular diffraction peaks in the different cubic systems of the Bravais lattices (SC, BCC, and FCC) are provided in Table 1-2

The allowed values for different cubic systems are provided in Table 1-3. An example of BCC and FCC systems is given in Figure 1-13.

Table 1-2. Selection rules for the diffraction peaks in cubic systems

Bravais lattice	Reflections present	Reflections absent
Simple Cubic (SC)	All	None
Body-centered cubic (BCC)	(h+k+l) = even	(h+k+l) = odd
Face-Centered Cubic (FCC)	h,k,l unmixed (either all odd or all even)	h,k,l mixed

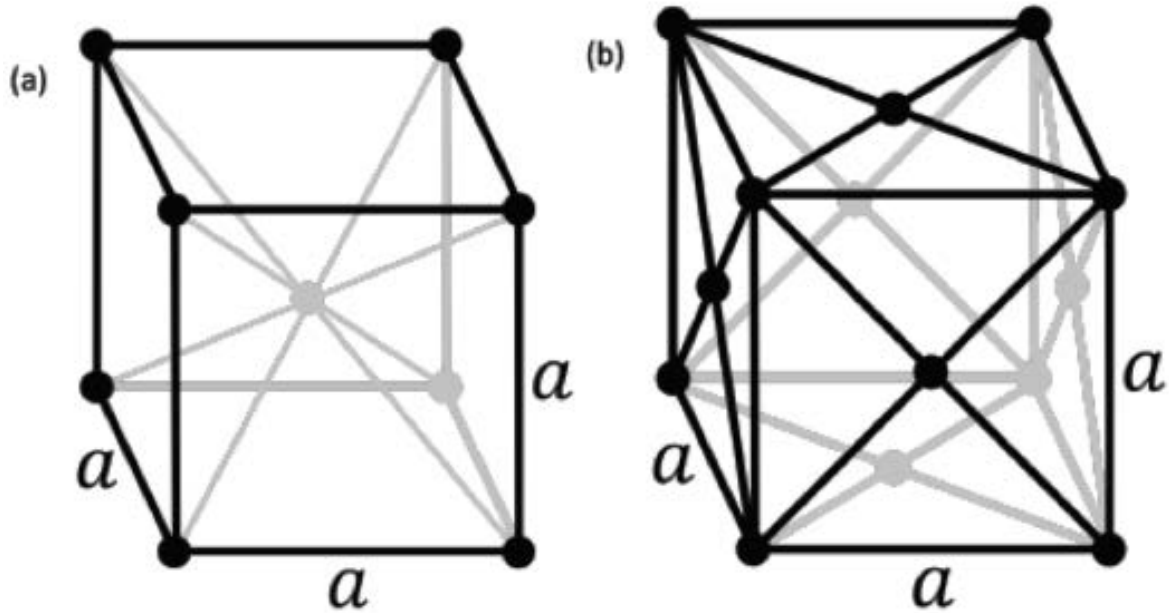

Figure 1-13. Unit cells of Fe (a), BCC, and Cu (b), FCC.

Table 1-3. Allowed list of values ($h^2+k^2+l^2$) of different atomic planes found in the cubic system

Forbidden number	Primitive, P	Face Centered Cubic, FCC	Body-Centered Cubic, BCC	Corresponding hkl
	1			100
	2		2	110
	3	3		111
	4	4	4	200
	5			210
	6		6	211
7				
	8	8	8	220
	9			221, 300
	10		10	310
	11	11		311
	12	12	12	222
	13			320
	14		14	321
15				
	16	16	16	400

We can then use Bragg's expression to characterize the structural changes observed in the multilayer systems. Numerically, this can be thought of as the radial distribution function (RDF), which reports the structural modifications either in the bulky Fe, Cu or at the interface. RDF is the probability to find an atom at the distance r of another identical atom, chosen as reference, as described in Chapter 2 on Numerical Methodology. Here, RDF is assimilated to the inter-plane distance given by the Bragg's relation (Equation (1.6)).

1-8. Conclusion

Throughout this chapter, we carried out an overview of the magnetic multilayer systems, from history to the technological application. We can conclude that the field of magnetism of multilayers is a relatively growing field based on its critical technological applications. The high demand to further miniaturized electronic devices is at the center of preoccupation in the scientific community. Additionally, the new properties presented by these artificially made materials have attracted much attention and the fundamental physics behind those unusual properties remains incompletely addressed; the thicknesses of different layers forming the multilayer systems have been shown to play an essential role in understanding such properties, but the debate remains open. For example, the thickness at which the maximum and the minimum of properties such as GMR occur, remains not well determined. Determining such thicknesses may help to increase the technological applicability of the magnetic multilayer systems.

Chapter 2 Numerical Methodology

2-1. Introduction

The recent trends in the methods of fabrication and characterization of magnetic multilayers have led to a growing interest in magnetic multilayer systems, not only for the understanding of the fundamental physics behind these artificially made materials but also for numerous technological applications. Besides these tremendous efforts in improving available techniques, a normalized protocol is still lacking. Many results present in literature rely on the methodology employed to fabricate the samples and can change considerably when switching to a new approach. The observed differences due to the techniques employed limit the transfer of technology for the applications at the industrial level. Numerical methods are often used to complement the experimental and theoretical techniques. This chapter covers the numerical approach used to simulate the multilayer systems that mimic the experimental systems, the Hamiltonian used to take into account the interacting particles, and an emphasis is made on the biased Monte Carlo Metropolis method with the simulated annealing that we used to characterized our systems.

2-2. Voronoï diagram approach applied to the preparation of the multilayer systems

The origin of the Voronoï diagram dates back to the 17th century when R. Descartes claims in his book on the principles of philosophy that the solar system consists of vortices[64]. In his illustration shown in Figure 2-1, one can see the decomposition of space into convex regions, each consisting of matter revolving around one of the fixed stars.

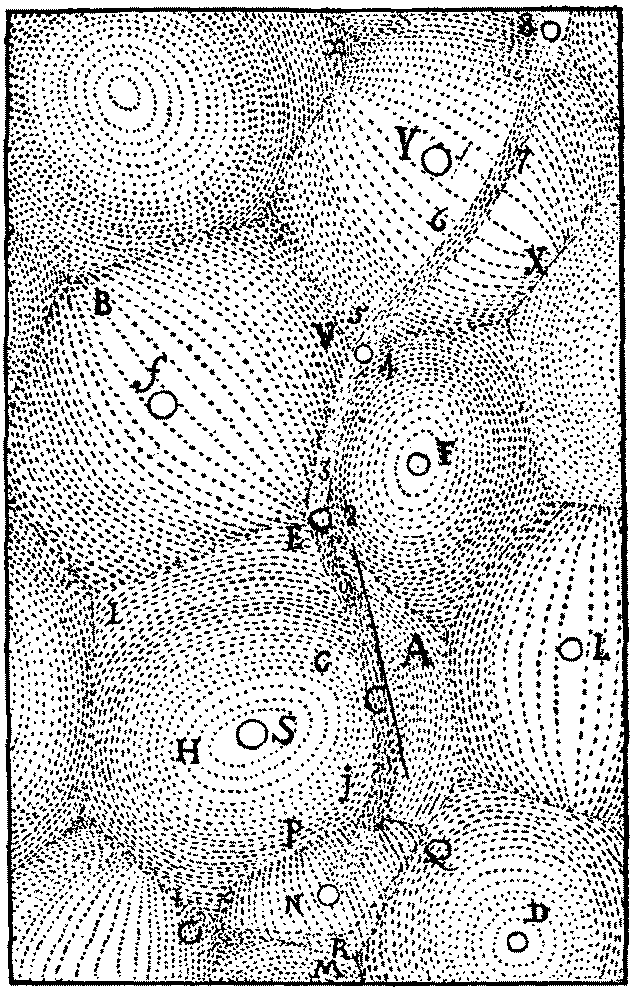

Figure 2-1. Descartes decomposition of the space into vortices [64].

A similar concept has been used in numerous fields, including Material Sciences, which is commonly known as Wigner-Seitz.

Dirichlet and Voronoï first introduced the Voronoï diagram in geometry[65, 66] and it was later linked to Delaunay triangulation. The construction of a Voronoï diagram consists of partitioning a plane into regions based on the distance to the points in a specific subset of the plane. This set of points (called a crystallographic cell) is specified beforehand. For each cell, there exists a corresponding region consisting of all points closer to the cell than to any other; these regions are called Voronoï cells. The Voronoï diagram of a set of points is dual to its Delaunay triangulation.

The general idea is that considering a set of “sites” of “generators,” a Voronoï diagram consists of a collection of regions that divide up the plane. Each point corresponding to one of the sites and

all the points in one region are closer to that site than any other site. The points located halfway between two sites correspond to the boundary. An illustration is given in Figure 2-2, where the point p is closer to the site p_1 than any other enumerated points, and p' is on the boundary between p_1 and p_3.

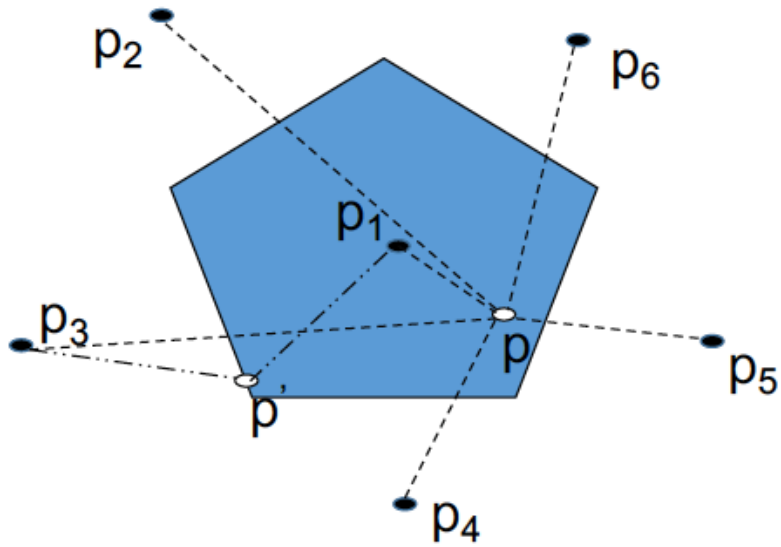

Figure 2-2. Example of the 2D construction of the Voronoï diagram. The distance from p to p_1 is less than the distance from p to any other points; p' is located at the boundary between p_1 and p_3

In 2-dimensional, the mathematical expressions of the Voronoï diagram are as follows: Let us define $p_i = (x_{i1}, x_{i2})$ and the corresponding vector $\vec{x}$. $P = \{p_1, p_2, ..., p_n\} \in \mathbb{R}^2$, where $2 \le n \le \infty$, and $p_i \ne p_j, i \ne j$, $\forall i, j = 1, 2, ..., n$ the set of points. The region is given by

$$V(p_i) = \{\overrightarrow{X} |, || \overrightarrow{x_i} - \overrightarrow{x_j} || \forall j \ni i \ne j\} \tag{2.1}$$

The Voronoï region p_i is the Euclidian distance. The ensemble of Voronoï regions in an arbitrary Voronoï is connected and convex. The Voronoï diagram of P is given by

$$V = \{V(p_1), V(p_2), ..., V(p_n)\} \tag{2.2}$$

We grew the multilayer systems according to the principle that each layer is characterized by its nucleation centers of coordinate (X_i, Y_i, Z_i, where i = 1 to n, n stands for the number of sites defined by the unit cell of each element) in the direct orthogonal base (O, I, J, K, where O stands for the origin, and I, J, or K standing for the unit coordinate for X, Y, or Z respectively). This arrangement aims to produce the initial step for each layer. The next step is to add atoms to the system, to make the layers grow in all directions until the structure reaches a specific limit fixed by the Voronoï cell conditions. We built each layer based on the following algorithm, where the simplified version is given by the flowchart in Figure 2-3.

Algorithm to build the multilayer systems based on Voronoï approach

Lest us suppose we want to build a multilayer system that contains N layers represented by their center C such as $C_i(x_i, y_i, z_i;\ i = 1,...,N)$. We need to define the vectors basis matrix, $MBasis$, which represents the coordinates transformation from the original basis (that of the element) to the cubic basis, and the atomic coordinates of atoms forming the unit cell in that basis, $C_R^i(i = 1,...,N_m)$, where Nm stands for the number of atoms in the unit cell. Each layer K_i is characterized by the position of its center, named here $PosCenter_i$, and the matrix orientation MR which takes into account the position of different Euler's angles $(\phi_i, \theta_i, \psi_i)$.

For $l = 0$ to $N - 1$ (choose N different layers with different centers)

Construct the matrix rotation $MR\{l\}$ (According to the orientation of Euler's angles)

Construct the transfer matrix $MT\{l\} = MR\{l\} * MBasis$ (It orients the matrix basis according to the Euler angles in the new coordinates system

For every possible displacement in the space (multiplicity)

Construct the displacement vector $DepR$

For $k = 0$ to $\mathrm{N}_m - 1$ (N_m represents the number of atoms per unit cell)

Calculate $CR\{lk\} = CR\{k\} + DepR$, the relative coordinates of the atom k

Calculate $Pos_k = MT\{l\} * CR\{lk\} + PosCenter_l$, the final position of the atom k

Calculate $d = dis\tan ce(Pos_k, \{C_i\})$ to check whether the new added atom is closer to the center l than any other center in the box (C_i is any other centers except C_l)

Is $d < C_l$? and $Pos_k < Pos_Max$?

If yes, then the new position is accepted

If no, then the new position is rejected.

End for

End for

End for

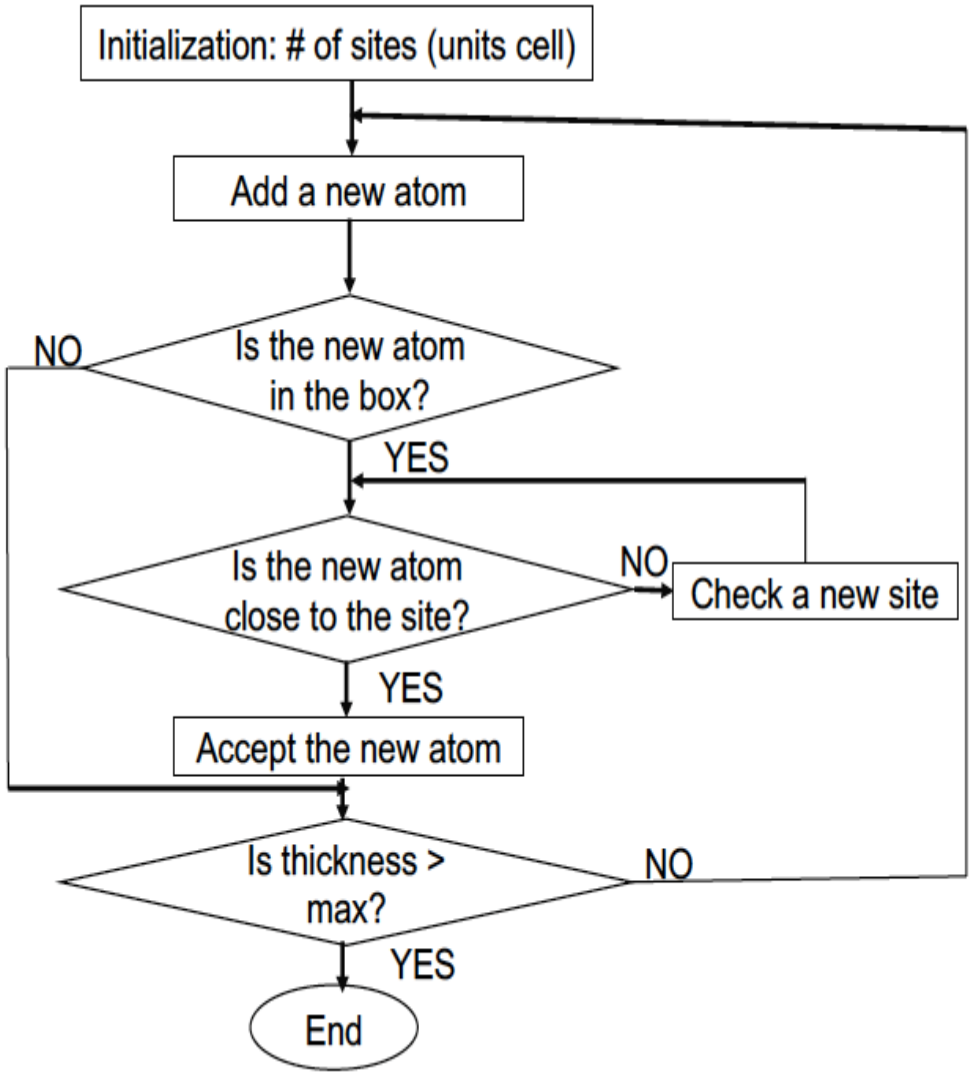

Figure 2-3. Flowchart to simulate a single layer based on Voronoï diagram.

We further superposed on top of one another on the y-direction. For each layer, we considered its directionality by using the Euler angles, which are chosen to orient the relative crystallographic axes of the layers. We further avoided finite size and surface effects by first choosing a simulation

box large enough to contain several layers and then performed simulations on a truncated box of much smaller size. Figure 2-4 shows an example of multilayer system constructed using the current approach.

A similar procedure can be used to build other types of a multilayer systems such as Fe/Cr.

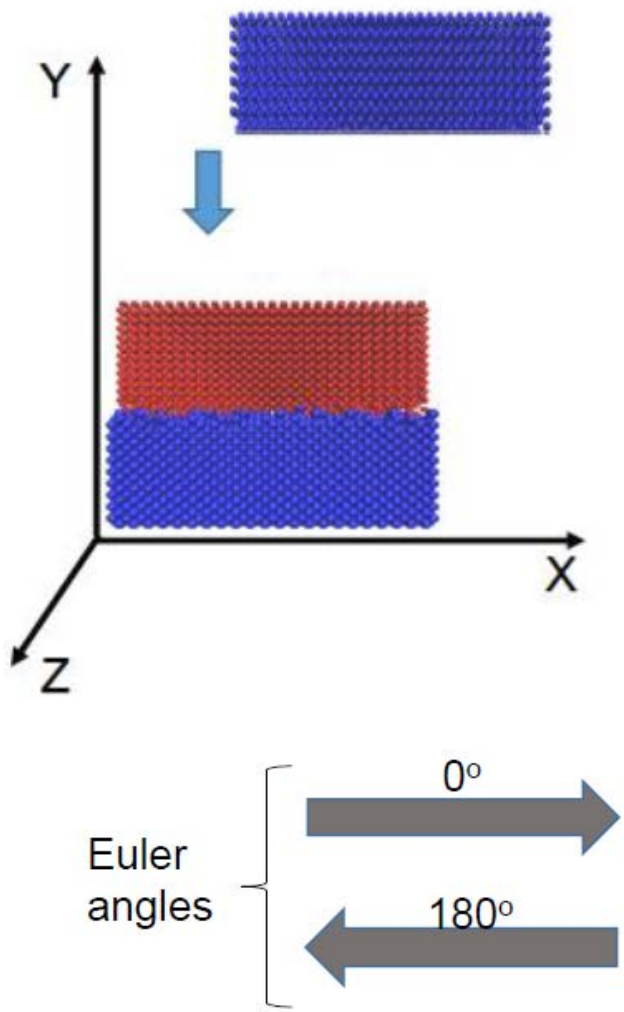

Figure 2-4. Example of a magnetic multilayer system composed of Fe (blue) and Cu (red) layer, prepared with the Voronoï method, used in our study. We have used the free boundary conditions by first choosing a large simulation box, and analyze a reduced box, as shown in the figure.

2-3. Definition of the form of the Hamiltonian used in this thesis

Since our multilayer systems are constituted of interacting particles, it is important to define the interaction energy among atoms. Depending on the system, four types of bonds can be used to define the interactions between atoms: The ionic bond, which is characterized by a transfer of electron, can be found in the ionic materials; the covalent bond (strong bond), which is characterized by the pairing of electrons by two atoms; the Van der Walls bonds (or weak bonds), which are a relatively weak bonds such as the electrostatic bonds; the metallic bonds, which are found in the metals such as iron and copper. The total energy term is defined using either empirical or semi-empirical potential functions.

Atomistic simulation techniques such as molecular dynamics or Monte Carlo require the use of interatomic potential derived from the first-principle calculations to provide exact results. However, due to the size (or the number of atoms in the system), it is often not possible to investigate material behavior using only first-principles calculations. Another convenient approach is a “semi”-empirical interatomic potential that can deal with more than a million of atoms. A good semi-empirical potential should be able to reproduce correctly various fundamental physical properties such as elastic properties, structural properties, magnetic properties, defect properties, surface properties, thermal properties, etc. The most widely used semi-empirical interatomic potential is the Embedded-Atom Method (EAM) first proposed by Daw and Baskes [67-70], which is based on density functional theory. Finis and Sinclair later introduce another critical version of the EAM from the second nearest moment approximation [71].

A successful and reliable interatomic potential for the multilayer Fe/Cu/Fe systems should be able to reproduce the physical properties of the interface FeCu or CuFe over the entire composition range, from one pure element side to the other pure element side, without changing potential parameters or formalism. This means that the potential should be able to describe individual elements using a common mathematical formalism. From this point of view, the modified embedded-atom method (MEAM) [72, 73] potential may be said to be highly applicable to multi-component systems, because it can describe interatomic potentials of a wide range of elements FCC, BCC, hexagonal close-packed, diamond, and even gaseous elements) using a common formalism and functional form. The MEAM was developed by Baskes [74], by modifying the

embedded-atom method [73] in such a way to include the directionality of bonding. In the original MEAM, interactions among only first-nearest-neighbor atoms were considered. The MEAM was modified once again by Baskes et al. (2NN MEAM) [72] to consider partially second-nearest-neighbor atoms interactions and to remove some critical shortcomings in the original MEAM. The expression of the total energy is given as follows

$$E = \sum_i [F_i(\overline{\rho_i}) + \frac{1}{2}\sum_{j(\neq i)} S_{ij}\phi_{ij}(R_{ij})] \tag{2.3}$$

Where F_i is the embedding function, which defines the energy to embed an atom of type *i* into the background electron density $\overline{\rho_i}$ at site *i*; S_{ij}, and $\phi_{ij}(R_{ij})$ are the screening factor and the pair interaction between atoms *i* and *j* separated by a distance R_{ij}, respectively. For the general calculations of the energy, the functional forms of the two terms, F_i and ϕ_{ij}, should be provided. The direct contribution to the energy on Equation (2.3) can be written as

$$E_i = F_i(\overline{\rho_i} / Z_i) + \frac{1}{2}\sum_{j(\neq i)} \phi_{ij}(R_{ij}) \tag{2.4}$$

Where the background density has been normalized to the nearest neighbors Z_i in the reference structure of type-*i* atom. For the first neighbors interactions, the energy function in Equation (2.4) defined for each atom of the reference structure as function of nearest-neighbor distance is given by

$$E_i^u(R) = F_i(\overline{\rho_i}^o(R) / Z_i) + \frac{Z_i}{2}\phi_{ii}(R) \tag{2.5}$$

$\overline{\rho_i^o}(R)$ is the background electron density for the reference structure of atom i and R is the nearest neighbor distance. We can then write the pair interaction for type-i atom as

$$\phi_{ii}(R) = \frac{2}{Z_i}\{E_i^u(R) - F_i(\overline{\rho_i^o}(R) / Z_i)\} \tag{2.6}$$

By replacing the expression of the pair interaction in Equation (2.4) we get the following term

$$E_i = \frac{1}{Z_i}\sum_{j(\neq i)} E_i^u(R_{ij}) + [F_i(\overline{\rho_i} / Z_i) - \frac{1}{Z_i}\sum_{j(\neq i)} F_i(\overline{\rho_i}^o(R_{ij}) / Z_i)] \tag{2.7}$$

On the Equation (2.7), the first term represents the average of the energy per atom of the reference lattice at each of the nearest neighbor distances. Equation (2.7) can be written in terms of electron density of the reference structure in the following form

$$E_i(R) = \frac{Z'}{Z_i} E_i^u(R) + [F_i(\rho_i^{a(o)}(R)Z'/Z_i) - \frac{Z'}{Z_i} F_i(\rho_i^{a(o)}(R))] \tag{2.8}$$

Where Z' is the number of nearest neighbors in the structure. The FCC and BCC have Z_i 12 and 8 respectively and the energy of the reference structure is given by

$$E_i^u(R) = -E_i^0(1 + a^*)e^{-a^*} \tag{2.9}$$

With $a^* = a_i(R/R_i^0 - 1)$ and $a_i = \sqrt{9B_i\Omega_i / E_i^0}$ or $a_i = \sqrt{K_i / E_i^0 R_i^0}$ where R_i^0 is the equilibrium nearest-neighbor distance, B_i is the bulk modulus, Ω_i is the atomic volume of the solid elements, and K_i is the diatomic force constant for the gaseous elements.

The embedding function in the general expression of the energy in Equation (2.3) can be written as a function of the electron density

$$F_i(\rho) = A_i E_i^0 \rho \ln \rho \tag{2.10}$$

Where A_i is defined using the values of the FCC-BCC energy difference derived from the ab initio local density approximation (LDA) calculations.

The atomic electron densities term is given by

$$\rho_i^{a(l)}(R) = e^{-b^*} \tag{2.11}$$

And the

$$b^* = \beta_i^{(l)}(R/R_i^0 - 1) \tag{2.12}$$

Where the parameters $\beta_i^{(l)}, l = 0 - 3$ are determined from the experiments.

In general, the first term of the Equation (2.3) is given in Equation (2.13)

$$F(\rho_i) = AE_c(\rho_i / \rho^{(0)}) \ln(\rho_i / \rho^{(0)}) \tag{2.13}$$

where the density is defined by $\rho_i = \rho^{(0)} G(\Gamma_i)$ with $G(\Gamma_i) = \frac{2}{1+e^{-\Gamma_i}}$ and $\Gamma_i = \sum_{h=1}^{3} t^h [\frac{\rho_i^{(h)}}{\rho_i^{(0)}}]^2$. In these expressions, $\rho_i^{(h)} = f(\rho_{ai})$ and $\rho_{ai} = \exp[-\beta_i(\frac{r}{r_e}-1)]$, $i = 0,1,2,$ and 3; where $\rho_i^{(h)}$ is the partial density (angular or spherical contribution) and ρ_{ai} is the electronic density.

The expression of the conventional pair correlation functions is given by Equation (2.14)

$$\phi(r_{ij}) = (\frac{2}{N_{neighbors}})[E^u(r_{ij}) - F(\rho^0(r_{ij}))] \tag{2.14}$$

where $E^u(r_{ij}) = -E_c(1+a^* + da^3)e^{-a^*}$ with $a^* = (\frac{9B\Omega}{E_c})^{1/2}(\frac{r_{ij}}{r_e}-1)$, $F(\rho^0(r_{ij})) = AE_c\rho^0(r_{ij})\log(\rho^0(r_{ij}))$, and $\rho^0(r_{ij}) = \exp(-b_0((\frac{r_{ij}}{r_e})-1))$ .The above parameters are defined for each element, Fe, and Cu in our simulations as well as the interface. Table 2-1 shows the parameters obtained from the first principle that we will use in our simulations.

Table 2-1. Parameters used in the energy function.

	Ec	Re	B	A	d	β_0	β_1	β_2	β_3	t_1	t_2	t_3	S
Fe-Fe	4.29	2.28	1.73	0.56	0.05	4.15	1	1	1	2.6	1.8	7.2	0.9112
Cu-Cu	3.54	2.555	1.42	0.94	0.05	3.83	2.2	6.0	2.2	2.72	3,o4	1.95	0.9112
Fe-Cu	Ec*	2.57	B*		d*								

$Ec^* = 0.75Ec_{Fe} + 0.25Ec_{Cu} + 0.158$, $B^* = 1.646(0.75B_{Fe} + 0.25B_{Cu})$, and $d^* = 0.75d_{Fe} + 0.75d_{Cu}$

2-4. Computational approach of characterization of magnetic multilayer systems

Modeling a physical system can be done using theory, laboratory prototypes, or numerical techniques. The theoretical models often use, especially in complicated many-body problems, macroscopic equations to describe the physical phenomenon of interest, thereby neglecting many microscopic details of the system. Numerical methods usually lack this approximation problem,

and they are generally inexpensive in comparison with experiments. Numerical methods also provide efficient benchmarks for theoretical models. They can address details of complex phenomena that can be difficult for theory as well as for experiments. Experimental difficulties may arise from complexity, expenses, danger, or hazardous condition of the phenomenon. For example, the presence of interdiffusion at the interface between two layers in the experimentally made multilayer system renders its study more complicated at the atomistic scale. Also, numerical techniques are versatile enough to combine or distinguish different physical phenomena, which have made them popular tools of analysis. The results of numerical methods are, however, subject to uncertainties that arise from, e.g., different approximations and the numerical techniques employed. It is, therefore, necessary to be cautious when expressing the results of numerical simulations, and theoretical and/or experimental findings should support them.

2-4-1. Molecular dynamics method to investigate the properties of interacting particles

The molecular dynamics method encompasses two general forms: one for systems at equilibrium, another for systems away from equilibrium. Equilibrium molecular dynamics is typically applied to an isolated system containing a fixed number of molecules N in a fixed volume V. Because the system is isolated, the total energy E is also constant; E is the sum of the molecular kinetic and potential energies. Thus, the variables N, V, and E determine the thermodynamic state [75, 76].

If we consider a system with N interacting atoms, we can define the internal energy E as follow

$$E = K + U \tag{2.15}$$

Where K is the kinetic energy given by

$$K = \sum_{i=1}^{N} \frac{1}{2} m_i \, |\overrightarrow{v_i(t)}|^2 \tag{2.16}$$

and U is the potential energy

$$U = U(\overrightarrow{r^{3N}(t)}) \tag{2.17}$$

The whole problem of the molecular dynamics becomes the determination of the function given in Equation (2.17). In general, it is not possible to evaluate the potential energy in Equation (2.17)

exactly. However, several methods exist, which use the first principle calculations to approximate its evaluation.

In NVE molecular dynamics, the positions $\mathbf{r}^{3N}$ are determined by solving Newton' equations of motion

$$\vec{F}_i = m\frac{\partial^2 \overrightarrow{r_i(t)}}{\partial^2 t} = -\frac{\partial U(\overrightarrow{r^{3N}(t)})}{\partial \vec{r}_i} \tag{2.18}$$

Here $\vec{F}$ is the force on *i* caused by the N-1 other molecules, m is the molecular mass, and U is the intermolecular potential energy. Integrating Equation (2.18) once yields the atomic momenta; integrating a second time produces the atomic positions. Repeatedly integrating for several thousand times provides individual atomic trajectories from which time averages can be computed for macroscopic properties. The problem now is to integrate Equation (2.18) for all the interacting particles, which is usually done by making approximation on the intermolecular potential energy [77, 78].

2-4-2. Monte Carlo versus Molecular dynamics

Although the physical and mathematical basis of the Monte Carlo might be less transparent to a novice than that for molecular dynamics, Monte Carlo is usually easier than molecular dynamics to code in a high-level language such as C or Fortran. Monte Carlo is also easier to implement for systems in which it is difficult to extract the intermolecular force law from the potential function. Systems having this difficulty include those composed of molecules that interact through discontinuous forces (forces starting to act on the system instantaneously at some positive time, either persisting or being withdraw suddenly); examples are the hard-sphere and hard convex-body models. Similar challenges arise in systems for which the potential function is a complicated multidimensional surface, such as might be generated by ab initio calculations [78].

For the determination of simple equilibrium properties such as the pressure in atomic fluids, Monte Carlo and molecular dynamics are equally effective: Both require about the same amount of computer time to reach similar levels of statistical precision. However, molecular dynamics more efficiently evaluate properties such as heat capacities, compressibilities, and interfacial properties.

Besides configurational properties, molecular dynamics also provides access to dynamic quantities such as transport coefficient and time correlation function. Such dynamics quantities cannot generally be obtained by Monte Carlo, although certain kinds of dynamic behavior may be deduced from Monte Carlo simulations.

Molecular dynamics also provide certain computational advantages because of the deterministic way in which it generates its trajectories. The presence of an explicit time variable allows us to estimate the length needed for a run; the duration must be at least several multiples of the relaxation time for the slowest phenomenon being studied. No such convenient guide is available for estimating the length required for a Monte Carlo calculation. Also, many kinds of small errors in the molecular dynamics program tend to accumulate with time and so become apparent as violations of conservations principles; in contrast, subtle mistakes in a Monte Carlo program may not blatantly advertise their presence.

2-4-3. Metropolis Monte Carlo statistical method to investigate the properties of interacting particles

Monte Carlo methods play an important role in computational physics, mainly when problems evolve a large number of interacting atoms. We will introduce the Monte Carlo method; emphasis will be made on concepts such as Markov chains and ergodicity. The Metropolis algorithm will be explained thoroughly as it constitutes an important part of the Monte Carlo implementation in this thesis.

The Monte Carlo method in computational physics is possibly one of the essential numerical approaches to study problems spanning all scientific disciplines. The idea is seemingly simple: Randomly sample a volume in d-dimensional space to obtain the estimate of an integral at the price of a statistical error. For problems where the phase space dimension is enormous, especially in the case when the dimension of the phase space depends on the number of degrees of freedom, and the Monte Carlo method outperforms any other integration scheme. The difficulty lies in smartly choosing the random samples to minimize the numerical effort.

The term Monte Carlo method was coined in the 1940s by physicists Ulam, Fermi, Von Neumann, and Metropolis (amongst others) working on the nuclear weapons project at Los Alamos National Laboratory [79]. Because random numbers (similar to processes occurring in a casino, such as the Monte Carlo Casino in Monaco) are needed, it is believed that this is the source of the name.

The idea behind the Monte Carlo approach comes from finding an approximate solution to the integration of space with a high dimension. In general, most standard integration schemes fail for high-dimensional integrals, and the space dimension of the phase space of typical physical systems is very large. For example, the phase space dimension for N classical particles in three space dimensions is d = 6N (three coordinates and three momentum components are needed to characterize a particle fully). This is even worse for the simple case of the N classical Ising spins, which can take the values ±1. In this case, the phase space dimension is 2^N, a number that grows exponentially fast with the number of spins! Therefore, integration schemes such as Monte Carlo methods, where the error is independent of the space dimension are of high importance in computational physics.

Classical Monte Carlo: Samples are drawn from a probability distribution, often the classical Boltzmann distribution, to obtain thermodynamic properties or minimum energy structures. Let us consider a system described by a Hamiltonian H in thermodynamic equilibrium with a heat bath at temperature T. The physical quantities such as the energy, the magnetization, the specific heat, the susceptibility, etc., generally called observable, are computed by performing a trace over the partition function Z. Within the canonical ensemble, where the temperature is fixed, the expectation value of the thermal average of an observable O is given by

$$< \mathrm{O} >= \frac{1}{Z}\sum_{s} \mathrm{O}(s) e^{-\mathrm{H}(s)/k_B T} \tag{2.19}$$

The sum is over all the states s in the system, and k_B is the represents the Boltzmann constant. Z is the partition function, where the expression is given by

$$Z = \sum_{s} \exp[-H(s)/k_B T] \tag{2.20}$$

Which normalizes the following equilibrium Boltzmann distribution

$$p_{eq}(s) = \frac{1}{Z} e^{-H(s)/k_B T} \tag{2.21}$$

The expression < > in Equation (2.19) represents the thermal average. The expression of the energy is given by

$$E = < H(s) > \tag{2.22}$$

And the free energy of the system is as follow

$$F = -k_B T \ln Z \tag{2.23}$$

All thermodynamic quantities can be computed directly from the partition function and expressed as derivatives of the free energy. Because the partition function is closely related to the Boltzmann distribution, it follows that if we can sample observables (e.g., magnetization) with states generated according to the corresponding Boltzmann distribution, a simple Markov-chain "integration" can be used to reproduce an estimate.

In general, it is not possible to evaluate the partition function Z exactly. The presence of the exponential term in the infinite series makes things even harder as it may include complex interactions among particles.

The sum in Equation (2.19) and Equation (2.20) is not possible to evaluate for a large number of states such as high dimensional space. It is possible to take the average over a finite number of states a subset of all possible states, if one knows the correct Boltzmann weight of the states and their respective probability. E.g., a small subset of all possible states is chosen at random with certain probability distribution p_s. The best estimate of a physical observable O will be

$$\mathrm{O}_N = \frac{\sum_{s=1}^{N} \mathrm{O}(s) p_s^{-1} \exp[-H(s)/k_B T)]}{\sum_{s=1}^{N} p_s^{-1} \exp[-H(s)/k_B T)]} \tag{2.24}$$

When N →∞, O(s) ≈ <O>. The problem now is how to choose the p(s) that will lead to the correct observable <O>. A natural choice is to consider that $p(s) = p_{eq}(s)$ and Equation (2.24) will become

$$\mathrm{O}_N = \frac{\sum_{s=1}^{N} \mathrm{O}(s)\exp[-H(s)/k_B T)]}{\sum_{s=1}^{N} \exp[-H(s)/k_B T)]} \tag{2.25}$$

This approach is analogous to the importance sampling Monte Carlo integration, and the final observable is given by

$$< \mathrm{O} >= \frac{1}{N}\sum_i \mathrm{O}(s_i) \tag{2.26}$$

Where the states S_i are now selected according to the Boltzmann distribution. The problem now is to find an algorithm that allows for a sampling of the Boltzmann distribution. The method is known as the Metropolis algorithm.

Implementation of the Metropolis algorithm: The metropolis algorithm was developed in 1953 at Los Alamos National Lab within the nuclear weapons program mainly by Rosenbluth and Teller families. To evaluate Equation (2.24), we can generate a Markov chain of successive states $s_1 \to s_2 \to ...$ The new state is generated from the old state with a probability given by the equilibrium Boltzmann distribution given in Equation (2.21). In the Markov process, the state s occurs with probability $p_k(s)$ at the kth time step, described by the following master equation

$$p_{k+1}(s) = p_k(s) + \sum_{s'}[T(s' \to s)p_k(s') - T(s - s')p_k(s)] \tag{2.27}$$

The sum is over all the states s' and the first term in the sum describes all processes reaching state s and the second term describes all processes leaving state s. The goal is that as $k \to \infty$ the probabilities $p_k(s)$ will reach a stationary distribution described by the Boltzmann distribution. The transition probabilities T can be designed in such a way that for $p(s) = p_{eq}(s)$ all terms in the sum vanishes, i.e., for all s and s' the detailed balance condition

$$T(s' \to s)p_{eq}(s) = T(s \to s')p_{eq}(s) \tag{2.28}$$

must hold. The condition in Equation (2.28) means that the process has to be reversible. Furthermore, when the system has assumed the equilibrium probabilities, the ratio of the transition probabilities only depends on the change in energy

$$\Delta H(s,s') = H(s') - H(s) \tag{2.29}$$

which can also be written as

$$\frac{T(s \to s')}{T(s' \to s)} = \exp[-(H(s') - H(s))/k_B T] = \exp[-\Delta H(s,s')/k_B T] \tag{2.30}$$

There are different choices for the transition probabilities T that satisfy Equation (2.30). Thus, T satisfies the general Equation $T(x)/T(1/x) = x, \forall x,$ with $x = \exp(-\Delta H/k_B T)$. There are two convenient choices for T that satisfy this condition:

1- Metropolis (also known as Metropolis-Hastings) algorithm: in this case, T(x) = min(1,x) and so

$$T(s \to S') = \Gamma^{-1}\ ,\ \Delta H \le 0 \tag{2.31}$$

$$T(s \to S') = \Gamma^{-1} e^{-\Delta H(s,s')/KT}, \Delta H > 0 \tag{2.32}$$

Where Γ^{-1} in Equation (2.31) and (2.32) represent the Monte Carlo time.

2- Heat bath algorithm. In this case, T(x) = x/(1+x) corresponding to an acceptance probability $\sim [1 + \exp(\Delta H(s,s')/k_B T]^{-1}$

In this thesis, we have used the Metropolis algorithm. The Metropolis algorithm is given as follow:

1 initialization (T, steps), starting configuration S

2 for (counter = 1 . . . steps) do

3 generate trial state S’

4 compute p(S → S’, T) and x = rand (0, 1)

5 if (p > x) then accept S’

6 O += O(S’)

7 done

8 return O/steps

After initialization, in line 3, a proposed state is generated by, e.g., rotating a spin. The energy of the new state is computed and henceforth the transition probability between states p = T(S → S’). A uniform random number x ϵ [0, 1] is generated. If the probability is larger than the random number, the move is accepted. If the energy is lower, i.e., ΔH < 0, the spin is always flipped. Otherwise, the spin is flipped with the probability p. Once the new state is accepted, we measure

the given observable and record its value to perform the thermal average at a given temperature. For Steps → ∞ the average of the observable converges to the exact value with an error inversely proportional to the square root of the number of steps. This is the core bare-bones routine for the Metropolis algorithm. In practice, several aspects have to be considered to ensure that the data produced are correct. The most important is the autocorrelation and equilibration times [80].

Markov chain: Markov chain is a sequence of states where the new state depends only on the old state. For example, [n] → [m] → [0]. The transition probability W_{nm} from n to m should be time-invariant and should depend only on the properties of the current states (n, m). $W_{nm} \geq 0$ and $\sum_m(W_{nm}) = 1$.

Equilibration step: To obtain a correct estimate of an observable O, it is imperative to ensure that one is sampling an equilibrium state. In general, the initial configuration of the simulation can be chosen at random and the system will have to evolve for several Monte Carlo steps before an equilibrium state at the given temperature is obtained. The time τ_{eq} until the system is in thermal equilibrium is called equilibrium time and depends directly on the system size, and increases with decreasing temperature. In general, it is measured in units of Monte Carlo Steps (MCS), i.e., 1 MCS = N particles update. All measured observable should be monitored as a function of MCS to ensure that the system is in thermal equilibrium. Some observables, such as energy, equilibrate faster than others (e.g., magnetization). Therefore, the equilibrium time of all observables measured needs to be considered.

Simulated annealing: Simulated annealing is probably the straightforward heuristic ground-state search approach. A Monte Carlo simulation is performed until the system is in thermal equilibrium. Subsequently, the temperature is quenched according to a pre-defined protocol until T close to zero is reached. After each quench, the system is equilibrated with simple Monte Carlo. The system should converge to the ground state, although there is no guarantee that the system will not be stuck in a metastable state.

Improved Monte Carlo, parallelization: There are many recipes on how to ideally select the position of the temperatures for parallel tempering Monte Carlo to perform optimally. When the

temperatures are too far apart, the energy distributions at the individual temperatures will not overlap enough, and many moves will be rejected based on Boltzmann criterion. The result is thus M independent simple Monte Carlo simulations run in parallel with no speed increase of any sort. If the temperatures are too close, CPU time is wasted. A measure for the efficiency of a system copy to traverse the temperature space is the probability (as a function of temperature) that a swap is accepted. A good rule of thumb is to ensure that the acceptance probabilities are approximately independent of temperature, between 20 - 80%, and do not show large fluctuations as these would signify the breaking-up of the random walk into segments of the temperature space. Following the recipe mentioned above, parallel tempering Monte Carlo already outperforms any simple sampling Monte Carlo method in a rough energy landscape. Still, the performance can be further increased as outlined below.

Quantum Monte Carlo: In addition to the Monte Carlo methods that treat classical problems, quantum extensions such as variational Monte Carlo, path integral Monte Carlo, etc. have also been developed for quantum systems. In these methods, random walks are used to compute quantum-mechanical energies and wave functions, often to solve electronic structure problems, using Schrödinger's equation as a formal starting point.

2-5. Metropolis Monte Carlo method to investigate the properties of magnetic multilayers

We have used the Metropolis-Monte Carlo combined with the energy function defined in Equation (2.3) to simulate the properties of Fe/Cu/Fe multilayers. To test the accuracy of the potential, we applied it to an alloy system composed of 50 % of Fe and 50 % of Cu atoms (see first part of the results section on the test of the model). The final structure after the Monte Carlo simulated annealing scheme showed that the bonds among atoms are conserved inside and outside the simulation box. Moreover, the fact that Fe and Cu atoms do not form agglomeratess of each type or the presence of atoms inside the simulation box after the simulated annealing Monte Carlo scheme justifies the choice of our interatomic potential.

We further minimized the total energy of the system given in Equation (2.3) using Monte Carlo simulations with the Metropolis algorithm, as described above. We fixed the initial system at a high temperature (> 800 K, above the Curie temperature of Fe nanoparticles) to allow the

movement of each atom. We then gradually cooled down following specifically the temperature scheme initially used by Fongang et al. [81], where the expression is given in Equation (2.33)

$$T_{k+1} = \gamma T_k \tag{2.33}$$

until the system reaches the equilibrium, where the energy no longer changes. For each step of temperature, the following steps were performed:

1- Calculate the energy of the system at a high temperature (initial state).
2- Randomly choose and displace an atom in any of the three directions Δx, Δy, or Δz.
3- Calculate the energy change ΔE due to the displacement and decide whether to accept the move based on Metropolis criterion:
   If $\Delta E < 0$, then accept the new configuration.
   If $\Delta E > 0$, then calculate $p = \exp(-\frac{\Delta E}{k_b T})$ (where k_b represents the Boltzmann constant and T the absolute temperature) and compare it with a random number u between 0 and 1. If p > u, accept the new configuration, otherwise keep the old one and restart at step 2.
4- Redo steps 1-3 for each block of temperature.

We adapted initial conditions from [25]; in addition, for complexity reason and in order to keep the structure close to that of bulk material far from the interface, we made the following modification: the choice of the atom to be subjected to the Metropolis algorithm depends on its distance to the closest interface. The following relation gives the probability choice

$$\omega = \exp(-\alpha x) \tag{2.34}$$

where α is an adjustable parameter comprised between 0.5 and 2 $Å^{-1}$, and x represents the distance from the considered atom to the nearest interface. This probability allows to avoid periodic boundaries conditions and to anneal the atomic structure only close to the interfaces, as atoms located far from the interface have a low but non-zero probability to be chosen for the move[81]. Interestingly, we have observed the maximum change of energy to be located only at the interface; the change far from the interface was almost negligible after we subjected the system to the simulated annealing Monte Carlo scheme. The flowchart given in Figure 2-5 provides the step by step biased Monte Carlo Metropolis algorithm we used in our simulations, where we added extra condition to choose an atom according to its distance from the interface.

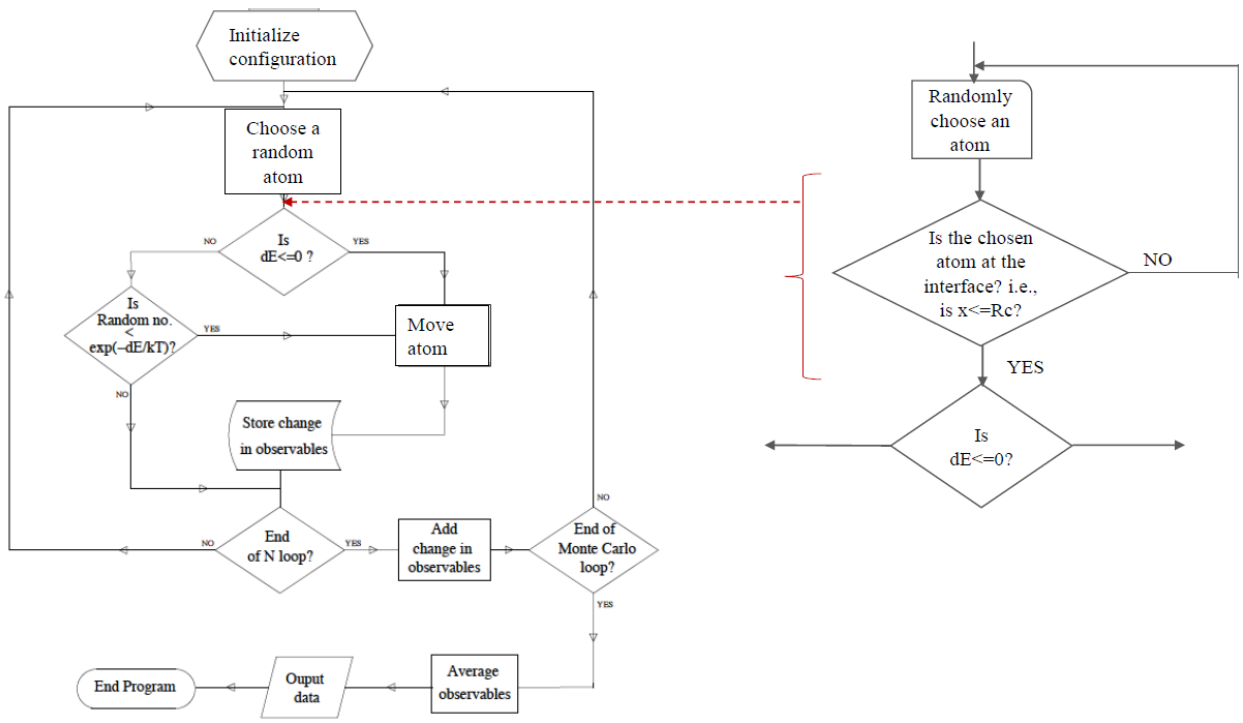

Figure 2-5. Flowchart of the biased classical Monte Carlo Metropolis algorithm used in our simulations

We further used the Heisenberg model where the Hamiltonian of the system is given by

$$\overrightarrow{H} = -\sum_{<i,j>} J_{ij} \overrightarrow{\sigma_i} \overrightarrow{\sigma_j} - g\mu_B h \sum_i \overrightarrow{\sigma_z^{(i)}} \tag{2.35}$$

Where J_{ij} denotes the spin-spin interaction, h represents the external field, μ_B, σ_i, and g represent the Bohr magneton, the individual spin, and Lande factor, respectively. J>0 for the ferromagnetic nearest neighbors, J<0 for the antiferromagnetic nearest neighbors.

The magnetization of the system can be obtained using the partition function defined in the previous chapter

$$< M > = < \sum_i \sigma_i > = -\frac{\partial F}{\partial h} = \frac{1}{\beta} \frac{\partial}{\partial h} \log Z \tag{2.36}$$

$\beta = 1/K_B T$ is the Boltzmann factor and the magnetization per spin will be given by Equation (2.37)

$$m = \frac{< M >}{N} =< \sigma > \tag{2.37}$$

where N is the number of total spin. If we consider the average field from the neighboring spins, we get the following relation

$$\in_i = -J \sum_{j=\{nn\}} \sigma_i \sigma_j - h\sigma_i = -Jz\sigma_i < \sigma > -h\sigma_i \tag{2.38}$$

Where z is the lattice coordination. Using the definition of the partition function defined in the previous chapter and replacing the expression of the Hamiltonian, we get

$$Z = \sum_{\sigma=\pm 1} e^{\beta\sigma(h_{mol}+h)} = 2\cosh(\beta(h_{mol}+h)) \tag{2.39}$$

Using Equation (2.38) we get

$$Z = 2\cosh(\beta Jz < \sigma > +\beta h) \tag{2.40}$$

Finally, the expression of the magnetization per spin becomes

$$m =< \sigma >= \frac{1}{\beta}\frac{\partial}{\partial h}\log Z = \tanh(\beta h + \beta Jzm) \tag{2.41}$$

Equation (2.41) gives the dependency of the magnetization on the external field h and the temperature. The critical temperature is provided by the Equation (2.42)

$$\beta = \frac{1}{Jz} \rightarrow T_c = \frac{Jz}{K_B} \tag{2.42}$$

Bellow the critical temperature, the relationships between m and T is given by the Mean-Field Theory

$$\frac{1}{K_B T} = \frac{1}{2Jzm}\log(\frac{1+m}{1-m}) \tag{2.43}$$

The equation gives the expression of the susceptibility

$$\chi = -\frac{\partial^2 F}{\partial h^2} = \frac{1}{T}\left[< m^2 > - < m >^2 \right] \tag{2.44}$$

Moreover, replacing $m = \sum_i \sigma_{i,}$ we get

$$\chi = \frac{1}{T}\sum_{i,j} < \sigma_i \sigma_j > \tag{2.45}$$

We used these two parameters, magnetization and susceptibility, to derive the magnetism of our multilayer systems.

In the Heisenberg model, the spins can rotate around itself, indeed allowing the spins to sample all possible conformations as seen in the real system; in contrast to the Ising model, which allows only two different configurations: spin-up and spin-down.

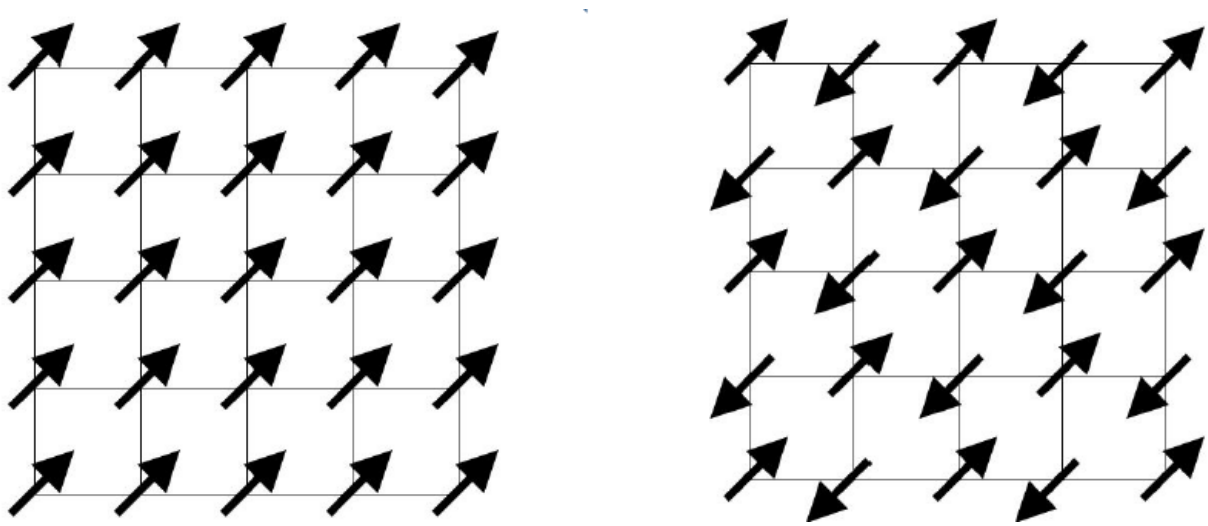

Figure 2-6. Example of the spins configuration used the Heisenberg model. Left panel shows ferromagnetic arrangement whereas the right panel shows the antiferromagnetic arrangement.

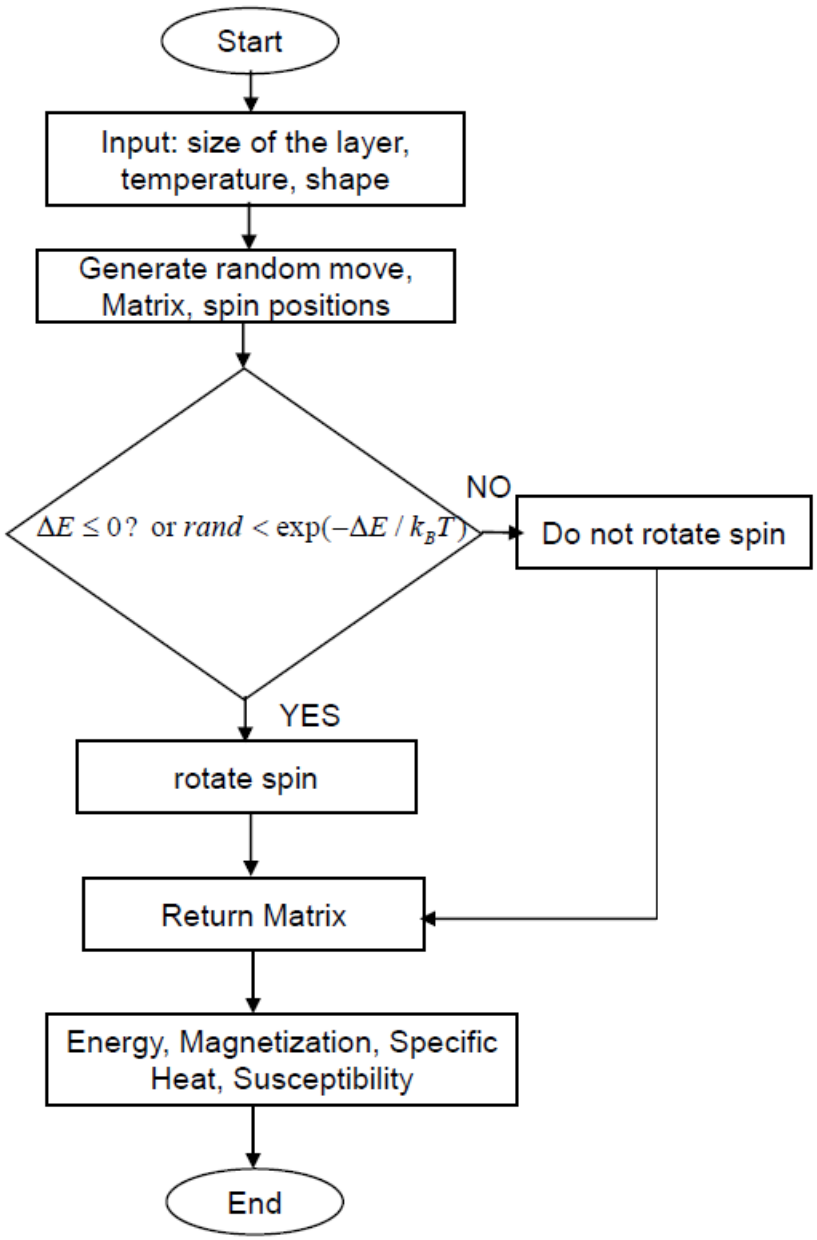

Figure 2-7. Flowchart describing the procedure to investigate the magnetic properties

2-6. Data analysis

We used a radial distribution function (RDF) to reproduce the change observed on the structures of layers and interfaces. An RDF $g(r)$ is the probability of finding an atom at the distance r of another identical atom chosen as a reference.

In statistical mechanics, the RDF (or pair correlation function g(r)) in a system of particles (atoms, molecules, colloids, etc.), describes how density varies as a function of distance from a reference particle.

If a given atom is taken to be at the origin, and if $\rho = N / V$ is the average density of particles, then the local time-averaged density at a distance r from the origin is $\rho g(r)$. This simplified definition holds for a homogeneous and isotropic system.

In simplest terms, it is a measure of the probability of finding a particle at a distance of r away from a given reference atom, relative to that for an ideal gas. The general algorithm involves determining how many atoms are within a distance of r and $r + dr$ away from a reference. Figure 2-8 shows an example of the RDF calculation, where the red particle is the reference atom, and blue atoms are those whose centers are within the circular shell, dotted in orange.

The radial distribution function is usually determined by calculating the distance between all atoms pairs and binning them into a histogram. The histogram is then normalized with respect to an ideal gas, where atoms histograms are completely uncorrelated. For three dimensions, this normalization is the number density of the system (ρ) multiplied by the volume of the spherical shell, which symbolically can be expressed as $\rho 4\pi r^2 dr$

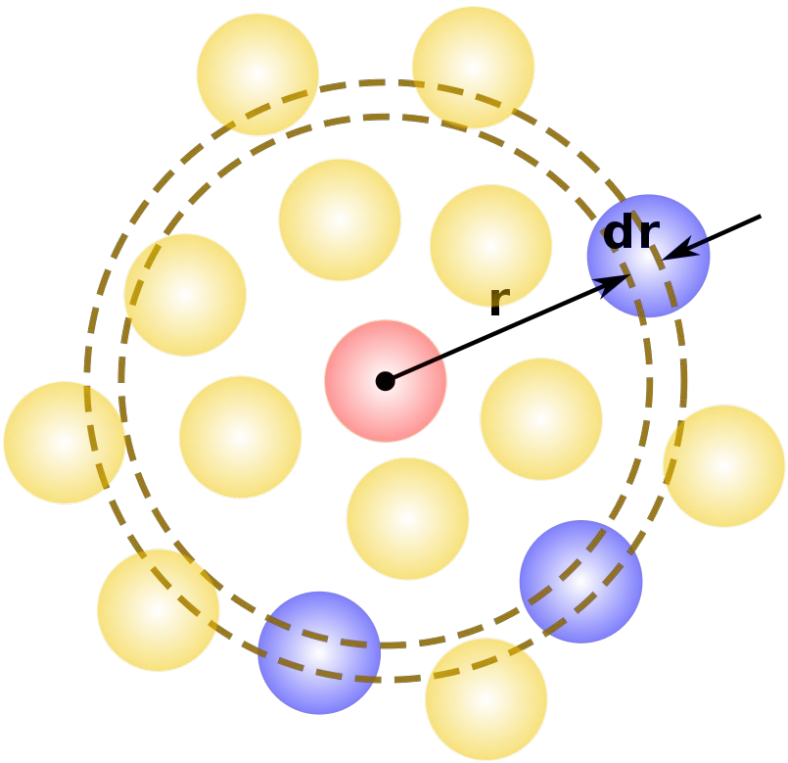

Figure 2-8. Example of the radial distribution function calculation. The pink atom at the center is taken as reference and atoms in blue are located at the distance r from the atom in pink.

2-7. Conclusion

We have presented in this chapter a few numerical techniques, commonly used to study magnetic multilayer systems. Particular attention was paid to the Monte Carlo, which we used to characterize the different multilayer systems obtained through the approach based on the Voronoï diagram. The various force fields used in atomistic simulations are related to the implementation of the interatomic potential. Due to the size limitation, most of those force fields use the interatomic potential derived semi-empirically by making convenient approximations. The modified-embedded atom method (MEAM) has been widely optimized to the study of pure Fe, pure Cu, and Fe-Cu alloy. We have briefly presented in this chapter the history of the MEAM. In the next section, we will use the numerical methodology presented here to build multilayers and investigate the different structural changes due to the reduced dimensionalities and their implications on the magnetic properties.

Chapter 3 Results and Discussion

3-1. Introduction

The discrepancies presented by different experimental techniques of preparation of magnetic multilayer systems have led to numerous alternative methods including the computer simulations. The computational-based approach allows the investigation of the structural, magnetic, and even optical properties of the multilayered systems, at the atomistic level. Thus, it provides insight into the detailed atomic structure of the system, which may be crucial in understanding the origin of interesting unusual properties observed in the nanomaterials or more specifically in the magnetic multilayer systems. For example, the different multilayer systems presented in the first chapter of this thesis, composed of Fe/Cr/Fe, Fe/Cu/Fe, Co/Cu/Co, etc., show results which are mostly based on different techniques used to prepare and/or to characterize the samples. The question of the spacer thickness, which is an essential factor in determining the coupling constant between the magnetic layers, remains debatable. The computational approach, could not only cast doubt on these different experiments but could also help in designing different samples before the experimental procedure, indeed, saving time and resources. This chapter presents our results of simulations on magnetic multilayer systems of Fe/Cu/Fe with thicknesses varying from 6 to 40 Å, conducted during this thesis. The first part of this chapter deals with the structural properties. and the structurally characterized systems are used in the second part to investigate the influence of the structural changes, due to the reduced dimensionality, on the magnetic properties, and the last section compares the current numerical results to the experiment ones.

We first characterized the pure elements of Fe and Cu, which will serve as the references to study the structural changes in our multilayer systems. Since Fe and Cu crystallize in the BCC and FCC systems, respectively, our RDF distance should match the interatomic distance that describes the relationships between the first, second, etc., nearest neighbors in each cubic system. Considering this approach, an example of the RDF of pure structures of Fe and Cu, obtained from the atomic visualization in Figure 3-1, is shown in Figure 3-2. We calculated the distance between the first,

second, etc., nearest neighbors, for the pure elements of Fe and Cu, which gave 2.48 Å, 2.86 Å and 2.56 Å, 3.61 Å respectively. Interestingly, these positions matched the first, second, etc., atomic planes given by the Bragg's law. We will use the structures shown in Figure 3-2 throughout this thesis to explain the changes due to the reduced dimensionalities either at the interface or in the bulk of the layers composing the system. This use of RDF is particularly interesting in the sense that the simulations can be compared to the experiments, as shown in Table 1-3, which gives the different values often observed when characterizing the cubic system with X-ray crystallography. We notice that X-ray crystallography is the most widely used method to characterize the change in the experimentally fabricated structures.

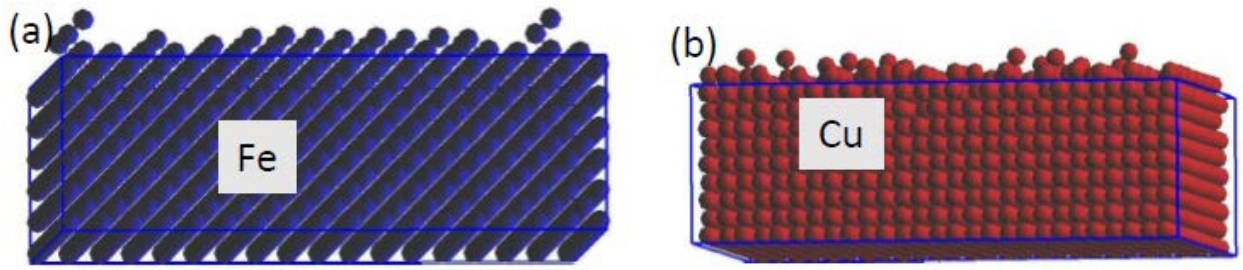

Figure 3-1. Atomic representation of the pure structures of (a) Fe (blue) and (b) Cu (red). The structures are obtained by Voronoï construction.

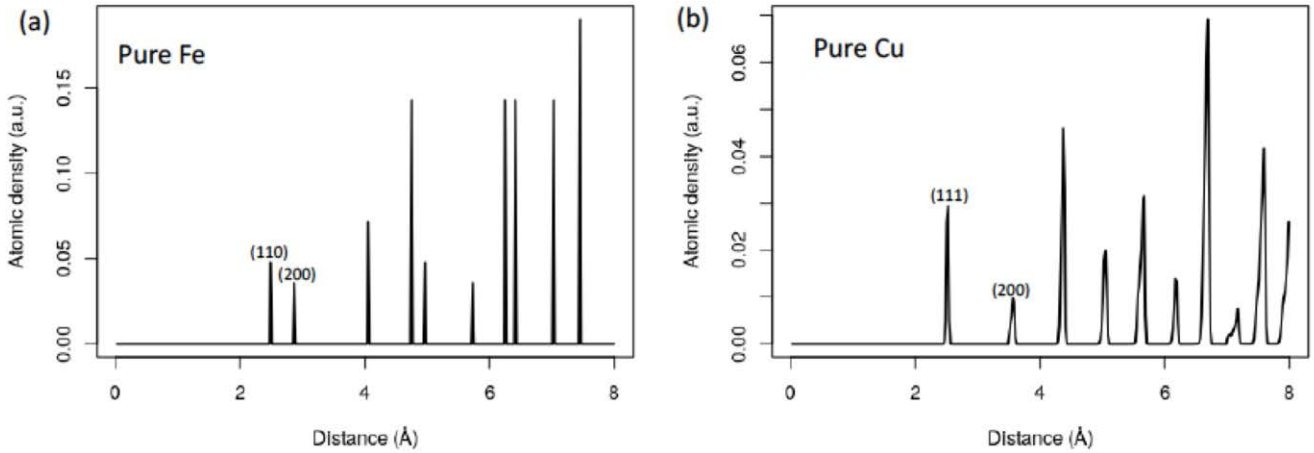

Figure 3-2. Radial distribution function (RDF) of pure bulky Fe (a) and Cu (b). The two first planes are also shown for both elements.

3-2 Structural properties of Fe/Cu/Fe multilayers

3-2.1 Test of the simulation model

We tested the capability of the model used in this thesis to simulate the properties of the system by conducting the simulated annealing procedure on a large amorphous system, with a thickness of 200 nm composed of 50% atoms of Fe and 50% atoms of Cu (Figure 3-3).

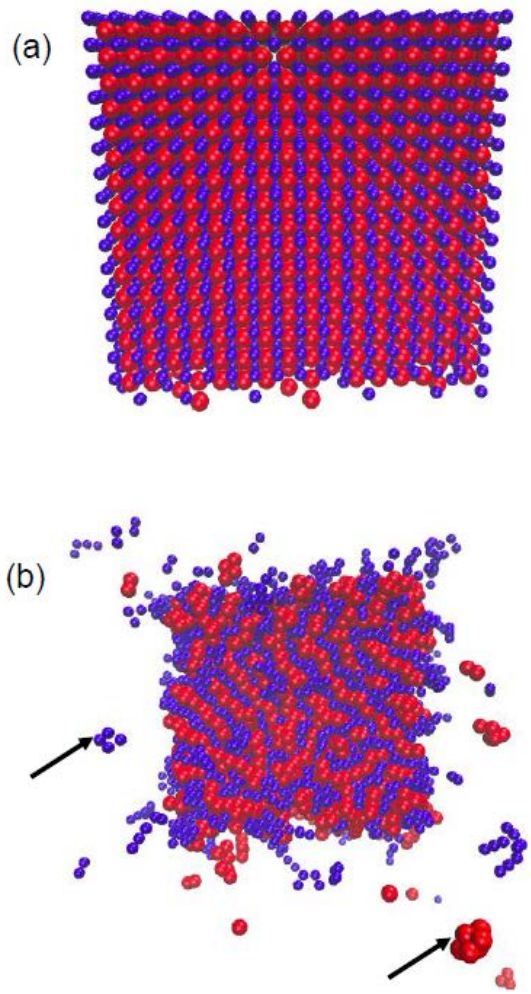

Figure 3-3. An amorphous system composed of 50% Fe (blue) and 50% Cu (red) before (a) and after (b) simulated annealing. One can see that even outside of the simulation box, atoms form agglomeratess of the same type; thus justifying the capability of our potential to reproduce the different interactions

As shown in Figure 3-4, one can see that the system before the simulated annealing process contains both the BCC and FCC structures. Also, the presence of a first small peak before the first atomic plane of the BCC structure is observed. This first little peak may be as a result of an undefined atomic plane due to the presence of Cu atoms. On the other hand, after simulated annealing, the pure BCC structure of Fe is completely recovered. Similar observations were made on the structure of Cu. We can justify this behavior by the fact that the number of atoms of each element is large enough (50%), and the atoms tend to form agglomerates of the same type, even at the bulk of the simulation box. This is not surprising; in fact, formation of agglomerates of the same kind reduces the energy of the system, which for each element is minimum when the structure is similar to that of the bulk material.

Similarly, Figure 3-5 shows the RDF of Cu before and after the simulated annealing process. One can see that the structure before the simulated annealing resembles a mixture of both FCC and BCC structures, due to the presence of Fe atoms and no preference to a particular type of agglomerates before the simulated annealing (Figure 3-5 a). When the system is cooled down, agglomerates of each type are formed, resulting in the structures similar to that of the bulk (Figure 3-5).

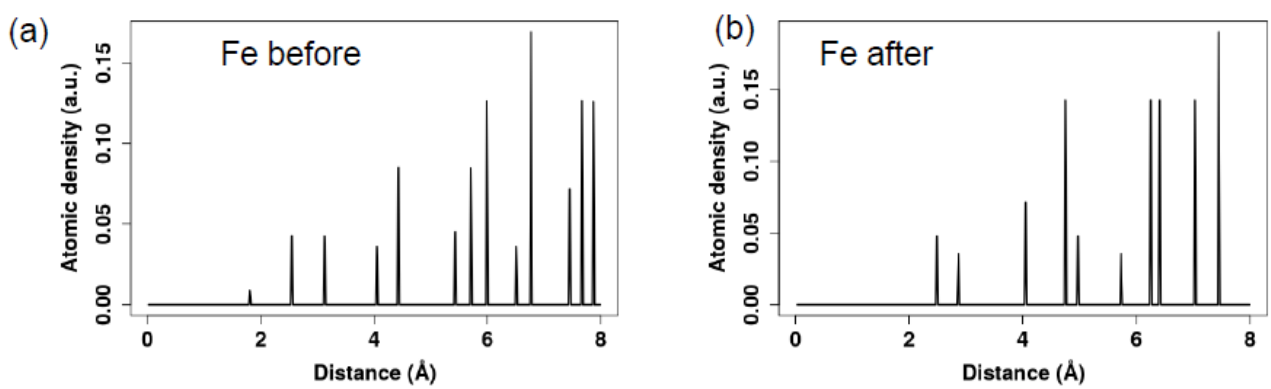

Figure 3-4. RDF of Fe before (a) and after (b) simulated annealing process. The conserved atomic density versus inter-plane distance is shown. One can also notice the absence of a few peaks from (b), which shows the distribution of the pure Fe after the simulated annealing process.

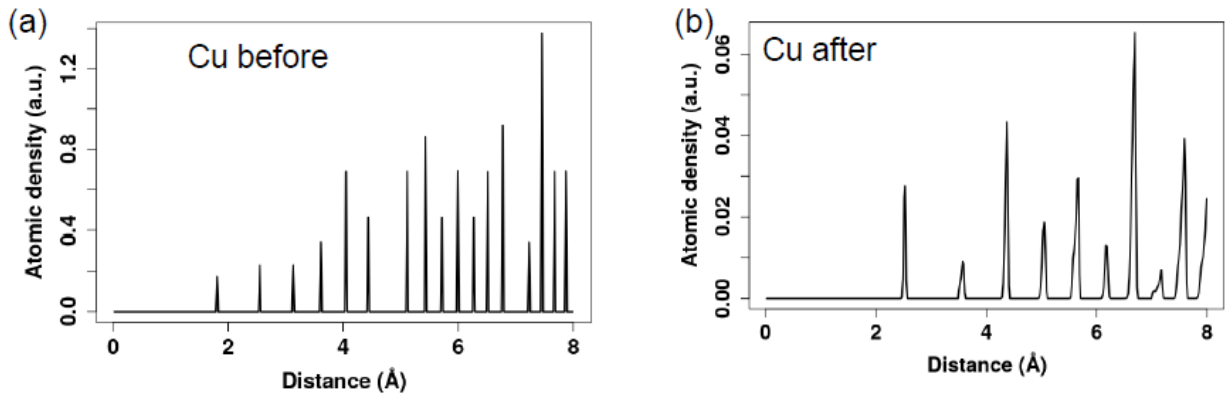

Figure 3-5. RDF of Cu before (a) and after (b) simulated annealing process. The conserved atomic density versus inter-plane distance is shown.

3-2.2 Properties of the magnetic bilayer systems

Numerous results present in the literature are based on bilayer systems. To get insight into the role played by a system with only two layers on the properties of the system, as compared with that of the multilayer systems (m >2, where m is the number of layers), we conducted the simulations on the bilayer systems Fe/Cu, by varying the thicknesses of both Fe and Cu layers and we compared the results with the experimental ones [26, 32, 82].

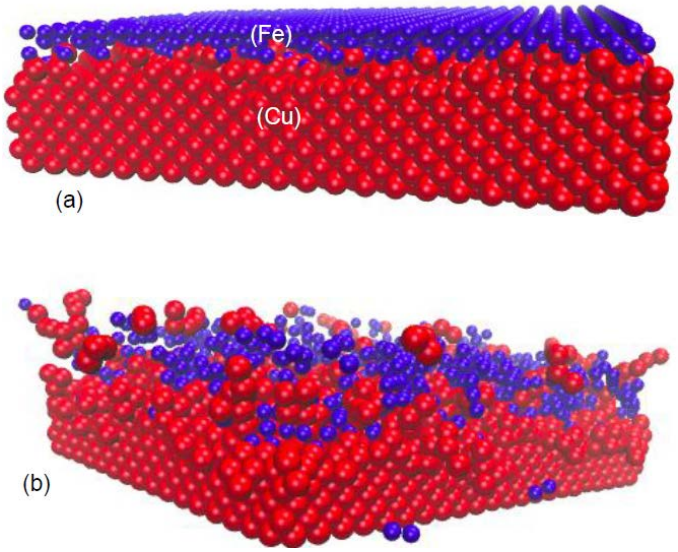

Figure 3-6. Structure of Fe/Cu (the thicknesses of Fe and Cu layers are 5 and 15 Å, respectively) before (a) and after (b) simulated annealing. One can see the presence of Fe atoms even in the bulk of Cu, due to their reduced size as compared to that of Cu.

The first system is Fe_5Cu_{15} (Å) (see Figure 3-6), where 5 and 15 are respectively the thicknesses of Fe and Cu in Å. Figure 3-7 shows the RDF_s after the simulated annealing process. It can be seen that the structure of Cu, FCC (a), is conserved, while that of Fe remains similar to the structure observed at the interface (b-d). This behavior is due to the large thickness of the Cu layer, therefore, leading to a high proportion of Cu atoms at the interface. It is interesting to see the persistence of the BCC structure of Fe, although for the short-range. This implies that the Fe layer remains magnetic, but with a reduced magnetism as was experimentally shown [26, 32]. We note in passing that both interfaces are represented by Fe-Cu, where Fe is deposited on Cu, and Cu-Fe, where Cu is deposited on Fe.

The behavior at the interface can be assimilated to that of Cu at least for the first atomic planes. At the bulk of the interface, both Cu and Fe coexist, but the atomic proportion is small to allow the formation of an agglomerates of the same type, which may lead to a mixed structure, FCC and FCC, at the interface. Before we test this hypothesis, we also kept the thickness of Cu low at 5 Å and we set that of Fe at 15 Å (Figure 3-8).

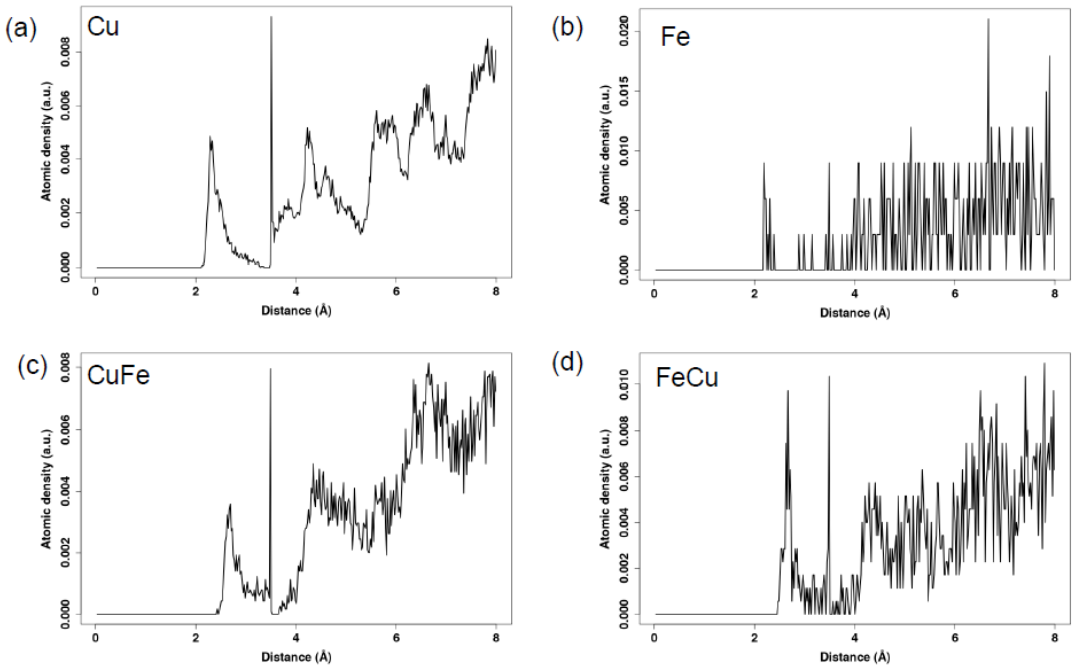

Figure 3-7. RDF of the bilayer system Fe_5/Cu_{15}. The FCC structure of Cu is conserved (a); the structure of Fe is similar to that of the interface (b-d). One can see that due to the lower thicknesses of both layers, 15 and 5 Å for Cu and Fe respectively, the structure of the bulk Cu is conserved through the system.

As a result, similar observations were made (Figure 3-9). This time, the structure of Fe, which is BCC, is reproduced at the bulk of the layer as well as at the interface (a, c, d). On the other hand, the structure of Cu is similar to that seen at the interface. This confirms the fact that in such bilayer systems, the structure of the system is dictated by the structure of the thickest layer. Furthermore, the interface and the thinner layer have a similar structure.

These findings are essential in a sense they may help to design multilayer systems, that are not only thinner but also present interfaces with similar properties as those of the bulk. Additionally, with the small interface, the interlayer coupling could be considerably reduced, indeed, resulting in the high transfer rate of those systems to the industrial scale. It is worth mentioning here that one of the limitations of the GMR composed of Fe/Cr/Fe is the high antiferromagnetic coupling between Fe and Cr. One of the active areas is to use noble metals, which have less antiferromagnetic coupling. This is particularly important in the industry of magnetic recording media.

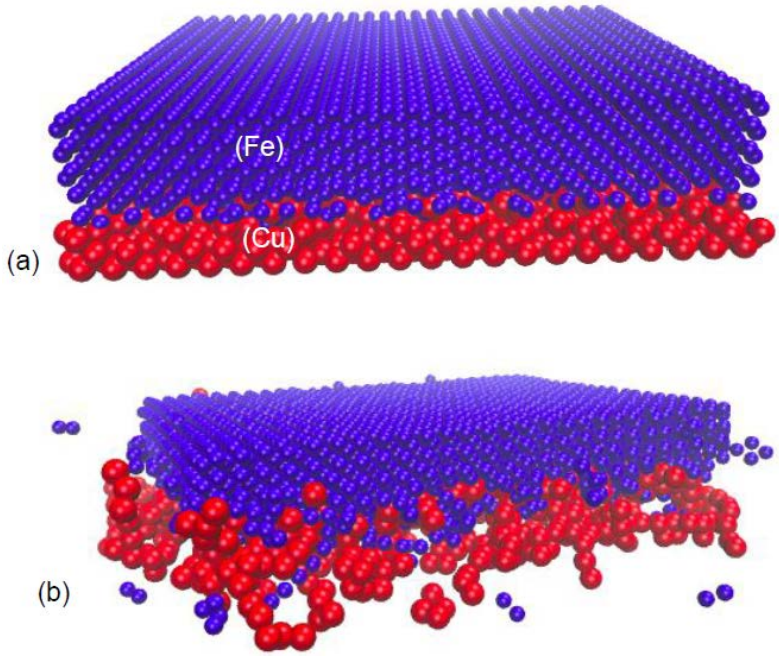

Figure 3-8. The bilayer $Fe_{15}Cu_5$ system before (a) and after (b) simulated annealing. Cu is completely at the interface due to its low thickness

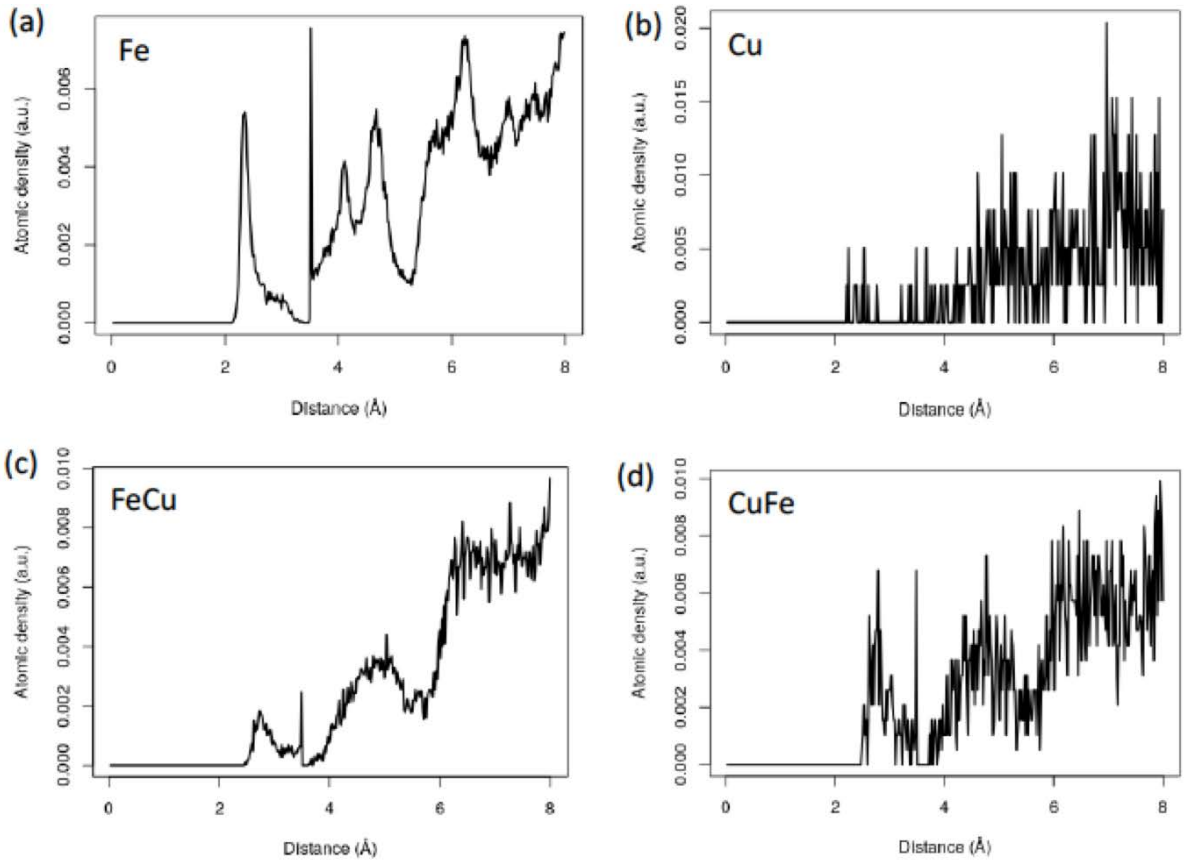

Figure 3-9. RDF of the bilayer system of Fe_{15}/Cu_5. The BCC structure of Fe is conserved (a); the structure of Cu is similar to that of the interface (b-d). One can notice the presence of the first atomic plan of the FCC structure of Cu. This is due to the large atomic radius of Cu as compared to that of Fe. Near the interface, Cu atoms tend to dominate and dictate the FCC structure of Cu.

We were interested here to know if increasing both thicknesses may lead to the formation of a agglomerates of different types. We then set both thicknesses at 35 Å (Figure 3-11). Two scenarios can be expected: whether Fe is deposited on Cu or vice versa. In past experiments, this phenomenon has sometimes led to the misinterpretation of the results and was assigned to the method used. We then first considered the case where Fe is deposited on Cu (Figure 3-10), which is similar to the bottom-up approach discussed in the Chapter 1. It is clear from the results that although the Cu layer is completely FCC (a), the structure of Fe remains similar to that seen at the interface, regardless of the Fe layer thickness (b). The first peak is identical to that seen in the pure

structure of Fe, and the second is formed between the second atomic plane of Cu and the third atomic plane of Fe. Beyond the first two atomic planes, the structure of the Fe layer tends to an amorphous structure, as the one observed in the structure of Fe_5/Cu_{15}. We then wonder if this is a property of Cu buffer, and we performed another set of simulations by switching both thicknesses.

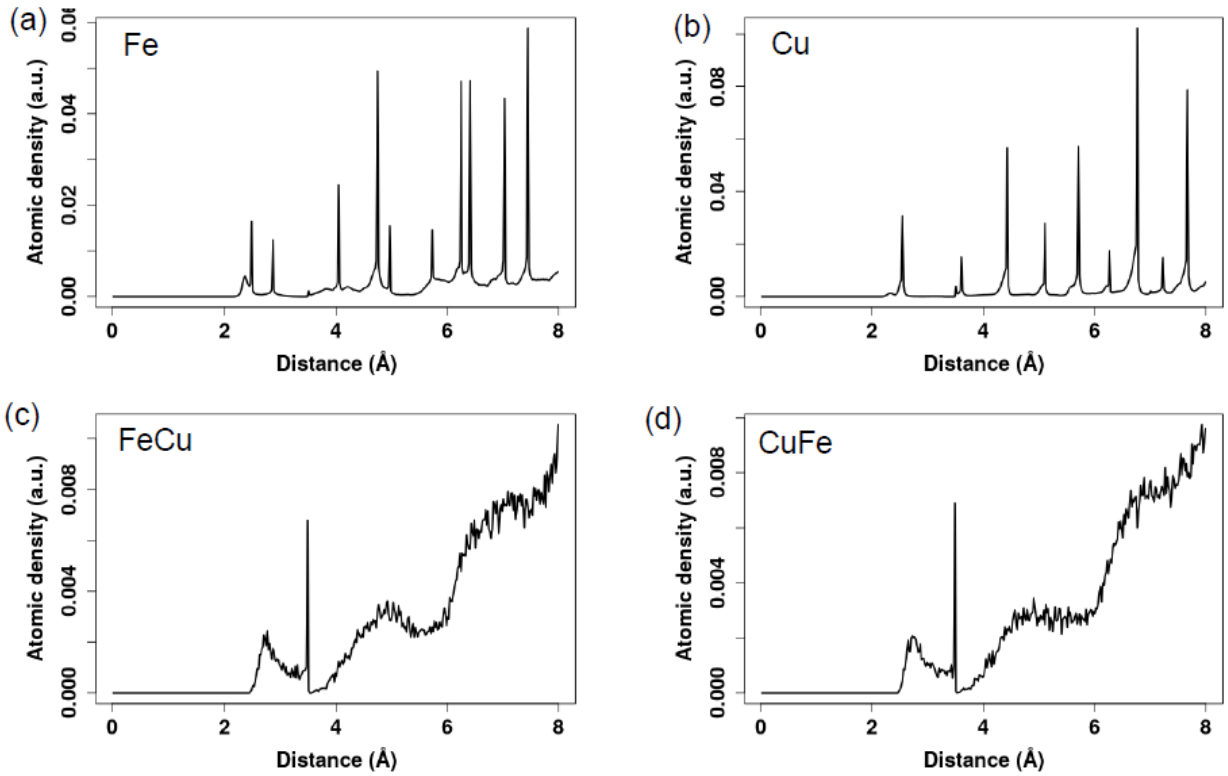

Figure 3-10. RDF of the Fe_{35}/Cu_{35}, when Fe is deposited on Cu, with the same thickness, 35 Å. The FCC structure of Cu is reproduced (a). The structure of Fe (b) is similar to that observed at the interface (c, d). These observations confirm the hypothesis that investigations on bilayer systems may take into account the substrate layer as it may primarily affect the structure of the system.

The results from the simulations are shown in Figure 3-12. One can notice that the roles have reversed. While it is clear that the structure of the Fe layer is similar to that of the pure Fe, the structure of the Cu layer is identical to that of the interface than pure Cu. Interestingly, the same amorphous system is observed above the second atomic plane corresponding to (200).

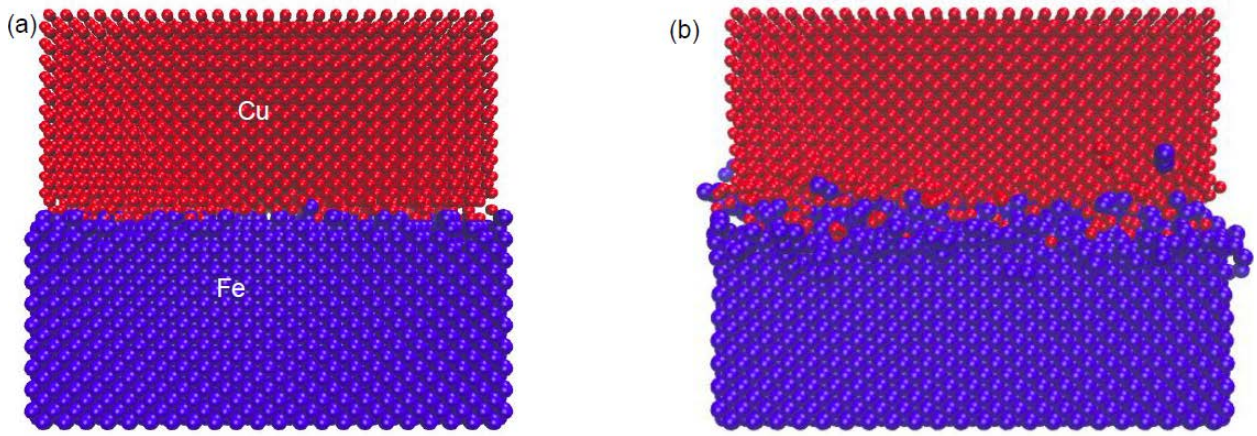

Figure 3-11. Structure of Fe_{35}/Cu_{35} before (a) and after (b) simulated annealing.

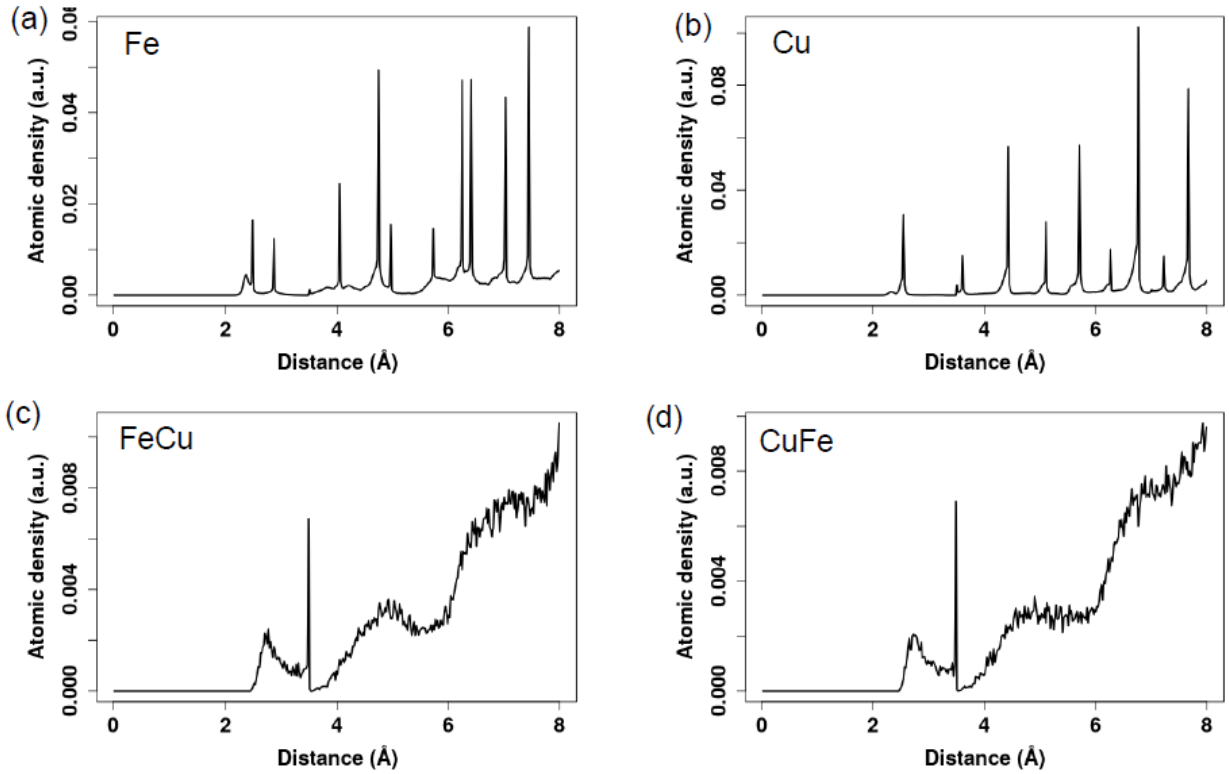

Figure 3-12. RDF of the Fe_{35}/Cu_{35}, when Cu is deposited on Fe, with the same thickness, 35 Å. The BCC structure of Fe clearly reproduced (a). Although the structure of Cu layer (b) is similar to that of the interface (c, d), the presence of the second peak less pronounced (b) implies the (200) second atomic plane of Fe. Both interfaces, Cu-Fe and Fe-Cu, show the same distribution.

These observations confirmed the high impact of the buffer layer on the structure of the adjacent layer. Can this behavior explain the discrepancies observed among different experimental techniques of elaboration and characterization of magnetic multilayer systems[26, 82, 83]. To answer this question, we further performed simulations on the magnetic trilayer systems with different values of thicknesses, from 6 to 40 Å. The results should hopefully shed light on the unusual properties of the bilayer systems.

3-2.3 Structural characterization of the trilayer systems

View the importance of multilayer systems composed on trilayers [14, 15, 38, 39, 84], we found interesting to perform simulations on the trilayer system to draw a compelling conclusion on the effect of the third layer. An example of a trilayer system studied in this work in given in Figure 3-13, which shows the trilayer system of Fe/Cu/Fe with a thicker spacer Cu layer. Let us recall that the system is obtained using the Voronoï approach. One can also see the presence of Cu atoms close to the bulk of Fe, implying the coexistence of both elements, although they are known as repulsive elements in nature, based on their phase diagram. The fact that both types of atoms prefer to coexist even far from the interface may also imply that forming a mixed structure is energetically favorable to the system than forming agglomerates of each type. The structure in Figure 3-13 was obtained for the trilayer $Fe_7/Cu_{25}/Fe_7$.

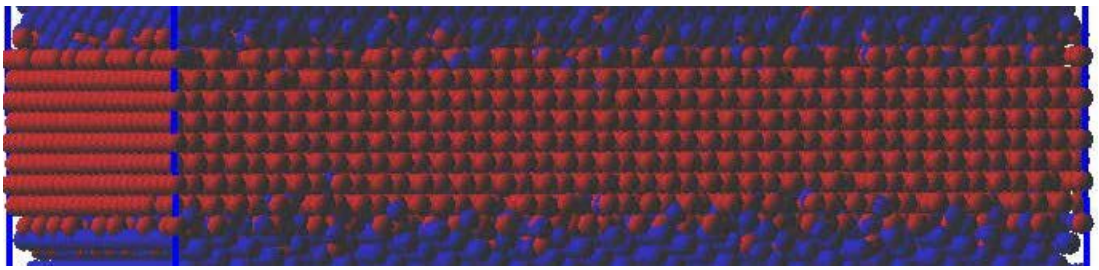

Figure 3-13. The trilayer system $Fe_7/Cu_{25}/Fe_7$. The atomic planes of Fe and Cu are shown in blue and red respectively. One can see that the Fe layers are almost consumed by the interfaces Fe-Cu and Cu-Fe.

We started this part by keeping the thickness of Cu fixed at 25 Å and gradually increased that of Fe from 7 to 34 Å, according to different experimental results present in the literature [23, 32]. As expected, the layer with high thickness tends to dictate the structural behavior of the whole system. However, compared to the case of bilayer systems, there may exist a specific critical thickness where both structures, FCC and BCC, are present in the system.

The results of the simulations of the $Fe_7/Cu_{25}/Fe_7$ system is shown in Figure 3-14. The structure of Cu, FCC, is shown in (a). The presence of Fe atoms at the interface can be visualized on the plot, where the first and second atomic planes of the BCC Fe are shown (a, b). This could indicate that if one of the layers forming the system has a thickness below the critical value, the system will preferably form mixed compounds at the interface and even a few atomic planes far from the interface. The structure of the interface remains dominated by that of the thickest layer (c, d).

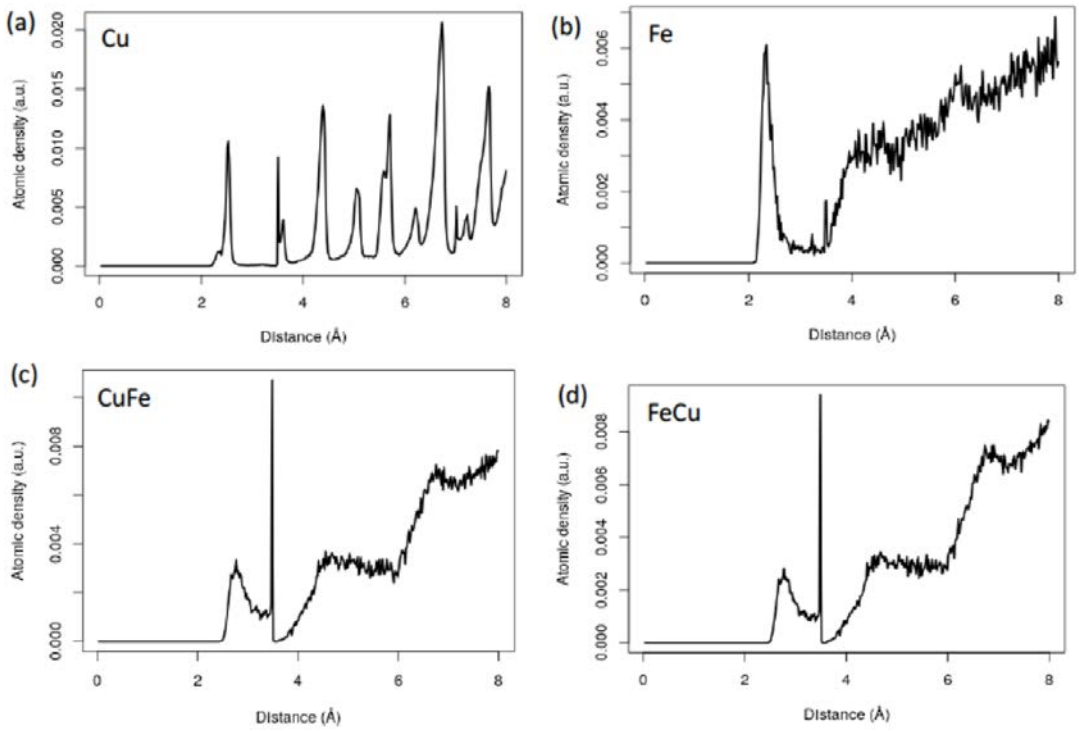

Figure 3-14. RDF of the $Fe_7/Cu_{25}/Fe_7$ system. At a sufficiently large value of the thickness of Cu (a) and lower value of the thickness of Fe (b), the FCC structure of Cu is conserved (a) while the Fe layer copies both FCC and BCC structures for its first two atomic planes and adopts an amorphous structure beyond. The presence of the FCC structure at the interface can be seen even beyond the first atomic planes (c, b). This means that the structure of the largest thickness dominates the system.

Increasing the thickness of the Fe layers led to a transition from amorphous to a structure close to that of the bulk Fe (Figure 3-15). Figure 3-16 ($Fe_{18}/Cu_{25}/Fe_{18}$) shows the results after the simulated annealing. The FCC structure of Cu is conserved while the BCC structure of Fe starts to form even beyond the fourth atomic plane. This implies that the different thicknesses in this regime are high enough to reproduce the bulk system. Furthermore, the mixed structure of the interface is less pronounced, probably due to the structural change in the Fe layer. This disturbance of the interface could also be explained by the fact that atoms of Fe, initially present at the interface, will prefer to join those of the bulk Fe, resulting in the structural rearrangement in both structure of Cu and the interface.

Predicting the correct critical value for which the structure of Fe remains BCC is essential to define the magnetism of the system. It has been shown that as long as the structure of Fe remains BCC, its net spontaneous magnetization is non-null.

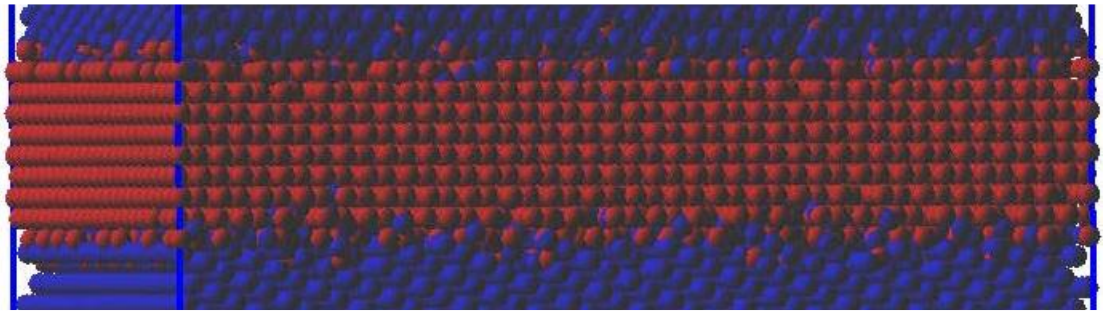

Figure 3-15. The trilayers system $Fe_{18}/Cu_{25}/Fe_{18}$. The atomic planes of Fe and Cu are shown in blue and red, respectively. One can see the formation of the atomic plane of Fe layers upon increasing its thickness. At the interface, atoms prefer to form agglomerates of the same type, leading to the transition from the amorphous to mixed FCC and BCC structures.

We further performed simulations where both elements have the same thickness on the system $Fe_{25}/Cu_{25}/Fe_{25}$. Its visualization is shown in Figure 3-17. One can see that even at the interface, atoms form agglomerates of the same type, which is the result of the formation of a mixed BCC and FCC interface, and each layer copying the structure of its bulk element respectively.

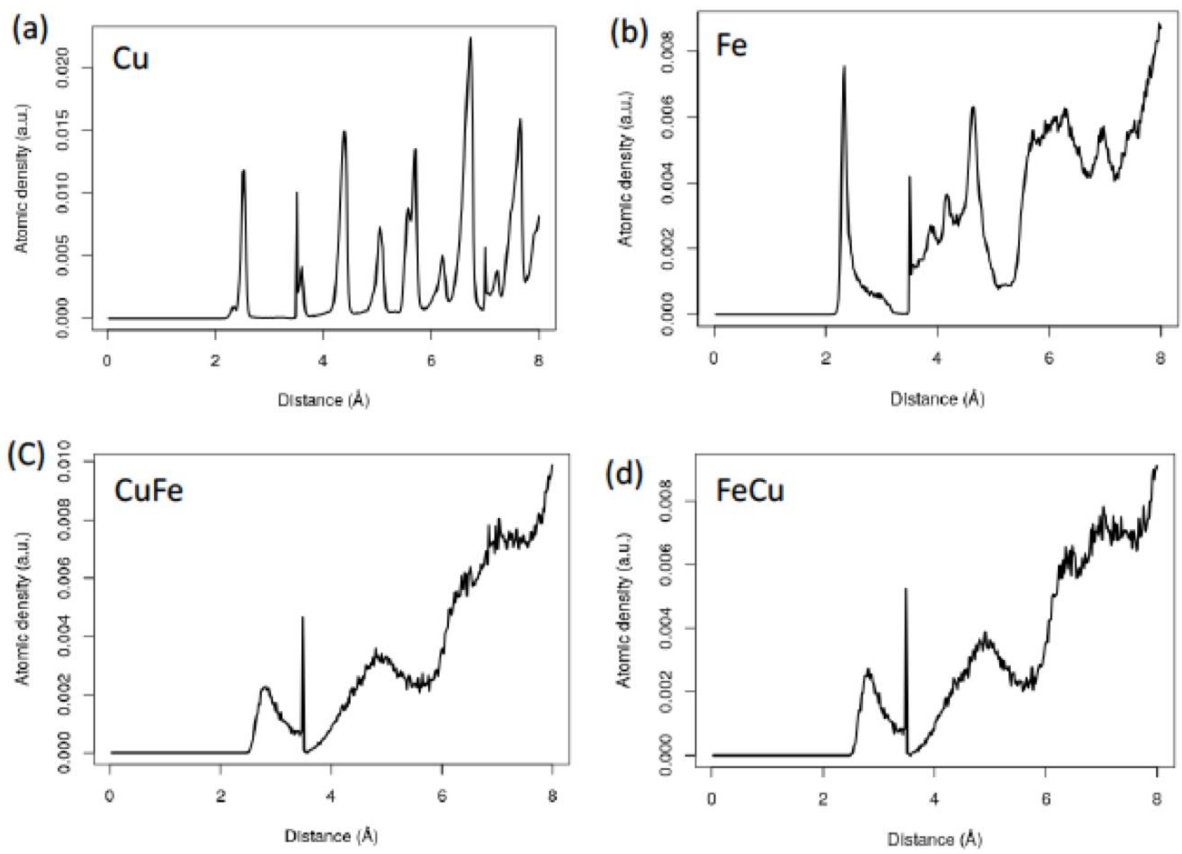

Figure 3-16. RDF of the $Fe_{18}/Cu_{25}Fe_{18}$ system. The Cu layer conserves its FCC structure regardless of the Fe layer. In contrast to the bilayer system, increasing the thickness of the Fe layer leads to a smooth transition from a mixture (FCC and BCC) to the BCC structure, as seen in the pure structure of Fe (b). The interface structures remain dominated by the FCC structure (c, d), although the first is disturbed due to the transition observed in the Fe structure.

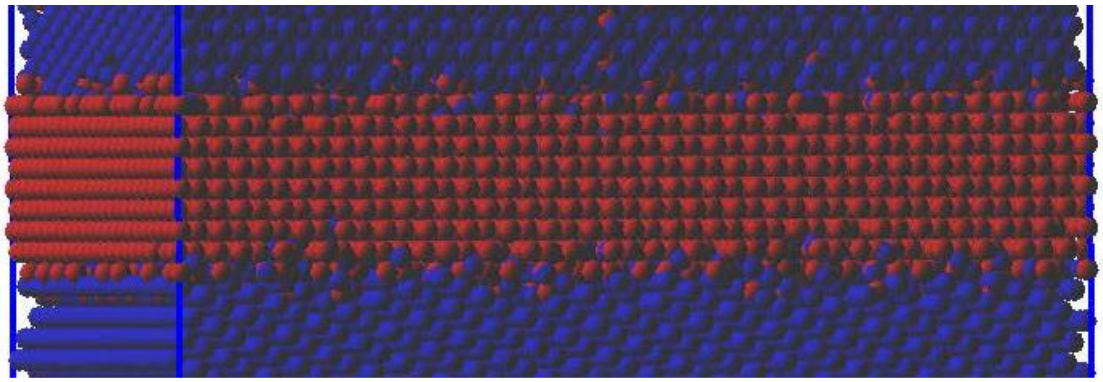

Figure 3-17. The trilayer $Fe_{25}/Cu_{25}/Fe_{25}$ system. The atomic planes of Fe and Cu are shown in blue and red, respectively. Each layer shows the well-pronounced atomic planes as a result of the formation of the structures similar to that of the bulk.

As a result, the conservation of the structure of layers Cu, FCC, and Fe, BCC is shown in Figure 3-18 (a, b). This behavior is not surprising since both layers are sufficiently thick to form agglomerates of each type, even when approaching the interface. This is in accordance with the structure of the interface, which shows a well-pronounced mixture of both structures, FCC and BCC Figure 3-18 (c, d). An interesting point here will be to observe the effect of this structural transition on the magnetic properties. Due to a growing demand in the miniaturized electronic devices, limiting the composition of such a system to a few atomic planes while still keeping at least the magnetic properties of the bulk system, could help the magnetic recording media industry to design new electronic devices with better features.

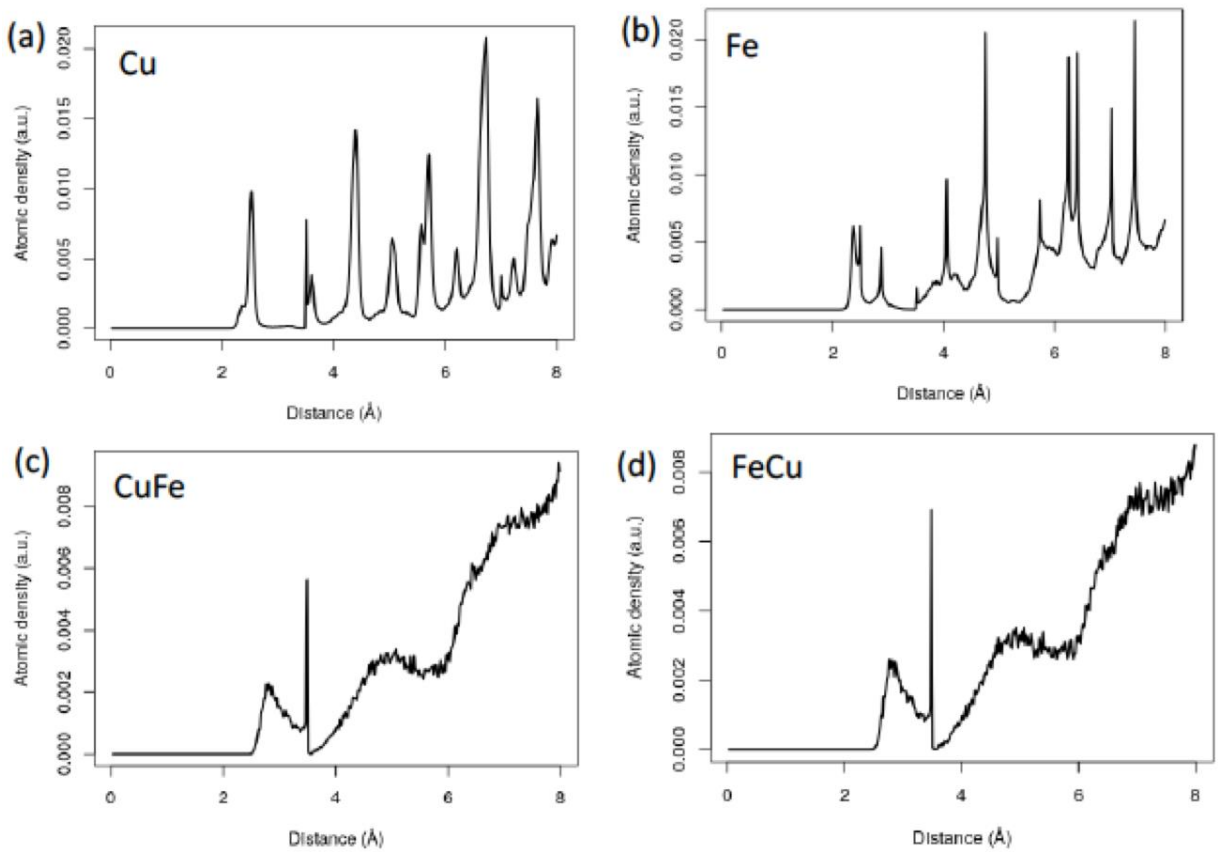

Figure 3-18. RDF of the $Fe_{25}/Cu_{25}/Fe_{25}$ system. Cu layer remains FCC (a), while the Fe layer shows the presence of the BCC atomic plan through the layer (b). The large atomic radius of Cu can justify the presence of the FCC structure in the Fe layer, a third small peak (b) compared to that of Fe, which dominates the interface. The interface shows a mixture of both FCC and BCC structure (c, d).

A further increase of the Fe thickness layer did not have much effect on the structural properties of the system, as shown in Figure 3-28. The structure of each layer is similar to that shown by the bulk system, Cu (FCC), and Fe(BCC), see Figure 3-19 a, b. The structure of the interface remains composed of both FCC and BCC structures (c, d).

Contradictory to the observations made on the bilayer systems, one can see that at a specific critical value of the thickness of the Fe layer (18 Å), its structure transitions towards the bulk one, leading to a structural rearrangement at the interface. The growth condition may affect the properties of the system, as was noticed by Ortega et al. [12, 85, 86]

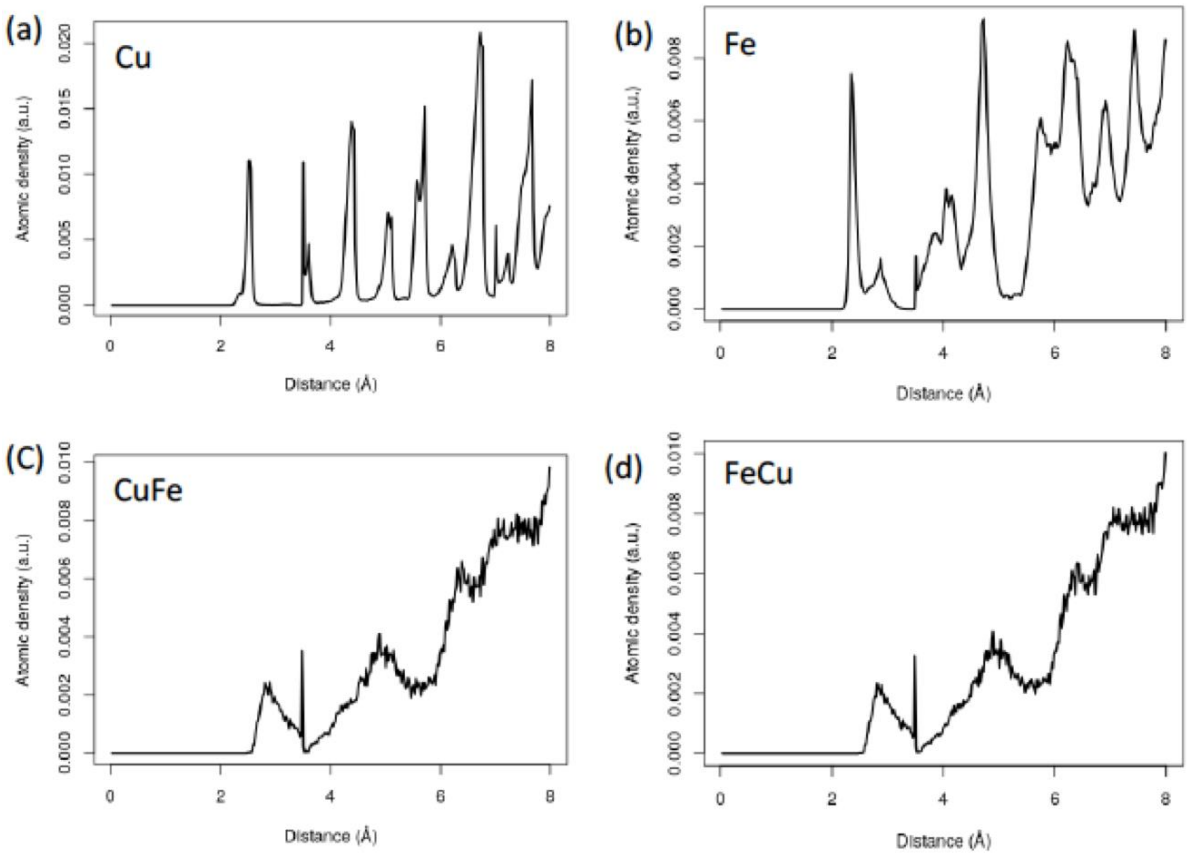

Figure 3-19. RDF of the $Fe_{34}/Cu_{25}/Fe_{34}$ system. No considerable change is observed either for the Cu layer, FCC (a), Fe layer, BCC (b) distorted at the interface by the presence of the Cu atoms, and both interfaces remain mixed dominated by the FCC structure.

This part discusses the change in the structure of magnetic multilayer systems Fe/Cu/Fe with variable spacer thickness. We gradually changed the thickness of the Cu layer and we used the RDF distribution to describe the structural rearrangement. The value of the width of the Cu layer varies from 6 to 40 Å, with the thickness of Fe kept fixed at 21Å. In general, we are expecting to see more structural change, due to the large atomic radius of Cu (around 3.615 Å), as compared to that of Fe, which about 2.860 Å. In fact, as the Cu's thickness increases, its atoms will quickly form an agglomerates of Cu, leading to an early phase transformation. We started the simulations on a $Fe_{21}/Cu_{6}/Fe_{21}$ trilayer system (see Figure 3-20 for reference).

Due to the low thickness of the Cu's layer, the Fe structure of the Fe layer is disturbed regardless of its large thickness. The BCC disturbed structure of the Fe layer (see Figure 3-21 a) is caused by the presence of large Cu's atoms at the interface, which are seen as large impurities in the crystal structure of Fe, that create dislocations, thus, leading to an irregular cell compared to the unit cell of the pure Fe. On the other hand, the presence of both structures, BCC and FCC is well pronounced in the structure of the Cu layer (Figure 3-21 b). This is due to the lower value of the thickness of the Cu layer in which Fe atoms are present even in the bulk of Cu (for reference, see Figure 3-13). At the interface, although dominated by the BCC structure, the second well-pronounced peak implies the presence of the FCC structure (Figure 3-21 c, d).

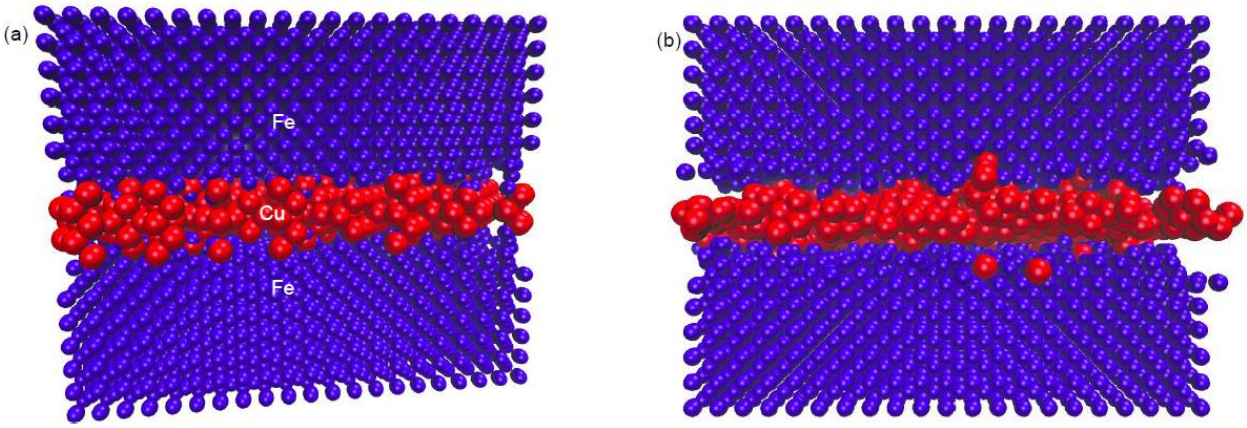

Figure 3-20 The trilayers $Fe_{21}/Cu_6/Fe_{21}$ system before (a) and after (b) the simulated annealing. The atomic planes of Fe and Cu are shown in blue and red, respectively. One can see the presence of Fe atoms even in the bulk of the Cu layer. Additionally, the atoms of Cu disturb the structure of the Fe layer on multiple planes, thus justifying the less pronounced structure of the Fe layer close to the interface. The interfaces remain dominated by the atoms of Fe, which impose the formation of the BCC structure.

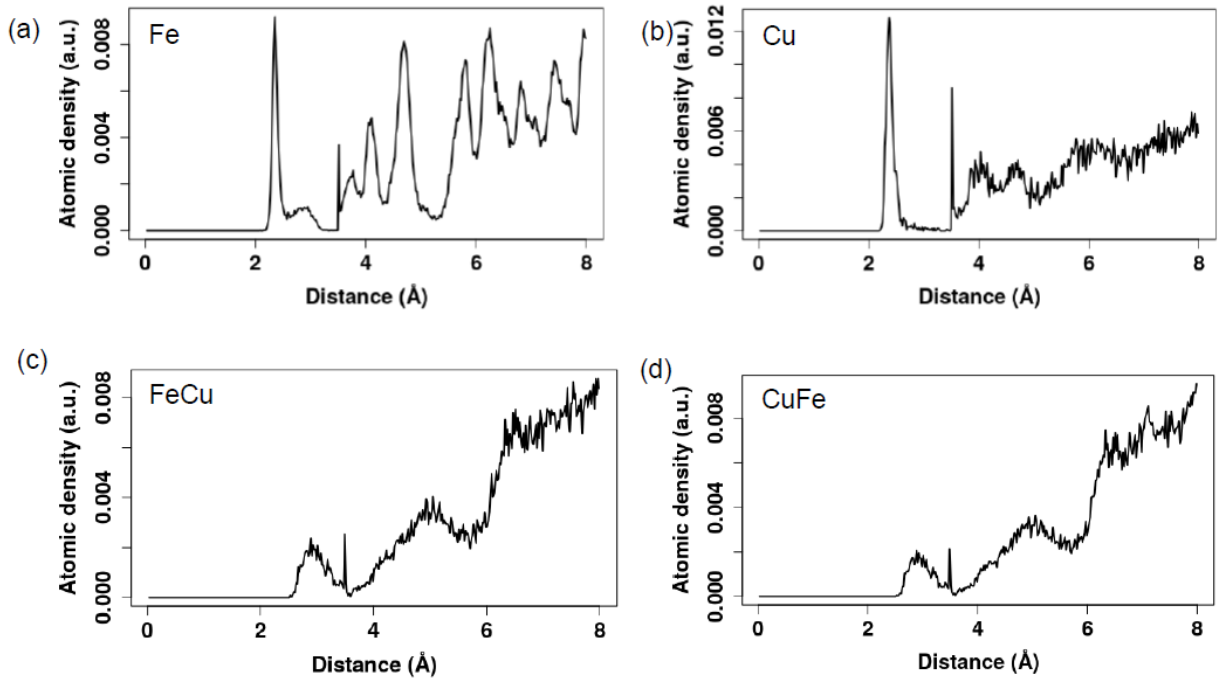

Figure 3-21. RDF of the $Fe_{21}/Cu_6/Fe_{21}$ system. (a) shows the conserved BCC structure of the Fe layer, although disturbed by the presence of Cu atoms on the first atomic planes. (b) shows the mixed structure (BCC and FCC) of the Cu, where the first peak implies the presence of BCC at the surface of Cu. The less pronounced presence of the BCC structure beyond the first atomic plane could be justified by the large atomic radius of the Cu, which limits the interpenetration of the Cu atoms into the Fe bulk. The interfaces are dominated by the FCC structure, probably due to its high proportion at the interface (c, d).

The transition from mixed structure to a structure close to that of bulk Cu was seen upon a slight increase in its thickness. The system was $Fe_{21}/Cu_{13}/Fe_{21}$ and the results are shown in Figure 3-23.

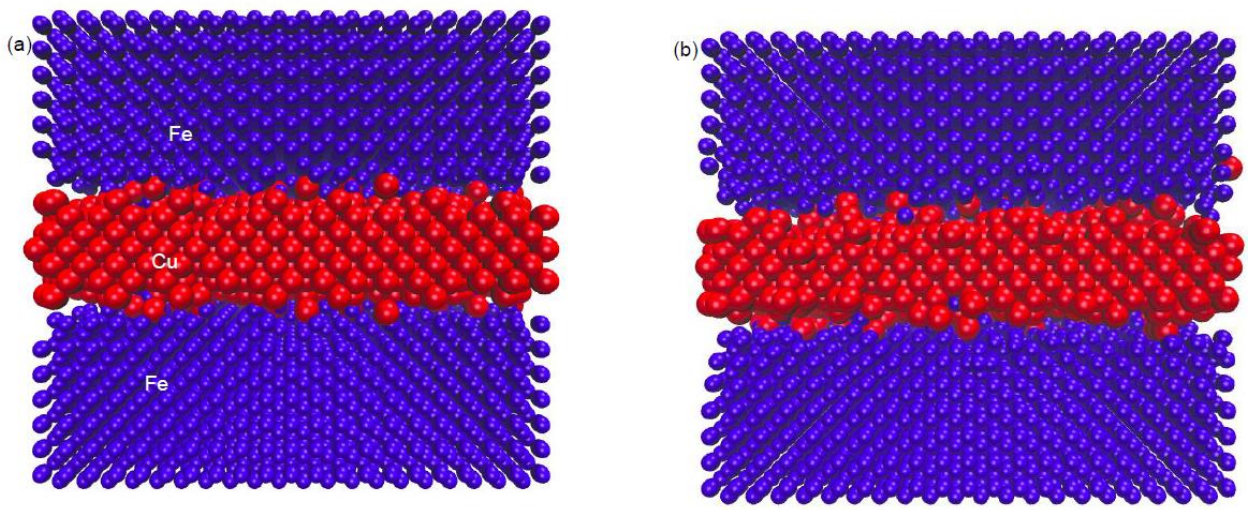

Figure 3-22 The trilayer system $Fe_{21}/Cu_{13}/Fe_{21}$ before (a) and after (b) the simulated annealing. The atomic planes of Fe and Cu are shown in blue and red respectively. One can see the formation of the different atomic planes of Cu, while the atoms of the interface tend to interact with atoms of the same type. These observations can help to explain the transition observed in Figure 3-23

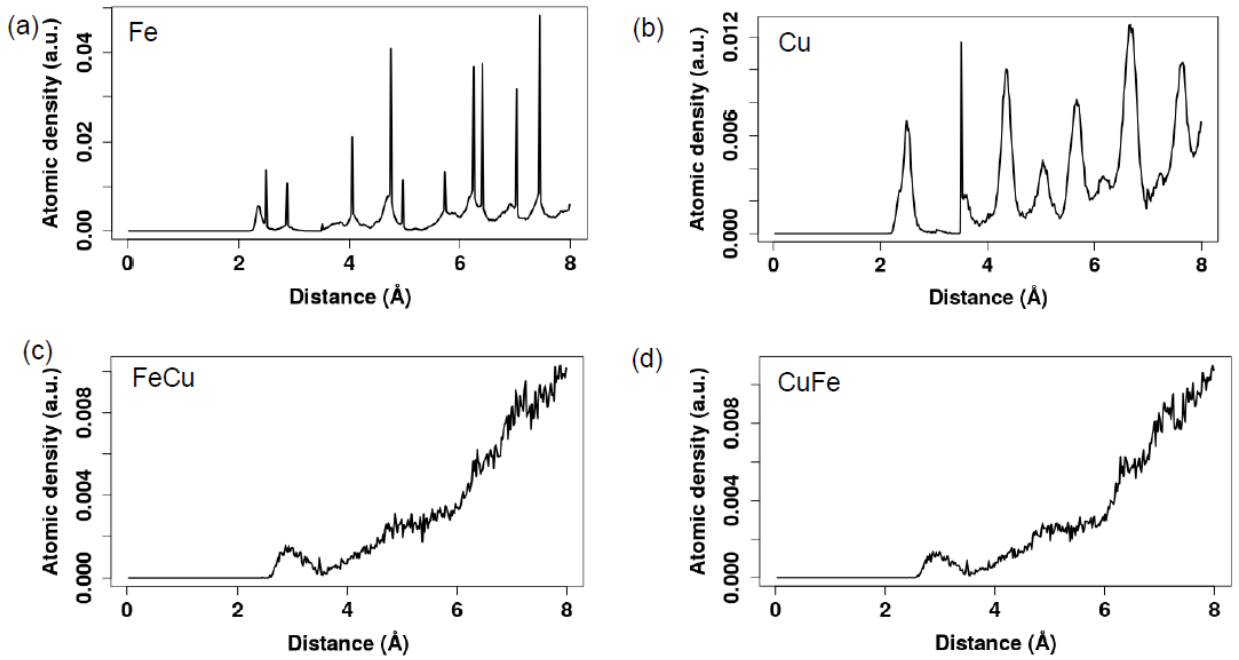

Figure 3-23. RDF of the $Fe_{21}/Cu_{13}/Fe_{21}$ system. Fe has conserved its BCC structure, less disturbed by the presence of the Cu atoms (a). During the growth process, atoms of Cu will tend to form an agglomerates composed uniquely of Cu atoms, thus limiting the disturbance of the Fe layer at the interface. (b) shows the FCC structure of Cu, while the effect of the transition is seen at the interface (c, d).

Amazingly, the structure of the Fe layer also changes upon the increase of the Cu's layer thickness, what was surprising as we were expecting more disturbance (Figure 3-23 a). One can see the disappearance of the Cu atoms on the first atomic planes of the Fe layer. As an explanation, we can say that when the atomic proportion of Cu atoms reduces at the interface, it leads to a structural rearrangement of the whole system. The structural rearrangement is seen on the structure of the interface, which shows a broader peak on the first atomic plane, but quickly transitions to an amorphous system (Figure 3-23 c, d). The structure of the Cu layer is pretty close to that of the bulk Cu, FCC (Figure 3-23 b).

A further increase of the Cu thickness layer to 24 Å (see Figure 3-24) leads to the disturbance of the structure of the Fe layer (Figure 3-25 a) as well as that of the interface (Figure 3-25 c, d). The structure of the Cu layer remains FCC (see Figure 3-25 for reference). The disturbance of the structure of Fe can be attributed to the fact that both Fe and Cu layers are large enough to form agglomeratess of each even at the interface. As a consequence, the amorphous structure initially present at the interface tends to become a mixture of BCC and FCC structures, and the structure of the Fe layer is highly disturbed due to the presence of Cu atoms with large size, which create more dislocations in the Fe cell. While it is known that Fe and Cu are non-miscible elements, it was shown that they could form a mixture of a few atomic planes at the interface [19]; indeed, supporting the behavior observed at the interface.

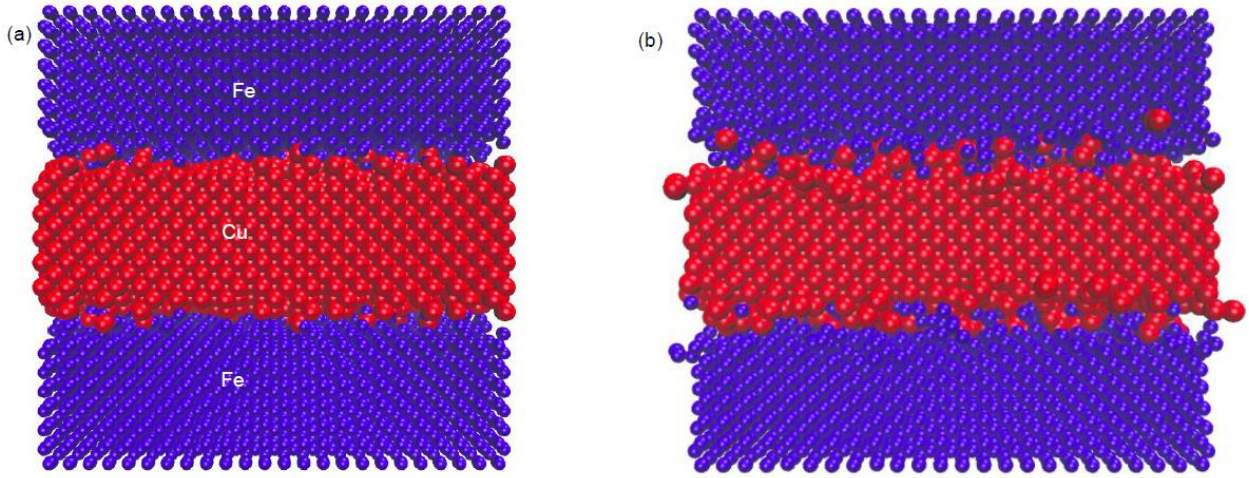

Figure 3-24. Visualization of the trilayer system $Fe_{21}/Cu_{24}/Fe_{21}$. before (a) and after (b) the simulated annealing. The atomic planes of Fe and Cu are shown in blue and red respectively.

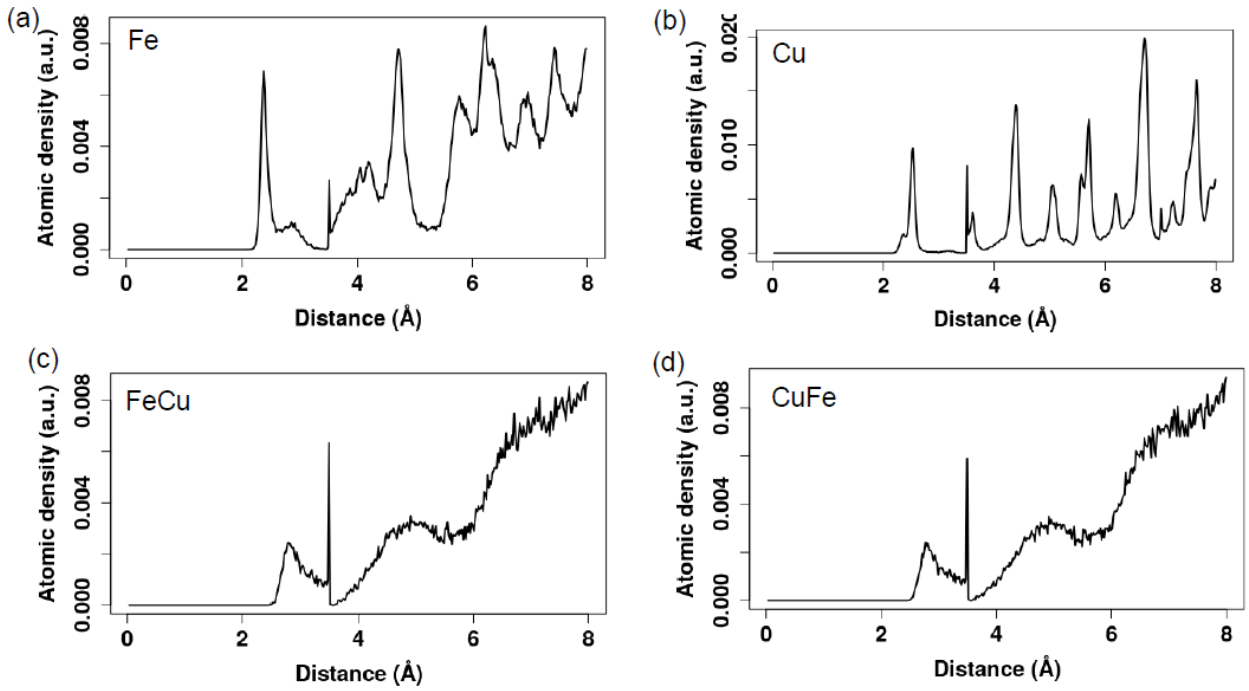

Figure 3-25. RDF of $Fe_{21}/Cu_{24}/Fe_{21}$ system. The disturbance is again seen at the interface of the Fe layer (a), which is still BCC, as the thickness of the Cu continues to grow. (b) shows the FCC structure of the Cu layer. In the presence of a high atomic proportion of Cu at the interface, Fe atoms will tend to copy the FCC structure of the interface (c, d) for the first atomic planes. This can justify the mixed structure dominated by the FCC of the interface.

A further increase of the thickness of the Cu layer to 40 Å leads to a more disturbance of the structure of the Fe layer (Figure 3-27 a). The FCC crystal structure of Cu can be seen in the Cu layer (Figure 3-27 b), while the presence of high Cu atomic proportion at the interface dictates the well pronounced FCC structure (Figure 3-27 c, d).

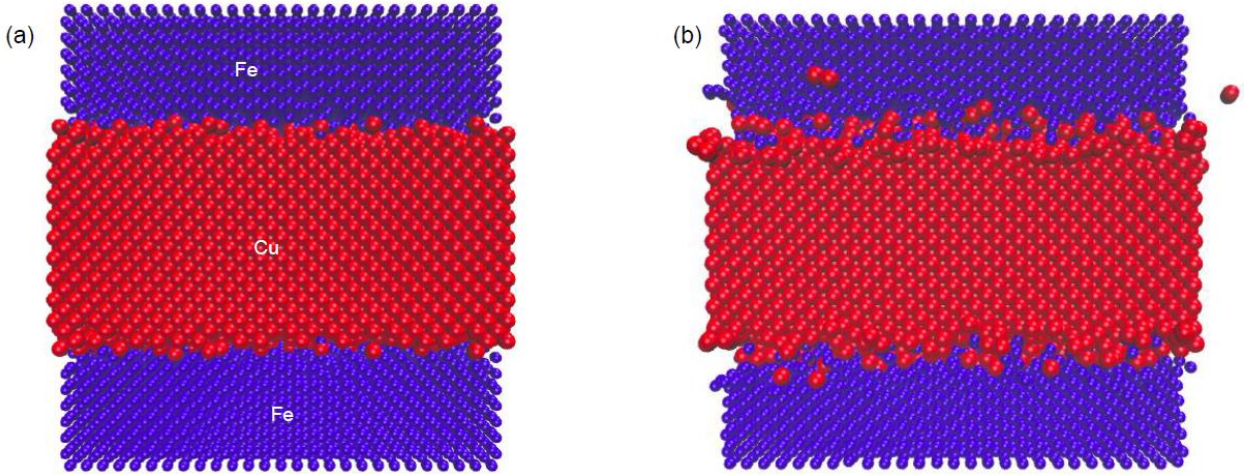

Figure 3-26. Structure visualization of $Fe_{21}/Cu_{40}/Fe_{21}$ before (a) and after (b) the simulated annealing. Increasing the thickness of Cu may disturb the structure of Fe.

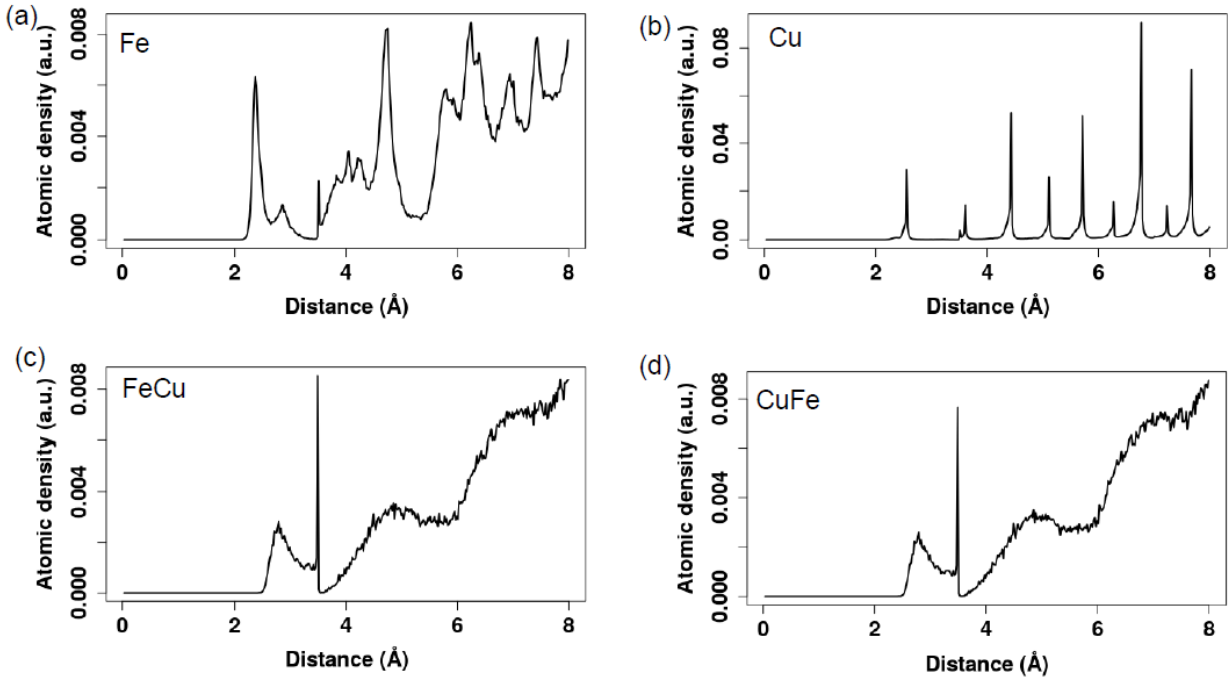

Figure 3-27. RDF of $Fe_{21}/Cu_{40}/Fe_{21}$ system. The disturbance of the Fe layer is seen upon a high increase of the Cu layer thickness. The structure of the Fe layer remains BCC but disturbed at the interface (a). (b) show the well-defined structure of the Cu layer as compared to the pure Cu, while the mixed structure of the interface is highly dominated by the FCC structure, second peak from the left (c, d).

We can conclude that the structural information of different layers is mostly based on the thickness of the individual layers forming the system. The nature of the interface is determined by the structure of each layer present at that interface. Below a particular critical value of the thicknesses, which we found to be 18 and 13 Å for the Fe and Cu layers, respectively, the structure of the interface is a mixture of both FCC and BCC structures. At the transition state, the mixed structure of the interface is less pronounced, and the amorphous system is observed where both Fe and Cu are miscible. The miscibility of Fe and Cu at the transition is an unusual phenomenon. In fact, in nature, Fe and Cu are immiscible elements based on their phase diagram. The miscibility of both elements has many technological advantages. For example, the presence of Cu atoms in the Fe matrix will induce antiferromagnetic coupling among the Fe magnetic moments, and upon applying a small external magnetic field, the anti-parallel magnetic moment of the Fe atom with easily align to the direction of the external magnetic field, leading to the ferromagnetic coupling. The value of the external field applied is relatively small because the atoms of the noble metal, Cu, present in the matrix are non-magnetic. This process is highly applied in magnetic recording media and magnetic sensors. The only drawback so far is due to the fact that these systems are made up of Fe/Cr/Fe, where Cr is an antiferromagnetic element. As a result, the antiferromagnetic coupling will be very high, thus, requiring a large external magnetic field to rotate the magnetic atoms of Fe in the direction of the utilized field. The large antiferromagnetic coupling has dramatically limited the transferability of the GMR-based Fe/Cr/Fe to the industrial level. These observations agree with the experiments[13, 26, 32, 82].

3-4. Magnetic properties of multilayer systems Fe/Cu/Fe.

After discussing the consequences of the change in the thicknesses of different layers on the structural properties, an interesting point would be to explore the effect of these changes on the magnetic properties. In this section, we performed simulations of the magnetic properties of Fe/Cu/Fe, with reduced dimensionalities due to the computational power, it requires to complete such high throughout simulations. We applied the Heisenberg model defined in the chapter 2 Numerical Methodology with the magnetization and its fluctuations represented by the susceptibility on the structurally characterized system to investigate the magnetic properties.

The first system is the trilayer $Fe_{34}/Cu_{25}/Fe_{34}$, where the size of the system was reduced compared to that of the structural investigation. We were interested in seeing the changes in the magnetization, the magnetic susceptibility, and the Curie temperature. As a reminder, the Curie temperature is the temperature below which the spontaneous magnetization can be observed. The Curie temperature of the conventional pure Fe is determined and is approximately 1053 K. It has been shown that the Curie temperature of the Fe element in a multilayer system is between 150 K and 350 K [9, 13, 87, 88]. The results of the simulations are shown in Figure 3-28. The relative values of the magnetization are shown in Figure 3-28 a. One can see that the magnetization curve is reproduced; additionally, the Curie temperature of the Fe layer is around 275.9 K. Similar values of the Curie temperature were also observed on magnetization curves at the interface and on the susceptibility of the Fe layer as well as that of the interface (Figure 3-28 b-d).

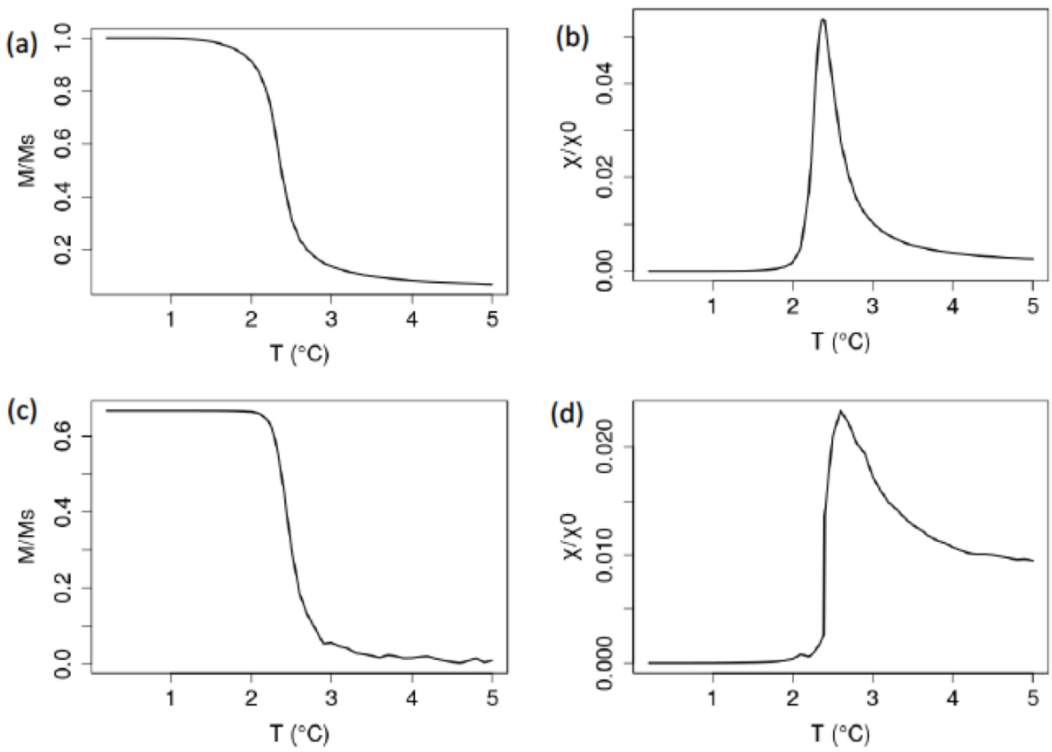

Figure 3-28. Multilayer system $Fe_{34}/Cu_{25}/Fe_{34}$. (a) and (c) show the magnetization of the Fe layer and the interface, respectively. The magnetic susceptibility if shown by (b) and (d) for the Fe layer and the interface, respectively. The Curie temperature of the system is around 275.9 K.

A decrease of the thickness of the Fe layer leads to a disturbed magnetization at the interface and a slight reduction of the Curie temperature (Figure 3-29 a, c). The reduced Fe atomic proportion can explain the origin of the disturbed magnetization at the interface, which has caused a structural rearrangement in the system. On the other hand, it could be due to the move toward the criticality region, where both element Fe and Cu are miscible at the interface, which is defined by an amorphous system. It is interesting to realize that the relative value of the susceptibility of the interface has dramatically increased, due to the perturbation of the magnetization, passing that of the Fe layer (Figure 3-29 b, d).

Owing to this hypothesis, we further reduced the thickness of the Fe layer to 18 Å, and the results are shown in Figure 3-30.

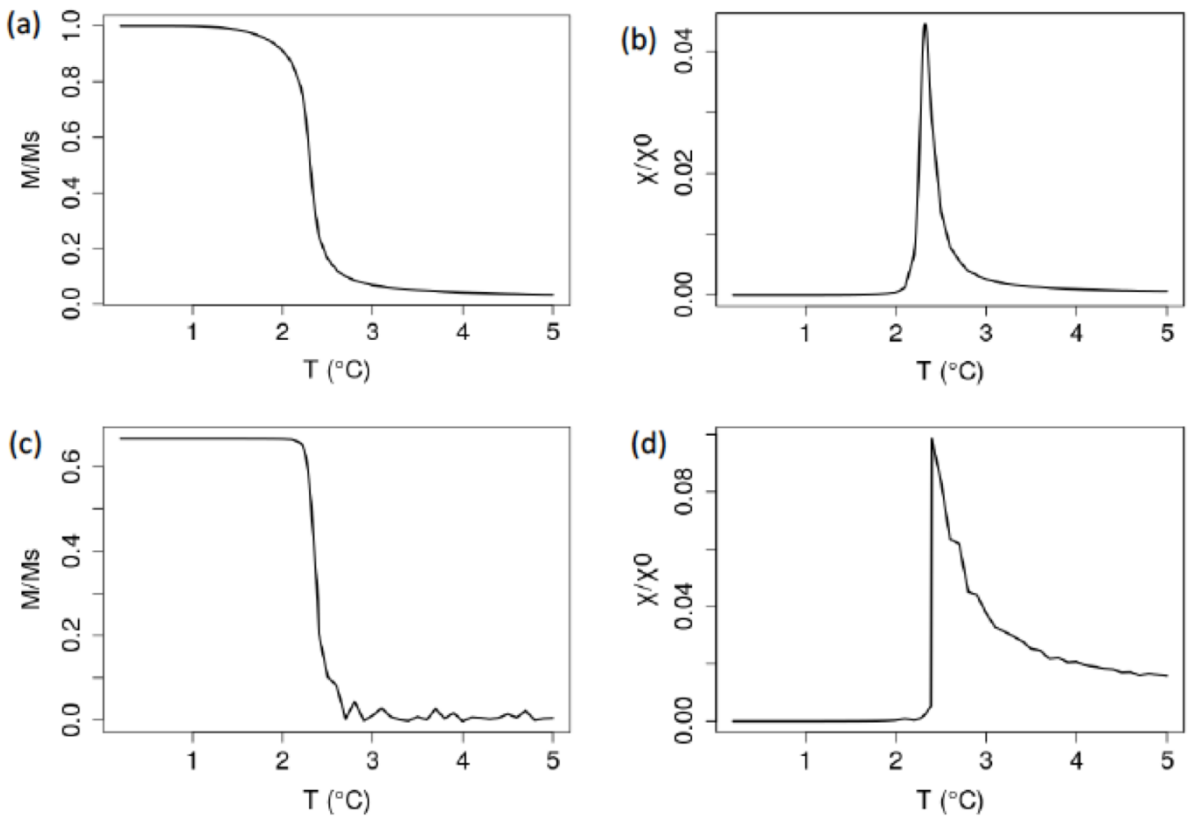

Figure 3-29. Multilayer system $Fe_{25}/Cu_{25}/Fe_{25}$. (a) and (c) show the magnetization of the Fe layer and the interface, respectively. The magnetic susceptibility if shown by (b) and (d) for both the Fe layer and the interface respectively. A slight increase in the Curie temperature of the system is observed, which is around 275.5 K. Additionally, one can observe the disturbance of the magnetization of the interface.

The decrease has led to a more disturbing interface magnetization (Figure 3-30 a, c). We can attribute this disturbance to the presence of Cu atoms in the matrix of Fe, which reduces the freedom of Fe atoms in the cell. Additionally, the susceptibility of the interface significantly increases upon decreasing the thickness of Fe (Figure 3-30). This could be due to the reduced Fe atomic proportion in the bulk of the Fe layer. It has been shown that the reduced dimensionalities in the multilayer systems result in an increase of surface atoms over volume atoms. According to the literature, an increase in susceptibility is expected. This means that we are expecting more increase of the relative susceptibility when decreasing the thickness of the Fe layer.

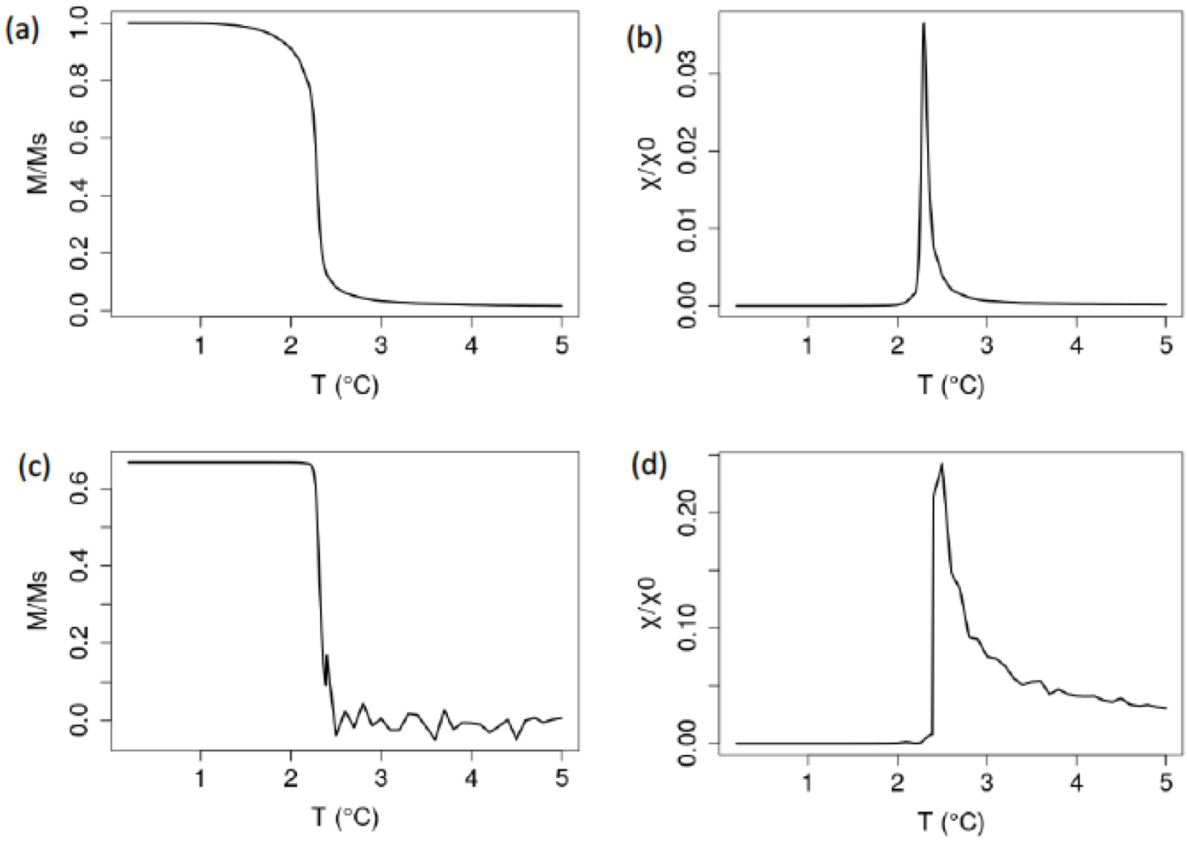

Figure 3-30. Multilayer system $Fe_{18}/Cu_{25}/Fe_{18}$. (a) and (c) show the magnetization of the Fe layer and the interface, respectively. The magnetic susceptibility if shown by (b) and (d) for both the Fe layer and the interface respectively. The disturbance of the magnetization of the interface is seen (c). The Curie temperature of the system remains close to 275.5 K.

As a result, the value of the relative susceptibility has dramatically increased (Figure 3-31 b, d). More importantly, the magnetization of the interface is even more disturbed above the Curie temperature, as shown in Figure 3-31 c. It would also be interesting to note the slight decrease of the Curie temperature with the reduction of the Fe layer thickness. As mentioned above, decreasing the thickness of Fe leads to an increase in the proportion of surface atoms. Contrarily to a single free Fe layer, the atoms present at the interface will encounter other types of atoms, here Cu atoms, which lead to a competition between both elements, either to form an agglomerates of each kind (above and below the critical regime) or to form an amorphous system (at the criticality). These hypotheses will be explored more thoroughly in our next investigations

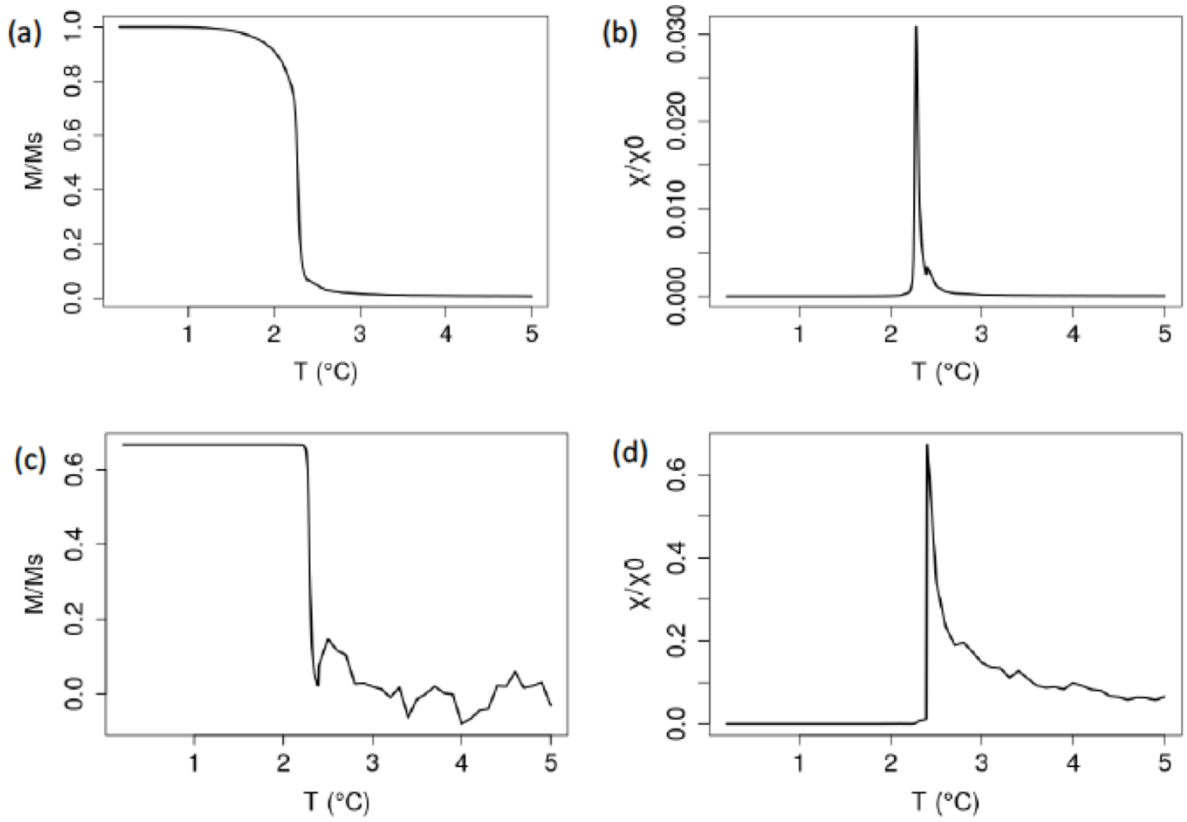

Figure 3-31. Multilayer system of $Fe_7/Cu_{25}/Fe_7$. (a) and (c) show the relative magnetization of the Fe layer and the interface, respectively. The relative magnetic susceptibility if shown by (b) and (d) for both the Fe layer and the interface, respectively. The high disturbance of the magnetization observed at the interface could be due to the presence of Cu atoms at the interface, which reduces the interlayer coupling between both layers of Fe.

3-5. Conclusion

Interface morphology plays a crucial role in determining the properties of magnetic multilayers. Spacer layer thickness, here the Cu layer, has been shown to control the nature of the interlayer exchange coupling between magnetic Fe layers during the study of the GMR effects [12, 23, 26, 38]. Depending on the spacer thickness, ferromagnetic or antiferromagnetic interlayer, exchange coupling can be observed. For example, in the case of the ultrathin spacer layer, the loss of antiferromagnetic coupling between adjacent magnetic layers can occur due to imperfections in the spacer layer. In contrast, in the case of thicker spacer layers an important reduction of the magnetization can be observed due to the low concentration of Fe atoms. However, the structural nature of the Cu layer and the thickness to which either of the exchange couplings is observed remain subjects of discussion. For example, Figure 3-21 showed the structure of the Cu layer similar to that of bcc Fe, for the first atomic plane of the ultrathin layer. Similar observations were previously reported [23, 26, 42]. Additionally, the transition observed for the thickness of the Cu layer at 13 Å has tremendous technological implications. These large structural rearrangements have many effects on the magnetic properties. For example, the direct coupling exchange between the two adjacent magnetic layers is likely to be ferromagnetic at low thickness of the Cu layer, which would explain the decrease in magneto-resistance below a certain critical spacer thickness as shown by the experiment. The observed metastable structures of Cu in Figure 3-21 or Fe in Figure 3-14 can be explained by the increase in atomic proportion at the interface with the layer's thickness, and the presence at the interface of almost all Cu atoms or all Fe atoms, thus forming a matrix with dominant Fe or Cu atoms. These assumptions are confirmed by the structures in Figure 3-13, in Figure 3-21 b, and Figure 3-14 where the interfaces are less dominated by the atoms of the thicker layer [5, 26].

On the other hand, upon the increase of the thinner layer thickness, although both layers have almost the same atomic proportion as the systems represented in Figure 3-23 and Figure 3-30, the interface tends to form a Fe-Cu alloy with an amorphous structure instead of metastable FCC and BCC structures. The smooth transition from metastable BCC to FCC or vice-versa for the critical values of 6 and 7 Å, for the Cu and the Fe layers, respectively. These transitions could explain the

observed expansion of the magneto-resistance with the increase of Cu thickness (for references, see [17, 82]). To get insight of the structural changes on the magnetic properties, the variations of the magnetization and the magnetic susceptibility on a reduced magnetic system were investigated. It was previously reported that the difference in the structure is accompanied by a significant decrease in the Curie temperature. The results of our simulation show a Curie temperature of around 276 K, which agrees with the experimental findings. Furthermore, we have also observed a significant variation of the magnetization at the interface and a substantial increase of the susceptibility as compared to the bulk counterpart. These observations could be confirmed by thorough experimental and theoretical investigations [27, 55, 86, 89].

General conclusion and future outlooks

The study of magnetic multilayer systems has attracted much attention in recent years. The considerable interest is not surprising, view the unusual properties they present and their technological applications. In this thesis, we aimed to understand the origin of these fascinating properties from the fundamental physics point of view. Although the research was purely theoretical and computational, the results were easily comparable to the existing experiments on magnetic multilayers. To have a realistic system that mimics the system obtained from experimental results, we used the approach based on the Voronoï diagram. This approach has been used in geometry since its introduction by Dirichlet and Voronoï. We applied this algorithm to construct the multilayer systems Fe/Cu/Fe.

Particles within the simulation box are thought to be interacting and these interactions were considered by defining the Hamiltonian of the system using the modified embedded atom method as the energy function. This approximation method of the energy function has been widely used to study metallic elements. The preliminary results of the simulations have reproduced the basic properties of each element in our study model. The defined energy function was implemented using the Monte Carlo algorithm with the Metropolis criterion.

The results of the simulations show that the structure of the system is highly sensitive to the variation of the thicknesses of individual layers. Indeed, it is possible to obtain at the interface the coexistence of multiple phases, e.g., body centered cubic (BCC), face centered cubic (FCC), and amorphous for particular values of thicknesses called critical values. It means that iron (Fe) and copper (Cu) can coexist for some specific layer thicknesses, what is surprising, considering that in nature, they are immiscible elements based on their phase diagram. Additionally, due to the large atomic radius of Cu, as compared to that of Fe, the critical value of the thickness of the Cu layer in the multilayer was found to be around 13 Å, much smaller than that of Fe, which is 18 Å. These values are in agreement with the experiment. We realize that the critical value is observed when either Cu or Fe undergoes a considerable structural change to adopt the structure of the bulk element.

The magnetic properties show a significant decrease of the Curie temperature of the Fe element, which is about 276 K as compared to that of the conventional bulk Fe, about 1053 K. The Curie

temperature is the temperature below which spontaneous magnetization can be observed. The results of our simulations show that by combining Fe and Cu in a specific configuration with reduced dimensionalities, we can tremendously reduce the Curie temperature. Furthermore, this reduced dimensionalities may be accompanied by the presence of magnetization at the interface, as we showed during our investigations.

The observed changes in the structural and magnetic properties have critical technological applications. For instance, the amorphous structure observed at the interface during the transition upon increasing the thickness could be explored in the magnetic recording media as well as magnetic sensors. One of the advantages of the Fe/Cu/Fe system, as compared to the most widely studied, Fe/Cr/Fe, is a less external magnetic field it requires to overcome the antiferromagnetic coupling, which was shown as the limitation of the Fe/Cr/Fe system.

As far as the future is concerned, we intend to conduct similar investigations on many other magnetic multilayer systems such as rare-earth/transition-metal, which presents interesting properties including antiparallel coupling between rare-earth and the transition metal.

References

[1] Hartmann, U. and R. Coehoorn, Magnetic multilayers and giant magnetoresistance : fundamentals and industrial applications. Springer series in surface sciences. Vol. 37. 2000: Springer-Verlag Berlin Heidelberg. x, 321 pages.

[2] Bland, J.A.C. and B. Heinrich, Ultrathin magnetic structures. Vol. 1. 1994: Springer. 4 volumes.

[3] Bogdanov, A.N., Magnetic Domains. The Analysis of Magnetic Microstructures. Low Temperature Physics, 1999. 25(2): p. 151-152.

[4] Visnovský, S., Optics in magnetic multilayers and nanostructures. 2006, Boca Raton: CRC/Taylor & Francis.

[5] Mardani, R., Fabrication of FM/NM/FM Hetero-Structure Multilayers and Investigation on Structural and Magnetic Properties: Application in GMI Magnetic Sensors. Journal of Superconductivity and Novel Magnetism, 2020. 33(2): p. 503-509.

[6] Gleiter, H., Nanostructured materials: Basic concepts and microstructure. Acta Materialia, 2000. 48(1): p. 1-29.

[7] Hovermann, K., et al., Syntheses and structural properties of 1,8-diazacyclotetradeca-3,5,10,12-tetraynes. European Journal of Organic Chemistry, 2000(12): p. 2291-2294.

[8] Benisch, C., et al., Syntheses and structural properties of cyclic tetrathiadiynes. European Journal of Organic Chemistry, 2000(13): p. 2479-2488.

[9] Chlenova, A.A., et al., Permalloy-Based Thin Film Structures: Magnetic Properties and the Giant Magnetoimpedance Effect in the Temperature Range Important for Biomedical Applications. Sensors (Basel, Switzerland), 2017. 17(8): p. 1900.

[10] Morón, C., et al., Magnetic Sensors Based on Amorphous Ferromagnetic Materials: A Review. Sensors (Basel), 2015. 15(11): p. 28340-66.

[11] Prudnikov, V.V., P.V. Prudnikov, and D.E. Romanovskiy, Monte Carlo simulation of magnetic multilayered structures with giant magnetoresistance effects. International Conference on Computer Simulation in Physics and Beyond 2015, 2016. 681.

[12] Afshari, M., M.E. Ghazi, and M. Izadifard, Structural and Magnetic Properties of Fe/Cu/Fe Trilayers. African Review of Physics, 2015. 10.

[13] Kuprin, A.P., et al., Magnetism and structure of Fe/Cu multilayers studied by low-temperature conversion electron Mossbauer spectroscopy. Journal of Applied Physics, 1999. 85(8): p. 5738-5740.

[14] Baibich, M.N., et al., Giant Magnetoresistance of (001)Fe/(001)Cr Magnetic Superlattices. Physical Review Letters, 1988. 61(21): p. 2472-2475.

[15] Binasch, G., et al., Enhanced magnetoresistance in layered magnetic structures with antiferromagnetic interlayer exchange. Physical Review B, 1989. 39(7): p. 4828-4830.

[16] van Noort, H.M., F.J.A. den Broeder, and H.J.G. Draaisma, Mössbauer study of Cu-Fe composition-modulated thin films. Journal of Magnetism and Magnetic Materials, 1985. 51(1): p. 273-279.

[17] Badia, F., et al., Magnetic properties of Fe/Cu multilayers. Journal of Magnetism and Magnetic Materials, 1991. 93: p. 425-428.

[18] Bakkaloğlu, Ö.F., A magnetic study of sputtered Fe/Cu multilayer films. Journal of Magnetism and Magnetic Materials, 1998. 182(3): p. 324-328.

[19] Shamsutdinov, N.R., A.J. Bottger, and F.D. Tichelaar, The effect of Cu interlayers on grain size and stress in sputtered Fe-Cu multilayered thin films. Scripta Materialia, 2006. 54(10): p. 1727-1732.

[20] Esaki, L. and L.L. Chang, New Transport Phenomenon in a Semiconductor ?Superlattice?, in Semiconductor Devices: Pioneering Papers. 1991, WORLD SCIENTIFIC. p. 732-735.

[21] Shinjo, T., Artificial multilayers and nanomagnetic materials. Proceedings of the Japan Academy. Series B, Physical and biological sciences, 2013. 89(2): p. 80-96.

[22] Grunberg, P., et al., Layered Magnetic-Structures - Evidence for Antiferromagnetic Coupling of Fe Layers across Cr Interlayers. Physical Review Letters, 1986. 57(19): p. 2442-2445.

[23] Lee, D.W., et al., Structural and magnetic properties of Cu/Fe multilayers. Physical Review B, 1999. 59(10): p. 7001-7009.

[24] Ueda, Y., et al., Magnetoresistance and magnetism in Fe-Cu alloys produced by electrodeposition and mechanical alloying methods. Materials Science and Engineering a-Structural Materials Properties Microstructure and Processing, 1996. 217: p. 371-375.

[25] Grafoute, M., et al., Structure of grain boundaries in nanostructured powders: a Monte-Carlo/EAM numerical investigation. European Physical Journal B, 2005. 45(3): p. 419-424.

[26] Pizzini, S., et al., Structure cristallographique de multicouches métalliques et magnétiques étudiées par spectroscopie d'absorption X. J. Phys. IV France, 1992. 02(C3): p. C3-185-C3-189.

[27] Zillgen, H., B. Feldmann, and M. Wuttig, Structural and magnetic properties of ultrathin Fe films deposited at low temperature on Cu(100). Surface Science, 1994. 321(1): p. 32-46.

[28] BenYoussef, J., et al., Correlation of GMR with texture and interfacial roughness in optimized rf sputtering deposited Co/Cu multilayers. Journal of Magnetism and Magnetic Materials, 1997. 165(1-3): p. 288-291.

[29] Cros, V., et al., Detection of the magnetization reversal in submicron Co particles by GMR measurements. Journal of Magnetism and Magnetic Materials, 1997. 165(1-3): p. 512-515.

[30] Dupuis, V., et al., From the superparamagnetic to the magnetically ordered state in systems of transition metal clusters embedded in matrices. Journal of Magnetism and Magnetic Materials, 1997. 165(1-3): p. 42-45.

[31] Dubois, S., et al., Perpendicular giant magnetoresistance in Co/Cu and permalloy/Cu multilayered nanowires. Journal of Applied Physics, 1997. 81(8): p. 4569-4569.

[32] Albini, L., et al., Magnetic and structural properties of Fe/Cu multilayers. Physica B-Condensed Matter, 2000. 275(1-3): p. 253-257.

[33] Kąc, M., et al., Structural and magnetic characterization of Fe/Cr/Fe tri-layers and Fe/Cr multilayers after swift Au ion irradiation. physica status solidi (a), 2008. 205(8): p. 1855-1859.

[34] Liebermann, L.N., D.R. Fredkin, and H.B. Shore, Two-Dimensional "Ferromagnetism" In Iron. Physical Review Letters, 1969. 22(11): p. 539-541.

[35] Shinjo, T., et al., Mössbauer evidence against the existence of magnetically “dead” layers. Physics Letters A, 1971. 36(6): p. 489-490.

[36] Exchange Coupling in Magnetic Multilayers, in Handbook of Magnetism and Advanced Magnetic Materials.

[37] Shinjo, T., Amorphous-to-crystalline transformation of ultrathin Fe Layers:57Fe Mössbauer study of artificial multilayers. Structural Chemistry, 1991. 2(3): p. (73)281-(80)288.

[38] Fert, A., et al., Giant magnetoresistance in magnetic nanostructures. Journal De Physique Iv, 1997. 7(C6): p. 151-161.

[39] Fettar, F., et al., Giant magnetoresistance in Co90Fe10/Ag multilayers with discontinuous magnetic layers. Journal of Magnetism and Magnetic Materials, 1997. 165(1-3): p. 316-319.

[40] Zhukov, A., et al., Giant magnetoimpedance in thin amorphous wires: From manipulation of magnetic field dependence to industrial applications. Journal of Alloys and Compounds, 2014. 586: p. S279-S286.

[41] Petroff, F., et al., Oscillatory interlayer exchange and magnetoresistance in Fe/Cu multilayers. Phys Rev B Condens Matter, 1991. 44(10): p. 5355-5357.

[42] Mosca, D.H., et al., Oscillatory interlayer coupling and giant magnetoresistance in Co/Cu multilayers. Journal of Magnetism and Magnetic Materials, 1991. 94(1): p. L1-L5.

[43] Parkin, S.S., Systematic variation of the strength and oscillation period of indirect magnetic exchange coupling through the 3d, 4d, and 5d transition metals. Phys Rev Lett, 1991. 67(25): p. 3598-3601.

[44] Dieny, B., et al., Giant magnetoresistive in soft ferromagnetic multilayers. Phys Rev B Condens Matter, 1991. 43(1): p. 1297-1300.

[45] Miyazaki, T. and N. Tezuka, Giant magnetic tunneling effect in Fe/Al2O3/Fe junction. Journal of Magnetism and Magnetic Materials, 1995. 139(3): p. L231-L234.

[46] Moodera, J.S., et al., Large magnetoresistance at room temperature in ferromagnetic thin film tunnel junctions. Phys Rev Lett, 1995. 74(16): p. 3273-3276.

[47] Yuasa, S., et al., Giant room-temperature magnetoresistance in single-crystal Fe/MgO/Fe magnetic tunnel junctions. Nat Mater, 2004. 3(12): p. 868-71.

[48] Parkin, S.S., et al., Giant tunnelling magnetoresistance at room temperature with MgO (100) tunnel barriers. Nat Mater, 2004. 3(12): p. 862-7.

[49] Iwasaki, S., Perpendicular magnetic recording. IEEE Transactions on Magnetics, 1980. 16(1): p. 71-76.

[50] Jesser, W.A. and J.W. Matthews, Evidence for pseudomorphic growth of iron on copper. The Philosophical Magazine: A Journal of Theoretical Experimental and Applied Physics, 1967. 15(138): p. 1097-1106.

[51] Macedo, W.A.A. and W. Keune, Magnetism of Epitaxial fcc-Fe(100) Films on Cu(100) Investigated in Situ by Conversion-Electron M\"ossbauer Spectroscopy in Ultrahigh Vacuum. Physical Review Letters, 1988. 61(4): p. 475-478.

[52] Fert, A., et al., Magnetic multilayers: oscillatory interlayer exchange and giant magnetoresistance. Journal of Magnetism and Magnetic Materials, 1992. 104-107: p. 1712-1716.

[53] Parkin, S.S.P., Dramatic enhancement of interlayer exchange coupling and giant magnetoresistance in Ni81Fe19/Cu multilayers by addition of thin Co interface layers. Applied Physics Letters, 1992. 61(11): p. 1358-1360.

[54] van Belle, F., C.A.F. Vaz, and J.A.C. Bland, Oscillatory interlayer coupling in bcc ${\mathrm{Co}}_{75}{\mathrm{Fe}}_{25}/\mathrm{Au}$ and fcc ${\mathrm{Co}}_{75}{\mathrm{Fe}}_{25}/\mathrm{Cu}$ multilayers. Physical Review B, 2007. 76(18): p. 184411.

[55] Cheng, S.F., et al., Structure and magnetic properties of magnetron-sputtered Fe/Cu multilayered thin films. Physical Review B, 1993. 47(1): p. 206-216.

[56] Pankhurst, Q.A., et al., A Mossbauer study of Fe(5 /spl Aring/)+Cu(50 /spl Aring/) multilayers. IEEE Transactions on Magnetics, 1994. 30(2): p. 778-780.

[57] Hahn, H., Gas phase synthesis of nanocrystalline materials. Nanostructured Materials, 1997. 9(1): p. 3-12.

[58] Blöschl, G., A. Viglione, and A. Montanari, 5.01 - Emerging Approaches to Hydrological Risk Management in a Changing World, in Climate Vulnerability, R.A. Pielke, Editor. 2013, Academic Press: Oxford. p. 3-10.

[59] Ramsden, J.J., Chapter 6 - Nanomaterials and their Production, in Nanotechnology, J.J. Ramsden, Editor. 2011, William Andrew Publishing: Oxford. p. 101-124.

[60] Jalali, H. and B.D. Gates, Monitoring and mapping imperfections in silane-based self-assembled monolayers by chemical amplification. Langmuir, 2009. 25(16): p. 9078-84.

[61] Mössbauer, R.L., Kernresonanzfluoreszenz von Gammastrahlung in Ir191. Zeitschrift für Physik, 1958. 151(2): p. 124-143.

[62] Pound, R.V. and G.A. Rebka, Apparent Weight of Photons. Physical Review Letters, 1960. 4(7): p. 337-341.

[63] Cadogan, J.M. and D.H. Ryan, MÖSSBAUER SPECTROSCOPY, in Handbook of Applied Solid State Spectroscopy, D.R. Vij, Editor. 2006, Springer US: Boston, MA. p. 201-256.

[64] Ferlin, F. and H. Chabot, Vortex Theories in the Early Modern Period, in Encyclopedia of Early Modern Philosophy and the Sciences, D. Jalobeanu and C.T. Wolfe, Editors. 2020, Springer International Publishing: Cham. p. 1-6.

[65] Voronoi, G., New applications of continuous parameters to the theory of quadratic forms. Journal Fur Die Reine Und Angewandte Mathematik, 1909. 136(1/4): p. 67-178.

[66] Horváth, Á.G., On the Dirichlet—Voronoi cell of unimodular lattices. Geometriae Dedicata, 1996. 63(2): p. 183-191.

[67] Daw, M.S. and M.I. Baskes, Semiempirical, Quantum-Mechanical Calculation of Hydrogen Embrittlement in Metals. Physical Review Letters, 1983. 50(17): p. 1285-1288.

[68] Daw, M.S., C.L. Bisson, and W.D. Wilson, Hydrogen Binding to Fixed Interstitial Impurities in Metals. Solid State Communications, 1983. 46(10): p. 735-738.

[69] Daw, M.S., C.L. Bisson, and W.D. Wilson, Calculations of the Binding of Hydrogen to Fixed Interstitial Impurities in Nickel. Metallurgical Transactions a-Physical Metallurgy and Materials Science, 1983. 14(7): p. 1257-1260.

[70] Daw, M.S., D.L. Smith, and T.C. Mcgill, Core Excitons for the (110) Surface of Zinc Blende-Iii-V Semiconductors. Solid State Communications, 1983. 47(6): p. 449-453.

[71] Finnis, M.W. and J.E. Sinclair, A simple empirical N-body potential for transition metals. Philosophical Magazine A, 1984. 50(1): p. 45-55.

[72] Lee, B.-J. and M.I. Baskes, Second nearest-neighbor modified embedded-atom-method potential. Physical Review B, 2000. 62(13): p. 8564-8567.

[73] Lee, B.-J., et al., Second nearest-neighbor modified embedded atom method potentials for bcc transition metals. Physical Review B, 2001. 64(18): p. 184102.

[74] Lee, B.-J., et al., Modified embedded-atom method interatomic potential for the $\mathrm{Fe}\text{\ensuremath{-}}\mathrm{Cu}$ alloy system and cascade simulations on pure Fe and $\mathrm{Fe}\text{\ensuremath{-}}\mathrm{Cu}$ alloys. Physical Review B, 2005. 71(18): p. 184205.

[75] Lamberti, V.E., et al., A Hands-On Introduction to Molecular Dynamics. Journal of Chemical Education, 2002. 79(5): p. 601.

[76] Li, J., Basic Molecular Dynamics, in Handbook of Materials Modeling: Methods, S. Yip, Editor. 2005, Springer Netherlands: Dordrecht. p. 565-588.

[77] Vollmayr-Lee, K., Introduction to molecular dynamics simulations. American Journal of Physics, 2020. 88(5): p. 401-422.

[78] Jorgensen, W.L. and J. Tirado-Rives, Monte Carlo vs Molecular Dynamics for Conformational Sampling. The Journal of Physical Chemistry, 1996. 100(34): p. 14508-14513.

[79] Metropolis, N., et al., Equation of State Calculations by Fast Computing Machines. The Journal of Chemical Physics, 1953. 21(6): p. 1087-1092.

[80] Walter, J.C. and G.T. Barkema, An introduction to Monte Carlo methods. Physica A: Statistical Mechanics and its Applications, 2015. 418: p. 78-87.

[81] Fongang, B., et al., Coupled structural and magnetic properties of ferric fluoride nanostructures part I: A Metropolis atomistic study. Journal of Magnetism and Magnetic Materials, 2010. 322(19): p. 2888-2892.

[82] Cobianu, C., et al., Characterization of the magnetic thin multilayers with vibrating sample magnetometer. Journal of Science and Arts, Universitatea Valahia din Targoviste-JOSA, 2012(4).

[83] Razouk, A., M. Sahlaoui, and M. Sajieddine, Hysteresis Properties of Magnetic/Non-Magnetic (M/NM) Multilayers: Monte Carlo Investigation. Journal of Superconductivity and Novel Magnetism, 2012. 25(5): p. 1623-1626.

[84] Fert, A. and S.F. Lee, Spin injection: Theory and application to Johnson's spin switch. Journal of Magnetism and Magnetic Materials, 1997. 165(1-3): p. 115-120.

[85] Ortega, M.D., et al., Dependence on growth conditions of surface anisotropy and magnetization reversal in Au/Co(0.8nm)/Au/MoS2. Journal of Magnetism and Magnetic Materials, 1997. 165(1-3): p. 487-491.

[86] Ressier, L., et al., Structural and magnetic study of Fe stripes and boxes patterned by the "Atomic Saw" method. Magnetic Ultrathin Films, Multilayers and Surfaces - 1997, 1997. 475: p. 239-244.

[87] Li, Y., et al., Catalytic synthesis and enhanced Curie temperature of ε-Fe3N@C nanostructure synthesized in a tetraethylenepentamine solution. Journal of Magnetism and Magnetic Materials, 2018. 465: p. 736-742.

[88] Krajewski, M., et al., Structural and magnetic properties of iron nanowires and iron nanoparticles fabricated through a reduction reaction. Beilstein journal of nanotechnology, 2015. 6: p. 1652-1660.

[89] Bader, S.D., E.R. Moog, and P. Grunberg, Magnetic Hysteresis of Epitaxially-Deposited Iron in the Monolayer Range - a Kerr Effect Experiment in Surface Magnetism. Journal of Magnetism and Magnetic Materials, 1986. 53(4): p. L295-L298.

Publication from this thesis

- Jules Berlin Nde Kengne, Bernard Fongang, and Serge S. Zekeng, Structural Properties of Fe/Cu Magnetic Multilayers: A Monte Carlo Approach. SPIN, 2018. **08**(03): p. 1850012.

SPIN
Vol. 8, No. 3 (2018) 1850012 (10 pages)
© World Scientific Publishing Company
DOI: 10.1142/S2010324718500121

SPIN Downloaded from www.worldscientific.com
by Mr. Reprints Desk on 10/08/18. Re-use and distribution is strictly not permitted, except for Open Access articles.

Structural Properties of Fe/Cu Magnetic Multilayers: A Monte Carlo Approach

Jules Berlin Nde Kengne*, Bernard Fongang†,‡ and Serge Zekeng*,§
*Laboratory of Material Science
Department of Physics, Faculty of Science
University of Yaoundé I, P. O. Box 812 Yaoundé
Centre, Cameroon

†Sealy Center for Structural Biology and Molecular Biophysics
University of Texas Medical Branch at Galveston
Galveston, Texas, USA
‡befongan@utmb.edu
§sergezekeng@yahoo.fr

Received 29 May 2018
Accepted 20 August 2018
Published 26 September 2018

Using atomistic Monte Carlo simulations, we investigated the impact of the interface on the structural properties of iron and copper (Fe/Cu) magnetic multilayers grown by Voronoi diagram. Interest in magnetic multilayers has recently emerged as they are shown to be promising candidates for magnetic storage media, magneto-resistive sensors and personalized medical treatment. As these artificial materials show large differences in properties compared to conventional ones, many experimental and theoretical works have been dedicated on shedding light on these differences and tremendous results have emerged. However, little is known about the influence of the interfaces on magnetic layers. Using numerical approaches, we show that the structure of each layer depends on its thickness and the interface morphology. The Fe and Cu layers can adopt either the body-centered-cubic (bcc) or face-centered-cubic (fcc) structure, while the interface can assume amorphous, bcc, fcc, or a mixture of bcc and fcc structures depending on the layer thicknesses. These results are in good agreement with the experiments. They could be helpful in understanding effects such as giant magneto-resistance from the structural perspective.

Keywords: Magnetic multilayers; Monte Carlo simulations; structural properties; GMR; Voronoi diagram; nanomaterial; computational physics.

1. Introduction

Metallic multilayer systems have gained much interest as they possess very different properties from bulk materials.[1,2] These artificial materials not only advance our understanding of the fundamental physics of nanomagnetism, but also have a wide range of technological applications such as magnetic recording media, magnetic storage and

§Corresponding author.

SPIN Downloaded from www.worldscientific.com
by Mr. Reprints Desk on 10/08/18. Re-use and distribution is strictly not permitted, except for Open Access articles.

magneto-resistive sensors.[1–4] Despite many experimental and theoretical progresses,[5–9] our understanding of those differences is still incomplete.

Many factors can contribute to the differences between multilayer systems and conventional bulk materials[6,10] One likely factor is the exchange coupling between thin films of ferromagnetic separated by nonmagnetic or antiferromagnetic metals. The striking properties of this exchange coupling have been used to explain the Giant Magneto-Resistance (GMR) phenomena.[1,11,12] The rationale behind the GMR, first observed in Fe/Cr multilayer systems, is that when varying the thickness of the Cr layer between two Fe layers, the magneto–resistance changed considerably inferring new and diverse properties to the multilayer material.[13–15] This phenomenon was later observed in other magnetic multilayers such as Fe/Cu.[6,7,16,17] However, the spacer thickness to which the oscillating coupling or the maximum of GMR is observed remains to be addressed. Moreover, the increasing percentage of atoms at the interface with the decreasing layer thicknesses can make structural properties of metallic multilayer systems to deviate significantly from those of their bulk counterparts.[18,19] Interface morphology could also be at the origin of the observed gap between experimental and theoretical coercivity measured in hard/soft multilayers. In fact, interface layer can reduce the effective crystalline anisotropy and coercivity in hard/soft multilayers, which could help explaining the observed paradox of coercivity and related energy.[20–23] Similarly, interface morphology also influences the Dzyaloshinkii–Moriya interaction (DMI) constants and skyrmions' behavior as mentioned in several studies.[24–26] The study of skyrmions is of great interest because of their excellent properties including their stability, small size and their low driving currents, making them better candidates than traditional magnetic domain walls for the development of next generation data storage.[24] In addition to the surface and interface effects, the electronic transport through multilayer structures can also affect the properties of magnetic multilayers.

Although many techniques have been developed for the preparation and characterization of magnetic multilayers, there are subtle differences among those techniques that can sometimes lead to misinterpretations of results.[27–30] For example, various deposition rates and growth temperatures can produce unexpected structural changes in the multilayer system.[31] Furthermore, soluble materials may experience unwanted interdiffusion at the interface, though multilayer systems made of Fe and Cu are often chosen for their mutual insolubility to reduce the interdiffusion.[32]

Besides the experimental approaches, numerical methods provide an alternative to study these systems.[9,33] However, it remains challenging to accurately model the structure of multilayer systems, mainly at the surface and interface, which critically influences the structure and the overall magnetic properties.[34,35] It is then desirable to have a numerical method of growing multilayer systems that better mimic experimental samples.

In this paper, we present a numerical study of the structural properties of metallic multilayers with variable layer thicknesses. We use Fe/Cu multilayer systems as model and investigate the structural changes using atomistic Monte Carlo simulations, which has been shown to accurately predict the properties of magnetic multilayers.[36,37] We use the Voronoi diagram method[38] to construct the numerical sample in order to make better comparison with the experiment.

2. Methodologies

2.1. *Construction of multilayer systems via Voronoi diagram*

We built multilayer systems based on Voronoi diagram.[19,38] Dirichlet and Voronoi first introduced the Voronoi diagram in geometry,[39] and it was later related to Delaunay triangulation. The construction of a Voronoi diagram consists of partitioning a plane into regions (sets of points). Any set of points (a crystallographic cell) is specified beforehand, and for each cell, there is a corresponding region consisting of all points closer to that cell than to any other. These regions are called Voronoi cells. The Voronoi diagram of a set of points is dual to its Delaunay triangulation. The general idea here is that given a set S of n points sites in the d-space, Voronoi diagram of S, $V_k(S)$, partitions the space into regions such that each point within a fixed region has the same k closest sites.

We grew our multilayer systems according to the principle that each layer is characterized by its nucleation center of coordinate (X_i, Y_i, Z_i, where $i = 1$ to n, n stands for the number of layers) in the direct orthogonal base (O, I, J, K, where O stands for the

SPIN Downloaded from www.worldscientific.com
by Mr. Reprints Desk on 10/08/18. Re-use and distribution is strictly not permitted, except for Open Access articles.

origin, and I, J or K standing for the unit coordinate for X, Y or Z, respectively). For each center, Euler angles are chosen in order to orient the relative crystallographic axes of the layers. This arrangement aims to produce the initial step for each layer. The next step is to add atoms to the system, to make the layers grow in all directions until the structure reaches a certain limit fixed by the Voronoi cell conditions. The detailed procedure used in this study can be found elsewhere.[19] We further avoided finite size and surface effects by first choosing a simulation box large enough to contain several layers and then performed simulations on a truncated box of much smaller size.

2.2. *Energy function and Monte Carlo simulations*

To mimic realistic samples, we used Modified Embedded Atom Method (MEAM) for the energy function of the system. While the current energy function can partially describe certain physical properties, it still suffers from certain accuracy problems. For example, Byeong *et al.*[40,41] showed that the results from MEAM for many body-centered-cubic (bcc) metals were in contradiction with the experimental ones[42,43]; they also showed that for a bcc structure, the energy of the (111) surface was smaller than that of the (100) surface.

The presence of multiple elements at the interface makes the problem even more complex for studying multilayer systems. Therefore, to overcome these difficulties, we used the variant of MEAM developed by Baskes *et al.*[44,45] for pure and alloy elements. This potential showed good agreement with the experiments in describing physical properties and surface energies.[45] Compared to EAM, MEAM has the advantage of being able to reproduce a wide range of structures including face-centered-cubic (fcc), bcc, hexagonal close-packed (hcp), etc. for different elements, using one common functional form. Equation (1) gives the form of the total energy used in this study:

$$E = \sum_i \left[F_i(\rho_i) + \frac{1}{2} \sum_{j(\neq i)} S_{ij} \Phi_{ij}(R_{ij}) \right], \qquad (1)$$

where F_i is the embedding function, ρ_i the background electron density at site i, S_{ij} the screen factor, and Φ_{ij} the pair interaction between atoms i and j separated by a distance R_{ij}. More details about the potential can be found elsewhere.[45]

To test the accuracy of the potential, we applied it to an alloy system composed of 50% of Fe and 50% of Cu atoms (data not shown). The final structure after Monte Carlo-simulated annealing scheme showed that the bonds among atoms are conserved inside and outside the simulation box. Moreover, the fact that Fe and Cu atoms do not form agglomerates of each type or the presence of atoms inside the simulation box after the simulated annealing Monte Carlo scheme justifies the choice of our interatomic potential.

We further minimized the total energy of the system given in Eq. (1) using Monte Carlo simulations with the Metropolis algorithm. Importance sampling Monte Carlo known as Metropolis Monte Carlo algorithm is based on the algorithm proposed by Metropolis *et al.*[46] We fixed the initial system at a high temperature (> 800 K) to allow the movement of each atom and we gradually decreased the temperature (as described in Ref. 38) until we reached the equilibrium, where the energy no longer changes (final temperature lower than 1 K). For each step of temperature, we performed the following steps:

(1) Calculate the energy of the system at a high temperature (initial state).
(2) Randomly choose and displace an atom in any of the three directions Δx, Δy or Δz.
(3) Calculate the energy change ΔE due to the displacement and decide whether to accept the move based on Metropolis criterion:
If $\Delta E < 0$, then accept the new configuration.
If $\Delta E > 0$, then calculate $p = \exp(-\frac{\Delta E}{K_b T})$ (where K_b represents the Boltzmann constant and T the absolute temperature) and compare it with a random number u between 0 and 1. If $p > u$, accept the new configuration, otherwise keep the old one and restart at step 2.
(4) Redo steps (1)–(3) for each block of temperature.

We adapted initial conditions from Ref. 19; in addition, for complexity reason and in order to keep the structure close to that of bulk material far from the interface, we made the following modification: the choice of the atom to be subjected to the Metropolis algorithm depends on its distance to the closest interface. The following relation gives the choice's probability

$$\omega = \exp(-\alpha x), \qquad (2)$$

where α is an adjustable parameter comprised between 0.5 Å^{-1} and 2 Å^{-1} as shown in a previous

SPIN Downloaded from www.worldscientific.com
by Mr. Reprints Desk on 10/08/18. Re-use and distribution is strictly not permitted, except for Open Access articles.

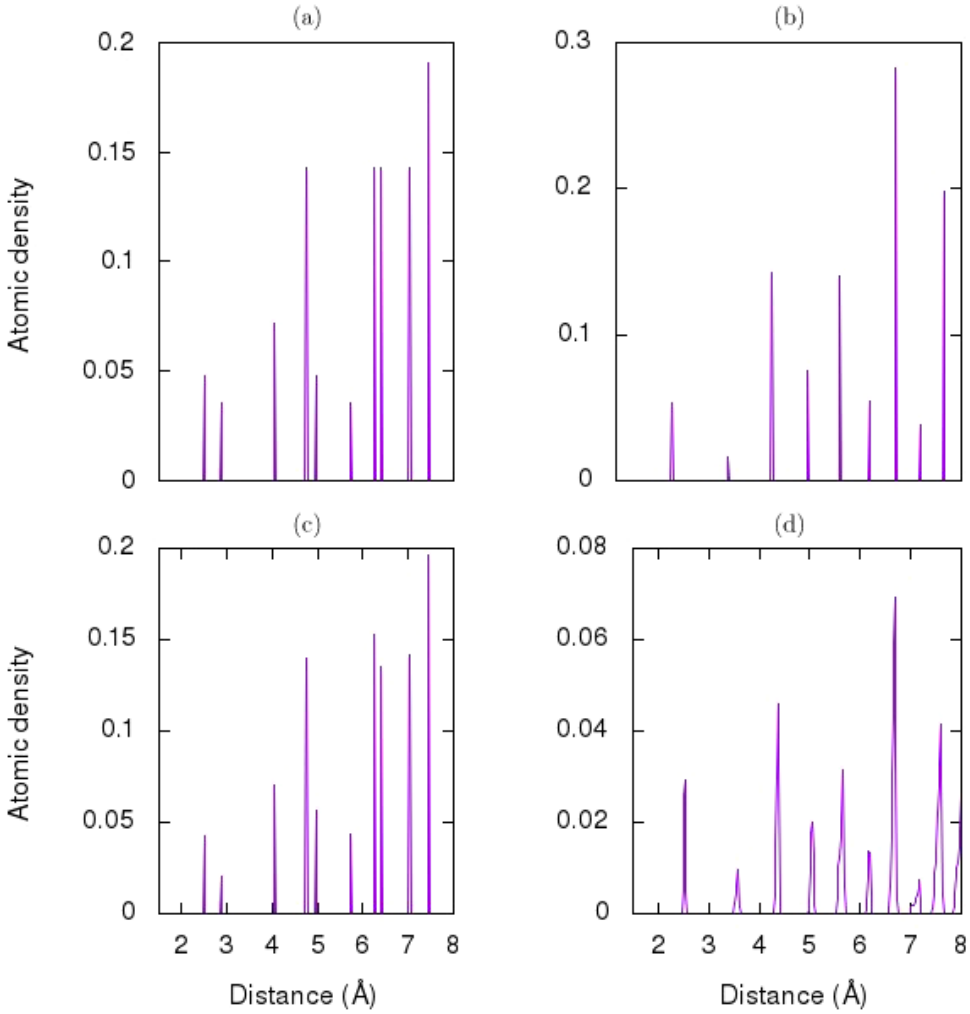

Fig. 1. RDF of pure elements (a) Fe and (b) Cu before and (c) Fe and (d) Cu after simulated annealing. The similarities between both structures before and after Monte Carlo-simulated annealing justify the fact that we neglected the relaxation of the whole system, thus, limiting computational time.

work,[38] and x represents the distance from the considered atom to the nearest interface. This probability allows us to avoid periodic boundary conditions and to anneal the atomic structure only close to the interfaces, as atoms located far from the interface have a low but nonzero probability to be chosen for the move. Interestingly, we have observed the maximum change of energy to be located only at the interface; the change far from the interface was almost negligible after we subjected the system to the simulated annealing Monte Carlo scheme [Figs. 1(c) and 1(d)].

2.3. *Structural characterization*

We further used a radial distribution function (RDF) to reproduce the change observed on the structures of layers and interfaces. A RDF $g(r)$ is the probability of finding an atom at the distance r of another identical atom chosen as reference. It provides a better description of the long-range order. The following relations give the distances (d_{Fe1}, d_{Fe2}, d_{Cu1} and d_{Cu2}), between first and second nearest neighbors for pure Fe and Cu structures, respectively: $d_{\mathrm{Fe1}} = a\sqrt{3}/2$, $d_{\mathrm{Fe2}} = a$, $d_{\mathrm{Cu1}} = a\sqrt{2}/2$ and $d_{\mathrm{Cu2}} = a$, where a stands for lattice parameter of Fe ($\sim$2.856 Å) or Cu ($\sim$3.597 Å). The obtained pure structures will be used in the following section as references.

3. Results and Discussion

In general, we numerically grew multilayers with variable thicknesses, set the adjustable parameter

SPIN Downloaded from www.worldscientific.com
by Mr. Reprints Desk on 10/08/18. Re-use and distribution is strictly not permitted, except for Open Access articles.

α to 2 Å^{-1}, and perform 5×10^5 Monte Carlo steps (MCSs) at each temperature. All the results were obtained after convergence of the Metropolis annealing procedure (no considerable change was observed in energy after a decrease of temperature).

We first mimicked the bulk structures of pure elements contained in our sample. Figure 1 shows the RDF obtained for Fe and Cu layers before (a, b) and after (c, d) simulated annealing. For each layer, it can be observed that the positions of peaks match the above-mentioned theoretical values (first and second nearest neighbors) for conventional elements of Fe and Cu structures. These results show the suitability of our method to mimic pure and experimental samples. While many experimental studies have been dedicated to bilayer systems,[3,8] we wondered whether the number of interfaces could have an impact on the structure of the system. Therefore, we started by studying systems composed of two layers and one interface. In order to gain insight into the role played by the interface on the structure of bilayers Fe/Cu, we proceeded to the analysis of Fe_5/Cu_{15}, Fe_{15}/Cu_5 and Fe_{35}/Cu_{35} (the subscripts denote thicknesses given in Å) bilayer systems. Figure 2 shows the RDF of the structures obtained after the Monte Carlo-simulated annealing scheme. As observed in Fig. 2(a), (case of Fe_5/Cu_{15} system), the system conserves the structure of the thickest layer, here fcc of Cu. A structure similar to that of fcc Cu is also observed at the interface [Fig. 2(b)], while the structure of Fe layer remains close to that of fcc Cu for short-range interactions [Fig. 2(a)] and amorphous far from the interface Cu/Fe. The absence of long-range order can be explained by the fact that almost all Fe atoms are located at the interface because of the ultrathin thickness of that layer, such a way that Fe atoms are embedded in the dominant element (here Cu), as interface thickness of Fe/Cu was shown to be around 4 Å.[9] Moreover, a similar behavior is observed when switching the thicknesses of Fe and that of Cu (Fe_{15}/Cu_5 system). Figure 2(c) shows the well-defined bcc structure of the Fe layer; interface structure [Fig. 2(c)] is similar to that of bcc Fe and the structure of Cu is amorphous far from the interface. We concluded that for bilayer systems, the thickest layer imposes its

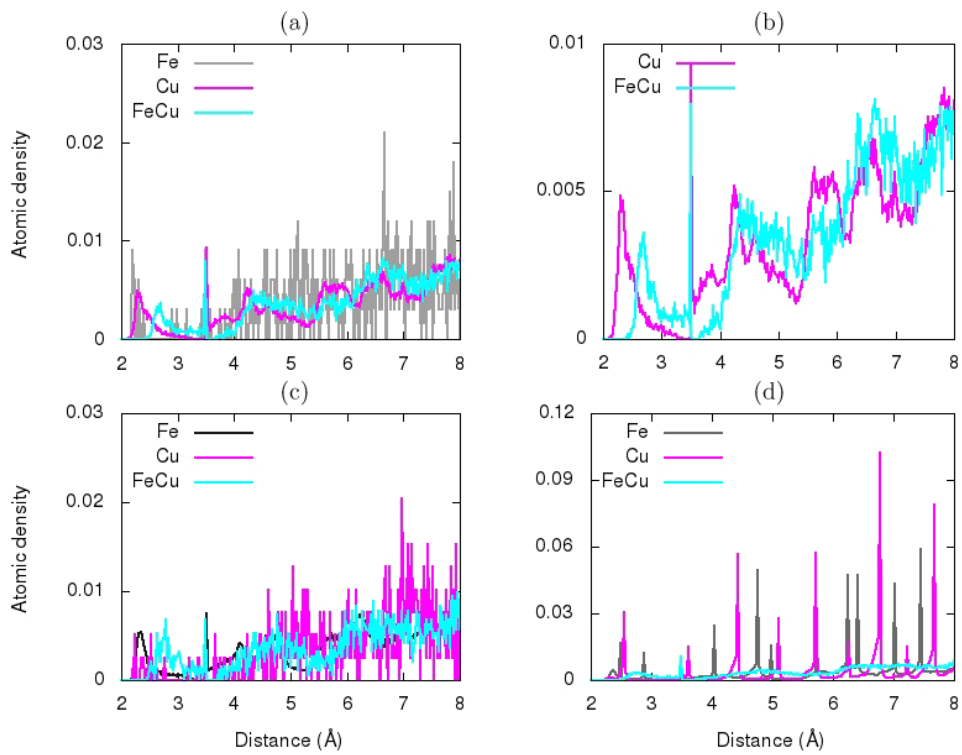

Fig. 2. RDF showing the structures of bilayers Fe/Cu systems for variable thickness of Fe (t_{Fe}) and Cu (t_{Cu}) layers. (a) with $t_{Fe} = 5$ Å and $t_{Cu} = 15$ Å, there is a structural similarity between the Cu layer and the interface, as confirmed in (b) (the structure of Fe layer is close to fcc for the first planes and amorphous beyond); (c) with $t_{Fe} = 15$ Å and $t_{Cu} = 5$ Å, the Cu layer is amorphous, and both Fe layer and interface adopt a bcc-like structure; (d) with $t_{Fe} = 35$ Å and $t_{Cu} = 35$ Å, there are well pronounced structures of Fe (bcc) and Cu (fcc) layers and an intermediary structure at the interface.

SPIN Downloaded from www.worldscientific.com
by Mr. Reprints Desk on 10/08/18. Re-use and distribution is strictly not permitted, except for Open Access articles.

structure to the system when the smallest layer has a thickness less than 15 Å.

Ultrathin layers first grow according to the structure of thickest layer (first atomic planes) and smoothly relax towards its bulk structure when increasing its thickness. We confirmed this observation when increasing the thicknesses of Fe and Cu to 35 Å (Fig. 2(d) for multilayer Fe_{35}/Cu_{35}). One can see the well-pronounced fcc and bcc structures of Cu and Fe layers, respectively, while the interface tends to adopt an intermediary structure. We can justify the presence of the intermediary structure at the interface instead of amorphous interface by the fact that the atomic proportion at the interface decreases with the increase in layer thicknesses as previously reported,[18,19] and atoms tend to be surrounded by the particles of same type. Albini *et al.*[8] and Jian-Tao *et al.*[47] previously observed similar results. We next went ahead and studied the system composed of multiple interfaces. We know from previous studies that GMR is commonly obtained from systems composed of three layers.[11–13] To study the impact of the second interface on the structure of the system and to accurately estimate the thickness of the spacer layer for which the maximum GMR could be observed, we carried out our investigations on trilayer systems. In order to further gain insight into the interfaces morphology and its impact on the structure of the system, we analyzed a series of multilayer systems, which showed a strong dependence of the structure at the interface on the thickness of layers and vice versa.

For instance, Fig. 3 presents the RDF obtained from the system $Fe_{21}/Cu/Fe_{21}$, with variable spacer thickness: $t_{Cu} = 6$ Å, 13 Å, 24 Å, and 40 Å.

One can see that for the ultrathin spacer (Fig. 3(a), system $Fe_{21}/Cu_6/Fe_{21}$), the structure of Fe layer remains bcc, while that of Cu layer tends to copy the metastable bcc structure for the first atomic planes and adopts an amorphous structure beyond. We observed the presence of Fe atoms even at the core of Cu layer (data not shown), confirming that Cu layer is not large enough to overcome the interface effect (i.e., its structure is more dominated

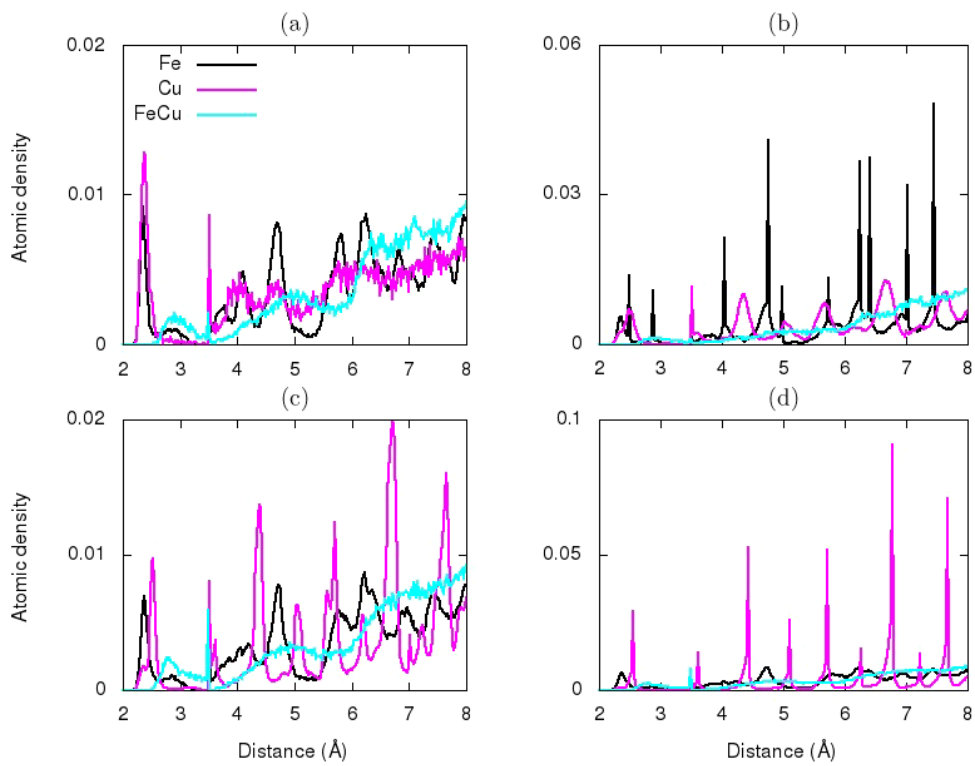

Fig. 3. Multilayer systems Fe/Cu/Fe with fixed thickness of Fe layer $t_{Fe} = 21$ Å and a variable thickness of the Cu layer t_{Cu}: (a) with $t_{Cu} = 6$ Å, the system adopts a bcc structure similar to that of Fe; (b) with $t_{Cu} = 13$ Å, the Cu layer undergoes a transition from metastable bcc to a structure similar to fcc of the bulk Cu, and the interface is largely amorphous; (c) with $t_{Cu} = 24$ Å, the bcc structure of the Fe layer coexists with the fcc structure of the Cu layer at the interface; (d) shows for $t_{Cu} = 40$ Å, the effect of the interface morphology and spacer thickness on the structure of Fe layer.

SPIN Downloaded from www.worldscientific.com
by Mr. Reprints Desk on 10/08/18. Re-use and distribution is strictly not permitted, except for Open Access articles.

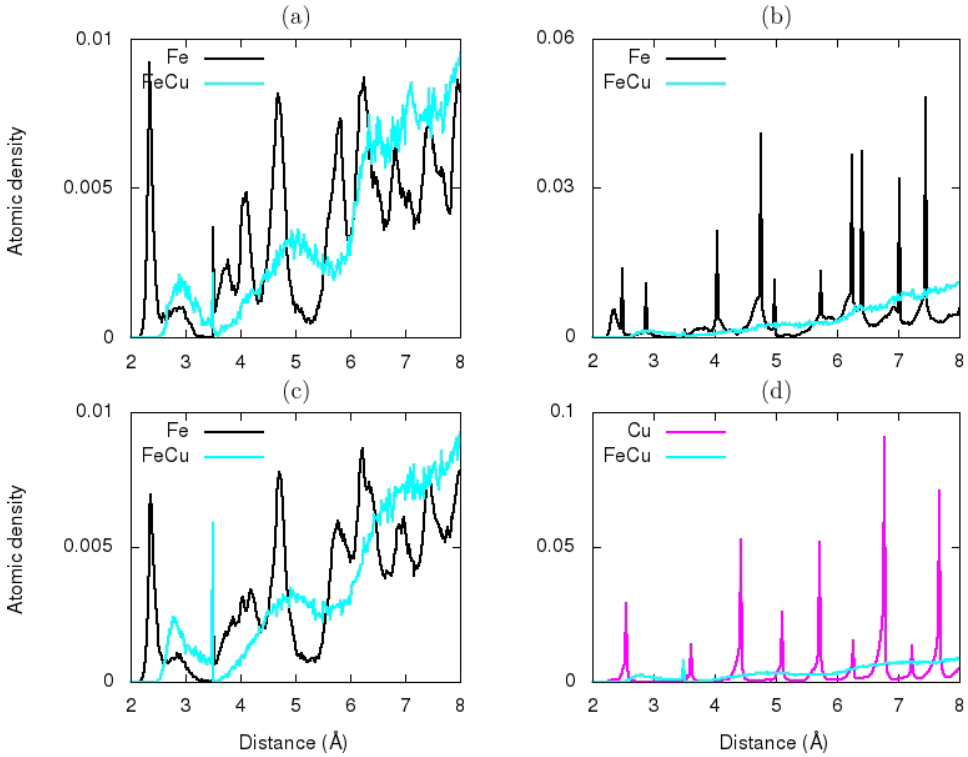

Fig. 4. Multilayer $Fe_{21}/Cu/Fe_{21}$ systems, with the thickness of the Cu layer varying from $t_{Cu} = 13$ Å to $t_{Cu} = 40$ Å. (a) Conserved bcc structure is observed at the interface; (b) critical point denoting the transition with an amorphous structure at the interface ($t_{Cu} = 13$ Å); (c) well-pronounced intermediary bcc and fcc interfaces for $t_{Cu} = 24$ Å; (d) shows the conserved structure of Fe and Cu with intermediary interface structure $t_{Cu} = 40$ Å.

by the interface structure, here bcc). Moreover, the lack of proper Cu-ordered structure even at the core of Cu layer could also be related to the presence of two interfaces, as t_{Cu} is not large enough to keep a single domain containing only Cu atoms. Compared to the results in Fig. 2(c), the metastable bcc Cu structure is well pronounced. This observed structure is probably the consequence of the second interface. While it is known that Fe and Cu are immiscible materials, it has been shown that Fe and Cu can form a mixture of few planes at the interface,[48] supporting a nonpronounced structure of bulk Cu for this system. The interface structure remains similar to that of bcc structure, as observed in Fig. 4(a). The peaks' positions are similar for both structures of Fe and interface of Fe/Cu.

Given that the above-mentioned structures of Cu and interface are still dominated by thickest layer (here Fe), we increased the spacer thickness and we observed the change on both structures (Fig. 3(b), system $Fe_{21}/Cu_{13}/Fe_{21}$). The structure of Cu tends to relax towards its fcc bulk structure while the peaks observed on the interface structure become broader. The observed structure at the interface [Fig. 4(b)] can be explained by the fact that increasing the spacer thickness leads to the decrease in the atomic proportion at the interface,[18,19] hence a tendency to form an interface mixture as atoms at the interface form bonds quasi-identical to those of the conventional material. We further noted that the order at the interface increases with the increase in t_{Cu}, this can also be explained by the fact that the density of Cu atoms at the interface reduces when t_{Cu} increases,[19] therefore Cu atoms tend to form fcc Cu-like structure and a mixture of bcc and fcc structures tend to be formed at the interface. The structure of Cu layer is well pronounced with the increase in t_{Cu} (Figs. 3(c) and 3(d) for the systems. $Fe_{21}/Cu_{24}/Fe_{21}$ and $Fe_{21}/Cu_{40}/Fe_{21}$, respectively) confirming the above observations. It can be seen on Fig. 3(c) that the observed Cu structure is similar to that of pure Cu shown in Figs. 1(a) and 1(b). This indicates that the spacer layer is large enough to reproduce the structure of bulk material; no change was observed with a further increase in spacer thickness [Fig. 3(d)]. Surprisingly, a considerable

SPIN Downloaded from www.worldscientific.com
by Mr. Reprints Desk on 10/08/18. Re-use and distribution is strictly not permitted, except for Open Access articles.

change was observed on the peaks' height of Fe structure when increasing the spacer thickness beyond a certain value, here 24 Å [Figs. 3(c) and 3(d)]. This observed behavior on the Fe layer structure can be explained by the fact that an increase in spacer thickness leads to the growth of first atomic planes (close to the interface Cu/Fe) according to the fcc structure and a smooth relaxation towards the bulk structure when approaching the core material. These observations will be further explained below. The structure at the interface remains intermediary between bcc and fcc as shown in Figs. 4(c) and 4(d). These observations are in good agreement with the experiments.[5,8]

To further investigate the correlation between interface morphology and the layers in presence, we studied systems with variable Fe thickness. Figure 5 shows the RDF for multilayer systems $Fe/Cu_{25}/Fe$, with Fe layer's thickness being varied: $t_{Fe} = 7$ Å, 18 Å, 25 Å and 34 Å. At the fixed t_{Cu}, it is observed that the structure of Fe depends on its thickness and the interface morphology. For example, when $t_{Fe} = 7$ Å, the structure of Fe layer tends to copy the fcc structure as it was shown experimentally.[3] [Fig. 5(a)]. The structure of the spacer layer, Cu, remains fcc as well as that at the interface. When increasing t_{Fe} from 7 Å to 34 Å [Figs. 5(b)–5(d)], a smooth transition is observed on the Fe structure from the less pronounced (here fcc-like structure) to the bulk bcc Fe structure [Fig. 5(d)] with a critical (or transitional) point observed around $t_{Fe} = 18$ Å [Fig. 5(c)]. It is noted that the structure of Cu layer remains fcc [Figs. 5(a)–5(d)] independently of Fe thickness while the interface tends to mimic the fcc structure for ultrathin Fe layers [Figs. 5(a) and 5(b)], and relaxes towards an intermediary structure for thicker Fe layers [Fig. 5(d)]. An amorphous interface structure is observed at the transition, $t_{Fe} = 18$ Å [Fig. 5(c)]. These results are in accordance with those previously obtained from experiments.[6]

Interface morphology plays a key role in determining the properties of magnetic multilayers. Spacer layer thickness (t_{Cu}) has been shown to control the nature of the interlayer exchange coupling between magnetic Fe layers during the study of the GMR effects.[5–7,13] Depending on the spacer thickness, ferromagnetic or antiferromagnetic

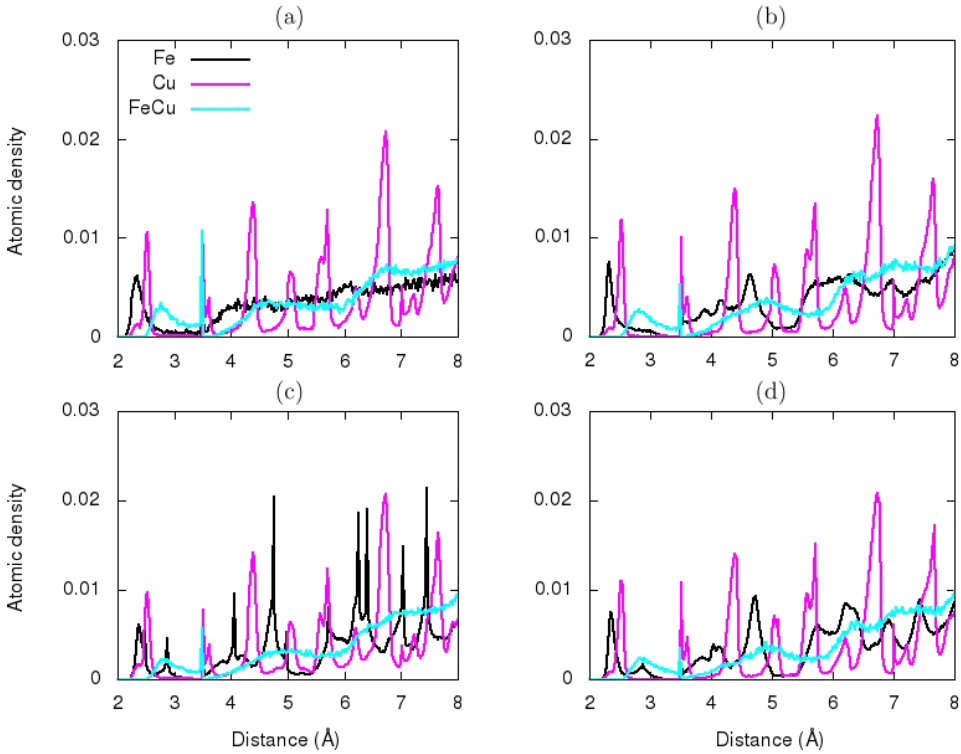

Fig. 5. Multilayer systems Fe/Cu/Fe with fixed thickness of the Cu layer $t_{Cu} = 25$ Å and variable thickness of the Fe layers, t_{Fe}: (a) with $t_{Fe} = 7$ Å, the system exhibits the fcc structure; (b) with $t_{Fe} = 18$ Å, the Fe layers shift towards the bulk bcc structure; (c) with $t_{Fe} = 25$ Å, the bcc structure of Fe layer is well pronounced; (d) $t_{Fe} = 34$ Å shows the well-pronounced intermediary interface structure and confirms the bcc structure of the Fe layer. Cu layer structure remains fcc independently of the Fe thickness.

SPIN Downloaded from www.worldscientific.com
by Mr. Reprints Desk on 10/08/18. Re-use and distribution is strictly not permitted, except for Open Access articles.

interlayer exchange coupling can be observed. For example, in case of ultrathin spacer layer, the loss of antiferromagnetic coupling between adjacent magnetic layers can occur due to imperfections in the spacer layer [Fig. 3(a)] while in the case of thicker spacer layers, an important reduction of the magnetic scattering can be observed due to the low concentration of Fe atoms [Fig. 3(d)]. However, the structural nature of the Cu layer and the thickness to which either of the exchange coupling is observed remain the subjects of discussion. For example, Fig. 3(b) shows the structure of Cu layer similar to that of bcc Fe for the ultrathin layers, as previously observed in Ref. 5. This implies that the direct coupling exchange between the two adjacent magnetic layers is likely to be ferromagnetic, explaining the decrease in magneto-resistance below a certain critical spacer thickness as shown in Ref. 5. The observed metastable bcc structure of Cu can be explained by the increase in atomic proportion at the interface with the layer's thickness, and the presence at the interface of almost all Cu atoms, thus forming matrix with dominant Fe atoms. This assumption is confirmed by the structure in Fig. 2(c) where the interface is less dominated by Fe atoms. Even though Cu layer has almost the same atomic proportion as the system represented in Fig. 3(a), it tends to form a Fe–Cu alloy with an amorphous structure instead of metastable bcc structure. Similarity in atomic proportion between Fe and Cu at the interface might explain this observation. The smooth transition from metastable bcc to fcc bulk Cu as observed on the graphs in Fig. 3 could be at the origin of the observed expansion of the magneto-resistance with the increase of Cu thickness, for reference, see Refs. 49 and 50. This transition could be helpful in explaining the observed antiferromagnetic interlayer exchange coupling for Fe/Cu/Fe multilayers.

4. Conclusion

We have investigated in this study the structural properties of metallic multilayers under the influence of interfaces using atomistic Monte Carlo simulations. We have shown that the structure of the layers depends on their thickness and the structure of the interface. Moreover, the structure of the interface can adopt that of the thicker layer, and switch to an intermediary structure of fcc and bcc, as the thickness of the thinner layer increases. These results are in good agreement with the experiments.

References

1. U. Hartmann and R. Coehoorn, *Magnetic Multilayers and Giant Magnetoresistance: Fundamentals and Industrial Applications* (Springer-Verlag, Berlin Heidelberg, 2000).
2. J. A. C. Bland and B. Heinrich, *Ultrathin Magnetic Structures* (Springer, Berlin, 1994).
3. C. Cobianu, M.-F. Stan, E.-O. Virjoghe and N. Fidel, *J. Sci. Arts* **4**, 451 (2012).
4. R. Gupta, A. Gupta, S. Chaudhari, M. Gupta and P. Allenspach, *Appl. Surf. Sci.* **238**, 254 (2004).
5. S. Pizzini, F. Baudelet, A. Fontaine, D. Chandesris, H. Magnan, A. Fert, F. Petroff and C. Marlière, *J. Phys. IV France* **2**, C3-185-C183-189 (1992).
6. D. W. Lee, D. H. Ryan, Z. Altounian and A. Kuprin, *Phys. Rev. B* **59**, 7001 (1999).
7. M. Afshari, M. E. Ghazi and M. Izadifard, *Afr. Rev. Phys.* **10**, 0004 (2015).
8. L. Albini, G. Carlotti, G. Gubbiotti, S. Loreti, C. Minarini, L. Palmieri and S. R. Teixeira, *Physica B* **275**, 253 (2000).
9. A. Razouk, M. Sahlaoui and M. Sajieddine, *J. Supercond. Novel Magn.* **25**, 1623 (2012).
10. P. Grunberg, R. Schreiber, Y. Pang, M. B. Brodsky and H. Sowers, *Phys. Rev. Lett.* **57**, 2442 (1986).
11. G. Binasch, P. Grünberg, F. Saurenbach and W. Zinn, *Phys. Rev. B* **39**, 4828 (1989).
12. M. N. Baibich, J. M. Broto, A. Fert, F. N. Van Dau, F. Petroff, P. Etienne, G. Creuzet, A. Friederich and J. Chazelas, *Phys. Rev. Lett.* **61**, 2472 (1988).
13. A. Fert, R. Morel, A. Barthelemy, V. Cros, J. L. Duvail, J. M. George, F. Parent, F. Petroff and C. Vouille, *J. Phys.* **7**, 151 (1997).
14. M. B. Salamon, S. Sinha, J. J. Rhyne, J. E. Cunningham, R. W. Erwin, J. Borchers and C. P. Flynn, *Phys. Rev. Lett.* **56**, 259 (1986).
15. C. F. Majkrzak, J. W. Cable, J. Kwo, M. Hong, D. B. McWhan, Y. Yafet, J. V. Waszczak and C. Vettier, *Phys. Rev. Lett.* **56**, 2700 (1986).
16. Y. Ueda, S. Ikeda, Y. Mori and H. Zaman, *Mater. Sci. Eng. A* **217**, 371 (1996).
17. Ö. F. Bakkaloğlu, *J. Magn. Magn. Mater.* **182**, 324 (1998).
18. H. Gleiter, *Acta Mater.* **48**, 1 (2000).
19. M. Grafoute, Y. Labaye, F. Calvayrac and J. M. Greneche, *Eur. Phys. J. B* **45**, 419 (2005).
20. G. P. Zhao and X. L. Wang, *Phys. Rev. B* **74**, 5 (2006).
21. G. P. Zhao, X. L. Wang, C. Yang, L. Xie and G. Zhou, *J. Appl. Phys.* **101**, 09J104 (2007).

22. G. P. Z. Wenjing Si, N. Ran, Y. Peng, F. J. Morvan and X. L. Wan, *Sci. Rep.* **5**, 16212 (2015).
23. J. C. Q. Zhao, J. Wang, X. Zhang, G. Zhao and Q. Ma, *Sci. Rep.* **7**, 4286 (2017).
24. G. P. Z. P. Lai, F. J. Morvan, S. Q. Wu and N. Ran, *Spin* **7**, 8 (2017).
25. G. P. Z. P. Lai, H. Tang, N. Ran, S. Q. Wu, J. Xia, X. Zhang and Y. Zhou, *Sci. Rep.* **7**, 8 (2017).
26. G. P. Z. Xichao Zhang, Hans Fangohr, J. Ping Liu, W. X. Xia, J. Xia and F. J. Morvan, *Sci. Rep.* **5**, 6 (2015).
27. H. Zillgen, B. Feldmann and M. Wuttig, *Surf. Sci.* **321**, 32 (1994).
28. M. T. Lin, J. Shen, W. Kuch, H. Jenniches, M. Klaua, C. M. Schneider and J. Kirschner, *Phys. Rev. B* **55**, 5886 (1997).
29. M. T. Lin, J. Shen, W. Kuch, H. Jenniches, M. Klaua, C. M. Schneider and J. Kirschner, *Surf. Sci.* **410**, 290 (1998).
30. J. Shen, P. Ohresser, C. V. Mohan, M. Klaua, J. Barthel and J. Kirschner, *Phys. Rev. Lett.* **80**, 1980 (1998).
31. A. Dittschar, W. Kuch, M. Zharnikov and C. M. Schneider, *J. Magn. Magn. Mater.* **212**, 307 (2000).
32. A. P. Kuprin, L. Cheng, D. W. Lee, Z. Altounian and D. H. Ryan, *J. Appl. Phys.* **85**, 5738 (1999).
33. V. V. Prudnikov, P. V. Prudnikov and D. E. Romanovskiy, *J. Phys. Conf. Ser.* **681**, 012016 (2016).
34. M. Zharnikov, A. Dittschar, W. Kuch, C. M. Schneider and J. Kirschner, *Phys. Rev. Lett.* **76**, 4620 (1996).
35. M. Zharnikov, A. Dittschar, W. Kuch, C. M. Schneider and J. Kirschner, *J. Magn. Magn. Mater.* **165**, 250 (1997).
36. P. V. Prudnikov, V. V. Prudnikov and M. A. Medvedeva, *JETP Lett.* **100**, 446 (2014).
37. P. V. Prudnikov, V. V. Prudnikov, M. A. Menshikova and N. I. Piskunova, *J. Magn. Magn. Mater.* **387**, 77 (2015).
38. B. Fongang, Y. Labaye, F. Calvayrac, J. M. Greneche and S. Zekeng, *J. Magn. Magn. Mater.* **322**, 2888 (2010).
39. G. Voronoi, *J. Reine Angew. Math.* **136**, 67 (1909).
40. B.-J. Lee and M. I. Baskes, *Phys. Rev. B* **62**, 8564 (2000).
41. B.-J. Lee, M. I. Baskes, H. Kim and Y. K. Cho, *Phys. Rev. B* **64**, 184102 (2001).
42. B. E. Sundquist, *Acta Metall.* **12**, 67 (1964).
43. H. E. Grenga and R. Kumar, *Surf. Sci.* **61**, 283 (1976).
44. M. S. Daw and M. I. Baskes, *Phys. Rev. Lett.* **50**, 1285 (1983).
45. B.-J. Lee, B. D. Wirth, J.-H. Shim, J. Kwon, S. C. Kwon and J.-H. Hong, *Phys. Rev. B* **71**, 184205 (2005).
46. N. Metropolis, A. W. Rosenbluth, M. N. Rosenbluth, A. H. Teller and E. Teller, *J. Chem. Phys.* **21**, 1087 (1953).
47. J.-T. Wang, L. Zhou, Y. Kawazoe and D.-S. Wang, *Phys. Rev. B* **60**, 3025 (1999).
48. N. R. Shamsutdinov, A. J. Bottger and F. D. Tichelaar, *Scr. Mater.* **54**, 1727 (2006).
49. H. M. van Noort, F. J. A. den Broeder and H. J. G. Draaisma, *J. Magn. Magn. Mater.* **51**, 273 (1985).
50. F. Badia, G. Fratucello, B. Martinez, D. Fiorani, A. Labarta and J. Tejada, *J. Magn. Magn. Mater.* **93**, 425 (1991).

SPIN Downloaded from www.worldscientific.com
by Mr. Reprints Desk on 10/08/18. Re-use and distribution is strictly not permitted, except for Open Access articles.